DISSERTATION

BEHAVIOR OF PARTIAL AND COMPLETE MONOLAYERS OF ARGON DEPOSITED ON GRAPHITE

Submitted by

Elijah Jude Flenner

Physics

In partial fulfillment of the requirements

For the Degree of Doctor of Philosopy

Colorado State University

Fort Collins, Colorado

Fall 2003

COLORADO STATE UNIVERSITY

August 28, 2003

WE HEREBY RECOMMEND THAT THE DISSERTATION PREPARED UNDER OUR SUPERVISION BY ELIJAH FLENNER ENTITLED BEHAVIOR OF PARTIAL AND COMPLETE MONOLAYERS OF ARGON DEPOSITED ON GRAPHITE BE ACCEPTED AS FULLFILING IN PART REQUIREMENTS FOR THE DEGREE OF DOCTOR OF PHILOSOPHY.

Committee on Graduate Work

Mark P. Hellfand

Ralf Feisner

Eugene L. Allgower

Richard D. Etters

Adviser

David A. Krueger

Department Head

ABSTRACT OF DISSERTATION

BEHAVIOR OF PARTIAL AND COMPLETE MONOLAYERS OF ARGON DEPOSITED ON GRAPHITE

This calculation examines the behavior of argon deposited on graphite for various densities in the temperature range of 30K and 90K. The densities studied were 0.39, 0.71, 1.00, 1.07, 1.14, 1.22, and 1.31 where a density of one corresponds to 0.0636 atoms/Å^2. For densities of 1.00 and below, two peaks were observed in the specific heat. A narrow peak around 47.3K and a broad peak around 50K. The narrow peak is identified with a rotational transition, and the broad peak is due to the melting transition, which corresponds to the loss of six fold bond orientational order. For densities of 1.07 and greater there is only one peak in the specific heat which is associated with the melting transition. Also, the motion of the atoms perpendicular to the substrate is determined to be an important aspect of the melting of complete monolayers.

Elijah Jude Flenner
Physics Department
Colorado State University
Fort Collins, CO 80523
Fall 2003

Contents

List of Tables

List of Figures

Chapter 1

Introduction

Even though the theory of melting has received much attention, no general theory exists. Most theories on melting are phenomelogical and require experimental information to determine thermodynamic properties around the melting transition. There has been some progress in understanding the mechanisms of melting. The most studied are theories based on the dislocation model of Kosterlitz and Thouless. While there is a three dimensional version of the dislocation model of melting, the two dimensional version has received more attention.

Kosterlitz and Thouless[1], Halperin and Nelson[2], and Young[3] (KTHNY) developed a theory of melting for two dimensional solids. The KTHNY theory predicts that the melting of two dimensional solids is continuous, which differs from the first order process always observed for three dimensional melting. This prompted experimental and theoretical studies on two dimensional and quasi-two-dimensional systems. One

of the most studied is rare gas atoms physisorbed on graphite. These systems are considered good approximations to two-dimensional systems since the absorbates are strongly attracted to the graphite surface so that there is little fluctuation in the direction perpendicular to the substrate. The atoms are mobile in directions parallel to the substrate due to lack of chemical bonds between the atoms and the surface.

Since the atom-atom interactions for rare gas atoms are all very similar, and the lateral variation of the graphite potential is weak compared to the atom-atom interactions, it was initially assumed that all the rare gases physisorbed on graphite would melt in a similar manner. This was not the case. Experimental evidence showed that the melting of the rare gas atoms on graphite to be quite different. Submonolayer xenon, krypton, and neon[4, 5] were determined to exhibit first order melting, but the order of the melting transition for argon is still debated[6, 7, 8, 9]. The difference in the melting characteristics is due to the difference in the relative strength of the interactions with the graphite substrate and the adatom-adatom interaction.

Chung published the first specific heat study of argon physisorbed on graphite in 1979[10]. He saw a broad peak with a maximum of about 8 $J/\mathrm{K}Nk_B$, where N is the number of absorbed atoms and k_B is Boltzman's constant, centered around 50K for densities smaller than one monolayer, the density at which atoms cover the whole surface. As the density approached one monolayer, the position of the specific heat peak moved up in temperature. Since the peak height was small compared to other rare-gas graphite systems, and the peak was broad, Chung concluded that the

melting of argon was continuous. In 1984, Migone[6] published a very accurate heat capacity measurement which exposed some additional features. Not only did he see a broad peak at 50K, but there was also a very narrow peak around 47.3K with a full width at half maximum (FWHM) of 0.3K. Migone interpreted the narrow peak as a signature of first order melting, and the broad peak due to a gradual loss of six-fold bond orientational order. At densities less than one half a monolayer, he also measured another peak centered around 55K corresponding to the 2D fluid-vapor transition. Migone calculated a 0.02 Nk_B entropy change per particle at the narrow specific heat peak by integrating under his measured specific heat peak. This change in entropy is about 15 to 20 times smaller than the entropy change at melting for other rare gas graphite systems.

Previous to Migone's work, McTague, Als-Nielsen, Bohr, and Nielsen[11] conducted a synchotron x-ray study to examine the melting of submonolayer argon on graphite. The x-ray scattering data observed the peak intensity of the (10) Bragg peak evolve continuously through the melting transition, and they saw no evidence for a first order melting transition. The peak width also increased rapidly from about 47.9K to 50K. In the experiment of McTague *et al.*, they list the melting temperature at 47.9K for densities less than one monolayer. In a later synchotron x-ray study by Nielsen *et al.*[7], similar results were found for submonolayer densities, but the melting temperature was between 48.13K and 48.41K. Nielsen found the melting temperature by fitting the correlation length to the KTHNY theory. They speculated that the

narrow specific heat peak could be due to loss of orientation order of the argon solid with respect to the substrate.

In 1978, a low energy electron diffraction (LEED) experiment was conducted by Shaw[12] that demonstrated that argon had a preferred orientation on the graphite surface. McTague and Novaco[13],in 1979, calculated how the lateral variation of the graphite substrate, the corrugation, could produce a preferred orientation of rare gas atoms with respect to the graphite. To see if there was a rotational transition, the rotation angle of the absorbed atoms was measured in 1990 by D'Amico[14] *et al.* They found that the rotation angle was nonzero below the melting transition, and into the fluid for a density below monolayer densities. It was concluded that the narrow specific heat peak was not due to loss of orientational order. D'Amico also determined the melting temperature to be around 50K. None of the scattering experiments could determine the cause of the narrow specific heat peak.

Zhang and Larese[8] conducted a compressibility experiment to examine the narrow specific heat peak. They found two compressibility peaks as they varied the density of the argon atoms at constant temperature on the graphite substrate. They identified the high density peak with the broad specific heat peak of Migone, and the other with the narrow peak. To determine the order of the transition, they compared their results with the compressibility peak of incommensurate methane, a known first order transition. There was an order of magnitude difference in height, and a factor of six difference in the FWHM of the two peaks. Also, under the assumption that the

narrow specific heat peak was first order melting, they calculated the change in the lattice constant using a two dimensional version of the Clausius-Clapeyron equation, and compared the results of the calculation to the experimental lattice parameter change. They found that the two methods differed by an order of magnitude. Using these results, they argued that the melting of argon physisorbed on graphite must not be first order. They were unable to determine the nature of the argon atoms between the two specific heat peaks, but they described it as having short range order, but with solid like characteristics.

Many computer simulations have been conducted to probe the nature of melting of argon on graphite[15, 16, 17, 18, 19, 20, 21, 22, 23, 24, 25]. Most of these do not include corrugation in the argon-graphite potential, which experiments suggest is important, but a few do. One of the first was a molecular dynamics simulation of Abraham[25] in 1983. Abraham used Lennard-Jones potentials for all the atom-atom interactions, including the interaction of the argon with the carbon. Abraham's simulations corresponded to a density less than a monolayer. He noticed liquid-like patches forming at around 47K, then the solid melted continuously, with the liquid-like patches growing larger, until it was completely melted around 55K. He also found the mobility of the argon atoms in the liquid phase to be greatly reduced compared to the case with no substrate corrugation. The melting behavior of argon in the simulations was also quite different than the melting behavior of krypton and xenon. Abraham's simulations demonstrated the importance of the corrugation on the melting of rare gas

atoms on graphite. Roth and Salazar[26] completed a molecular-dynamics simulation of argon physisorbed on graphite in 1998. A broad melting transition was observed around 135K for a complete monolayer, and second layer promotion was observed before melting.

A basic phase diagram can be constructed from the experimental results, figure 1.1. The solid and liquid phases can either cover the whole surface, or form solid and liquid patches. For submonolayer densities, the melting temperature is debated but is at a temperature between 47K and 51K. For complete monolayers, the melting temperature depends on density and increases very rapidly with density.

The present work tries to answer the questions posed by experiment and looks at the nature of melting, specifically two dimensional melting. The second chapter deals with general properties of rare-gas atoms on graphite, with an emphasis on the specifics of argon on graphite. Also described is the structure of the basal plane of graphite, and the structure of the argon atoms absorbed on the basal plane. The influence of the graphite surface on the structure of the argon atoms will be described. Also, chapter 2 will describe what is meant by a two dimensional solid and how the phase diagram might be affected by the presence of the substrate.

The third chapter will outline the Monte Carlo simulations, and the techniques used to study argon physisorbed on graphite. The details of the interactions and method used to find all the calculated quantities will be described. The fourth chapter will describe the results of the Monte Carlo simulations. The fifth chapter will review

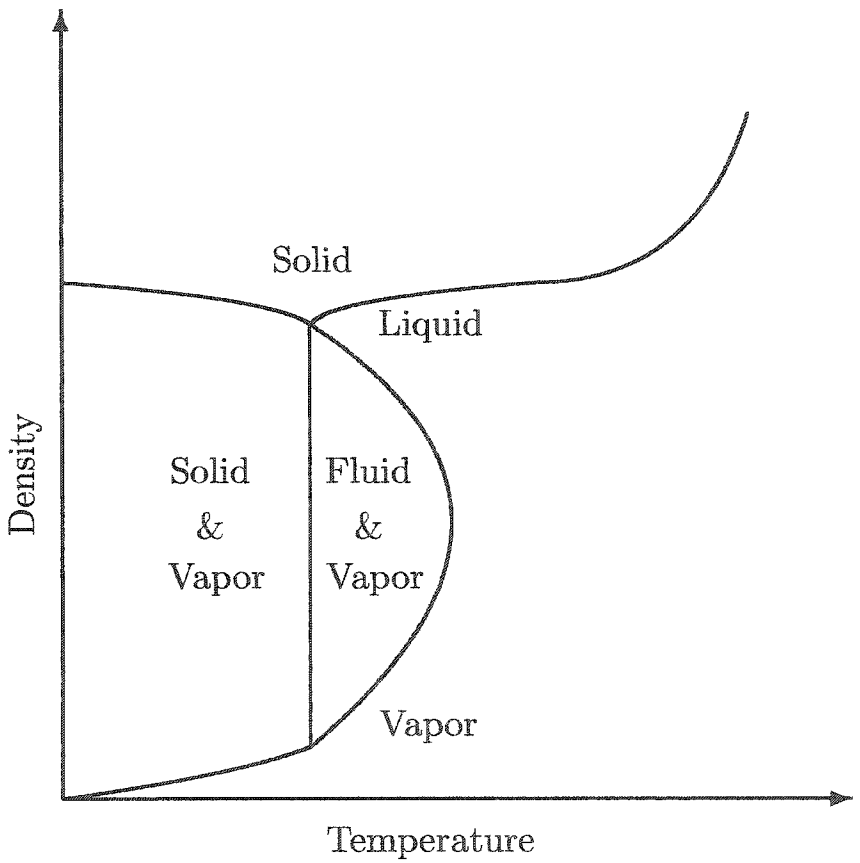

Figure 1.1: Main aspects of the phase diagram that can be determined from experiment.

the conclusions that can be drawn from this work, and discuss what else needs to be done to determine the behavior of argon physisorbed on graphite. The final chapter summarizes the results of these simulations.

Chapter 2

Background

This chapter describes some of the background information needed to understand the phase diagram of argon physisorbed on graphite. It is divided into two sections. The first section describes the structure of argon physisorbed on graphite. The second section describes what is meant by a two dimensional solid, and some of the properties of 2D solids.

2.1 Structure

To understand the melting of argon physisorbed on graphite, we need to know some information about the structure of graphite, as well as the structure of the argon atoms in the two dimensional solid phase. Graphite forms a two dimensional hexagonal lattice in the (001) plane, see figure 2.1. The nearest neighbor distance within planes is 1.42Å, and the separation between basal planes is 3.37Å. Argon atoms are attracted

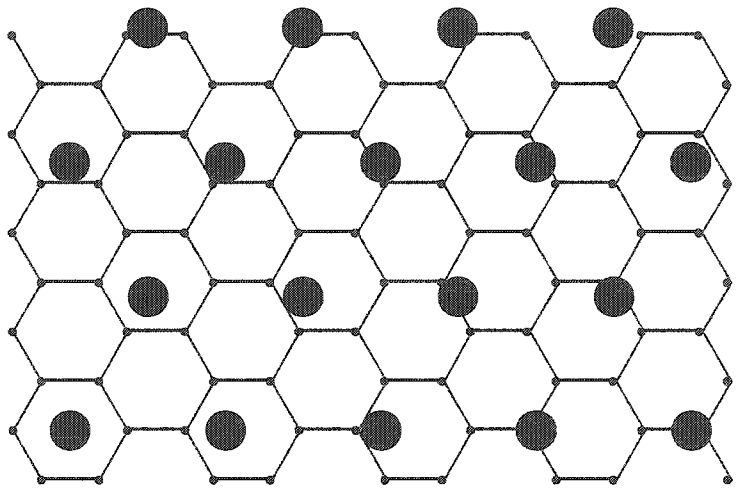

Figure 2.1: Argon atoms on graphite basal plane. The filled circles represent the mass centers of the argon atoms. The argon atoms are aligned with a $(\sqrt{3} \times \sqrt{3})$R30° symmetry direction and are separated by 3.86Å. For a $(\sqrt{3} \times \sqrt{3})$R30° structure, all the atoms would be in the center of a graphite hexagon.

to the carbon atoms in the graphite for distances greater than ~3.8Å. When the argon atoms are closer than ~3.8Å to a carbon atom, the electron clouds overlap and a repulsive force results.

For two isolated argon atoms, the interaction energy only depends on the separation of the argon atoms. The multi-body corrections are around 2% of the dispersion energy, thus they are small. On a smooth substrate, this implies that the argon atoms will form a close packed two dimensional solid, i.e. a two dimensional triangular lattice. In figure 2.1, this structure along with the underlying graphite structure is shown. The separation between the argon atoms in the figure is 3.86Å, the low temperature value obtained from neutron scattering of argon overlayers[27].

The distance between any two graphite hexagon centers is not equal to the argon atomic spacing, thus the argon atoms in this dense packed arrangement are incommensurate with the graphite substrate and all the argon atoms are not located above the center of a graphite hexagon. Krypton physisorbed on graphite does form a solid in which the average position of all the atoms are above the centers of the graphite hexagons, and is commensurate with the graphite substrate. There is one krypton atom for every three graphite hexagons, and the krypton structure is referred to as $(\sqrt{3} \times \sqrt{3})$R30° commensurate. In this study, a density of one will correspond to one atom per three graphite hexagons, the density with respect to a $\sqrt{3} \times \sqrt{3}$ structure.

The argon atoms are attracted to the individual carbon atoms, and the interaction energy of an argon atom with the surface depends on how close the argon atom is to

each individual carbon atom. A single atom on the surface will try to minimize the interaction energy between itself and as many carbon atoms as possible. The result is that the minimum energy for a single argon atom on the surface would be above the middle of a graphite hexagon, and the maximum of the energy occurs over a carbon atom. Thus the interaction energy of the argon atom with the graphite surface varies across the surface. This has some profound consequences. One is that the argon solid has a preferred orientation with respect to the graphite surface, which is not along one of the directions of high symmetry of the substrate.

The orientation of the argon solid on the graphite substrate plays a role in the phase diagram, so it is important to understand why they have orientational order with respect to the substrate. The following argument is due to a calculation by Novaco and McTague[13]. The periodic potential is included as a linear term in the Hamiltonian, and a static strain of the solid argon results. The result is that each atom behaves as a displaced harmonic oscillator, with the size of the displacement depending on where the adatom is above the substrate. The displacement of each atom results in a periodic change in the density, which is referred to as a mass density wave. The lowest energy state is one in which the argon lattice is rotated approximately 3° with respect to a $(\sqrt{3} \times \sqrt{3})$R30° structure. For long wavelength distortions, the rotation angle depends on the lattice constant and the ratio of the longitudinal and the transverse sound velocities, and does not depend on the strength of the substrate corrugation.

2.2 Two Dimensional Solids

The order parameter for a crystalline lattice is the thermal average of the Fourier transform of the density

$$\left\langle \hat{\rho}(\vec{G}) \right\rangle = \left\langle \frac{1}{N} \sum_{n=1}^{N} e^{i\vec{G}\cdot\vec{x}_n} \right\rangle \tag{2.1}$$

where the angle brackets represent thermodynamic averages, $\vec{G}$ is a reciprocal lattice vector of the triangular argon solid, and $\{x_n\}$ is the position of particle n. Let $\vec{x}_n = \vec{R}_n + \vec{u}_n$ where $\vec{R}_n$ is a lattice site. Then,

$$\left\langle \hat{\rho}(\vec{G}) \right\rangle = \frac{1}{N} \sum_{n=1}^{N} e^{i\vec{G}\cdot\vec{R}_n} \left\langle \exp\left(i\vec{G}\cdot\vec{u}_n\right) \right\rangle \tag{2.2}$$

For a harmonic solid

$$\left\langle \hat{\rho}(\vec{G}) \right\rangle = \frac{1}{N} \sum_{n=1}^{N} e^{i\vec{G}\cdot\vec{R}_n} \exp\left(-\frac{1}{2} \left\langle (\vec{G}\cdot\vec{u}_n)^2 \right\rangle \right) \tag{2.3}$$

The mean square vibrational amplitude reduces the value of the order parameter for the lattice.

In 1966, Mermin and Wagner[28] showed that thermal fluctuations destroy the long range translational order in an infinite two dimensional system with continuous symmetry for all temperatures greater than zero. The main points of the argument can be understood by looking at a two-dimensional Debye solid. The mean square deviation of a particle from its equilibrium position is

$$\left\langle u^2 \right\rangle = \int_{\omega_L}^{\omega_D} \frac{2\hbar}{m\omega} \left(\frac{1}{e^{\hbar\omega/k_B T} - 1} + \frac{1}{2} \right) \frac{\omega}{\omega_D^2} d\omega \tag{2.4}$$

where m is the mass of the argon atom, ω_D is the Debye frequency[29]. The lower limit ω_L is governed by the size of the system. We can set $\omega_L \approx v q_L$ where $q_L = \pi/L$

and L is the linear dimension of the argon solid. At low temperatures we can expand the exponential, thus

$$\langle u^2 \rangle \approx \frac{2\hbar}{m\omega_D^2} \int_{vq_L}^{vq_D} \frac{k_B T}{\hbar\omega} d\omega \approx \frac{2a^2 k_B T}{\pi^2 m v^2} \ln(L/a) \tag{2.5}$$

where a is the nearest neighbor distance and v is the velocity of sound in the solid. By letting $L \to \infty$ in equation 2.5, it can be seen that equation 2.3 is zero in the thermodynamic limit. But the two-dimensional solids are not infinitely large. Using reasonable values for T and v, the quantity $2k_B T/\pi^2 m v^2$ is on the order of 10^{-3}. Thus, for the deviations from equilibrium to be around 10% of the nearest neighbor distance, the argon solid would need to be approximately 10^{21} kilometers long, and the argon solid has to be very large for the order parameter for the crystal to be close to zero. Therefore, the order parameter for a two dimensional argon crystal would be zero for an infinite lattice. This also implies that while the positions of the atoms separated by a large distance are not correlated, the local environment of the argon atoms does not deviate much from a triangular lattice. The presence of the graphite substrate on the long-range translational order will be discussed later.

Using similar arguments as above, it can be shown that there is algebraic decay of the density-density correlation function[29, 30]

$$G_\rho(\vec{r}) = \left\langle \rho(\vec{r})\rho(\vec{0}) \right\rangle \sim |\vec{r}\,|^{-\eta(T)}. \tag{2.6}$$

An infinite two dimensional solid does have long range bond orientational order[31].

A useful order parameter for a triangular solid is

$$\psi_6(\vec{r}) = e^{6i\theta(\vec{r})} \tag{2.7}$$

where $\theta(\vec{r})$ is the orientation of the nearest neighbor bond angles with respect to an arbitrary axis. The correlation function of the orientational order parameter $G_\theta(\vec{r}) = \langle \psi_6^*(\vec{r})\psi_6(\vec{0})\rangle$ approaches a constant for large $|\vec{r}\,|$. A two dimensional solid is characterized by algebraic decay of the translational correlation function $G_\rho(\vec{r})$, and long-range order of the bond angle correlation function $G_\theta(\vec{r})$.

The two-dimensional solid phase would be expected to undergo a melting transition to an isotropic fluid phase characterized by exponential decay of translational correlations. The KTHNY theory predicts that a continuous melting transition of a two dimensional solid occurs in two steps[2]. The first step is a transition from a two-dimensional solid characterized by algebraic decay of $G_\rho(\vec{r})$ and long-range orientational order to a hexatic phase with exponential decay of $G_\rho(\vec{r})$ and algebraic decay of $G_\theta(\vec{r})$. The exponent of the algebraic decay of $G_\theta(\vec{r})$ in the hexatic fluid is between 1/3 and 1/4. The second step is another phase transition from the hexatic fluid to an isotropic fluid in which there is an exponential decay of $G_\rho(\vec{r})$ and $G_\theta(\vec{r})$. It is possible for there to be a first order solid to isotropic liquid phase transition within the framework of the KTHNY theory, if the transition from solid to hexatic fluid occurs at the same temperature as the transition from hexatic fluid to isotropic liquid[2].

While an ideal two-dimensional solid with continuous symmetry cannot have long

range translational order, it is possible that the substrate locks the argon solid into a commensurate structure with the substrate periodicity. The commensurate, or partially commensurate, structure only requires that a subset of the reciprocal lattice vectors of the argon lattice is equal to a subset of the reciprocal lattice vectors of the graphite substrate. It does not require all the reciprocal lattice vectors to be equal. The partially commensurate solid would have long range translational order since the graphite solid has long range translational order. Even if solid argon is not partially commensurate, reciprocal lattice vectors of the argon and graphite basal plane can still be very close, making it very difficult to determine if the system is partially commensurate or an oriented, floating solid. Also, the argon atoms are not restricted to motion in a two dimensional plane. Motion perpendicular to the graphite substrate is expected to be small, but may affect the 2D nature of argon absorbed on graphite.

Chapter 3

Simulation Details

Monte Carlo simulations were conducted using the Metropolis algorithm to study the melting of argon physisorbed on graphite. The simulations utilized accurate potentials so that quantitative comparisons could be made with experiment. This chapter will start with explaining the interactions used in these simulations. Also the specifics of how the specific heat, the lattice constant, the rotation angle, and the order parameters were calculated will be described.

3.1 Interaction Potentials

It is assumed that the potential energy of the system can be determined by a sum of the form

$$U = \sum_{i<j=1}^{N} U_{Ar-Ar}(|\vec{x}_i - \vec{x}_j|) + \sum_{i<j=1}^{N} V_{SM}(\vec{x}_i, \vec{x}_j) + \sum_{i=1}^{N} V_{Ar-Gr}(\vec{x}_i) \qquad (3.1)$$

where U_{Ar-Ar} is the argon-argon two body potential, V_{Ar-Gr} is the argon-graphite potential, and V_{SM} is the substrate mediated interaction. In equation 3.1, N is the number of argon atoms and $\vec{x}_i$ is the position of the ith atom. The substrate-mediated interaction depends on the separation of the atoms as well as the height of the atoms above the substrate.

There are many good argon-argon potentials that have been proposed. A HFD-B form of the potential by Aziz and Chen[32] and modified by Aziz and Slamen[33], was chosen for its ability to accurately predict second virial coefficients, thermal conductivity, and thermal diffusion data of bulk argon. The energy of two argon atoms separated by a distance r is given in equation 3.2, and plotted in figure 3.1.

$$\begin{aligned} U_{Ar-Ar}(r) &= \epsilon\left[A\exp\left(-\alpha r+\beta r^2\right)-f(r_{ij})\left(\frac{C_6}{(\frac{r}{R_m})^6}+\frac{C_8}{(\frac{r}{R_m})^8}+\frac{C_{10}}{(\frac{r}{R_m})^{10}}\right)\right] \\ &\text{where} \\ f(r) &= \begin{cases} 1 & \text{if } \frac{r}{R_m} > D \\ \exp\left(-(\frac{DR_m}{r}-1)^2\right) & \text{if } \frac{r}{R_m} < D \end{cases} \end{aligned} \tag{3.2}$$

An anisotropic Lennard-Jones potential of Carlos and Cole[34], given in equation 3.3, was chosen for the argon-graphite interaction.

$$\begin{aligned} U_{Ar-Gr} = \sum_{i=1}^{N}\sum_{j=1}^{M} 4\epsilon\Bigg(&\left(\frac{\sigma}{r_{ij}}\right)^{12}\left[1+\gamma_R(1-\frac{6}{5}\cos^2\theta)\right] \\ &-\left(\frac{\sigma}{r_{ij}}\right)^{6}\left[1+\gamma_A(1-\frac{3}{2}\cos^2\theta)\right]\Bigg) \end{aligned} \tag{3.3}$$

The angle θ is the angle between the vector $\vec{r}_{ij}$ which connects an argon atom i with a carbon atom j to the surface normal. N is the number of argon atoms and M is

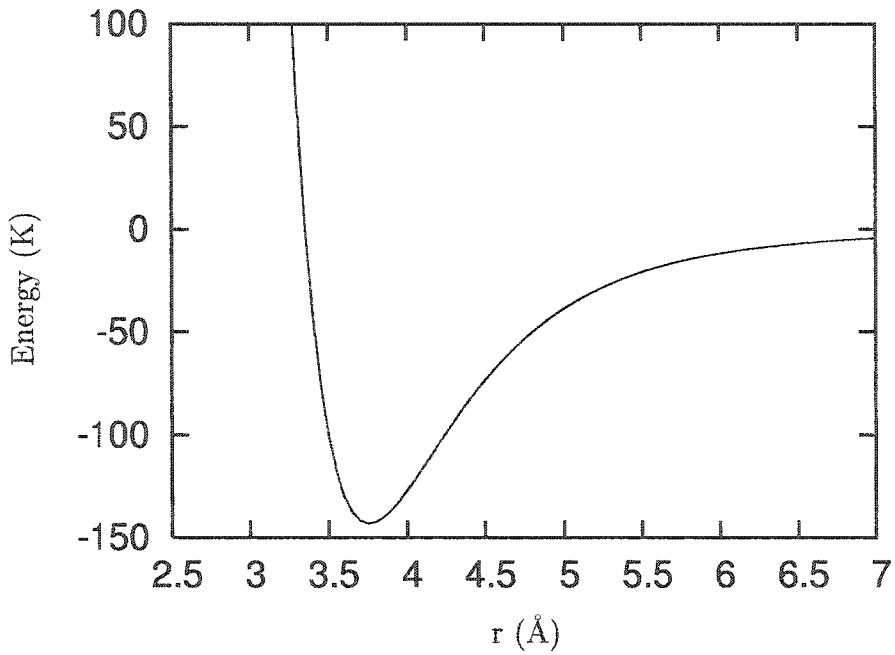

Figure 3.1: Argon-argon interaction potential.

the number of carbon atoms. The parameter γ_A is associated with the anisotropy of the attractive part, and γ_R is associated with the anisotropy of the repulsive part. The angular dependence is due to the directional dependence of the polarizability of the carbon atoms in the graphite substrate.

The argon-graphite potential was Fourier transformed with respect to the reciprocal lattice vectors of the graphite substrate. Representing an adatom-substrate potential in terms of a Fourier transform with respect to the reciprocal lattice vectors of the substrate was developed by Steele[35]. This results in the argon-graphite potential taking the form

$$V_{Ar-Gr} = E_0(z) + \sum_{n=1}^{\infty} E_n(x, y, z) \tag{3.4}$$

where z is the direction perpendicular to the substrate, and the xy plane is parallel to

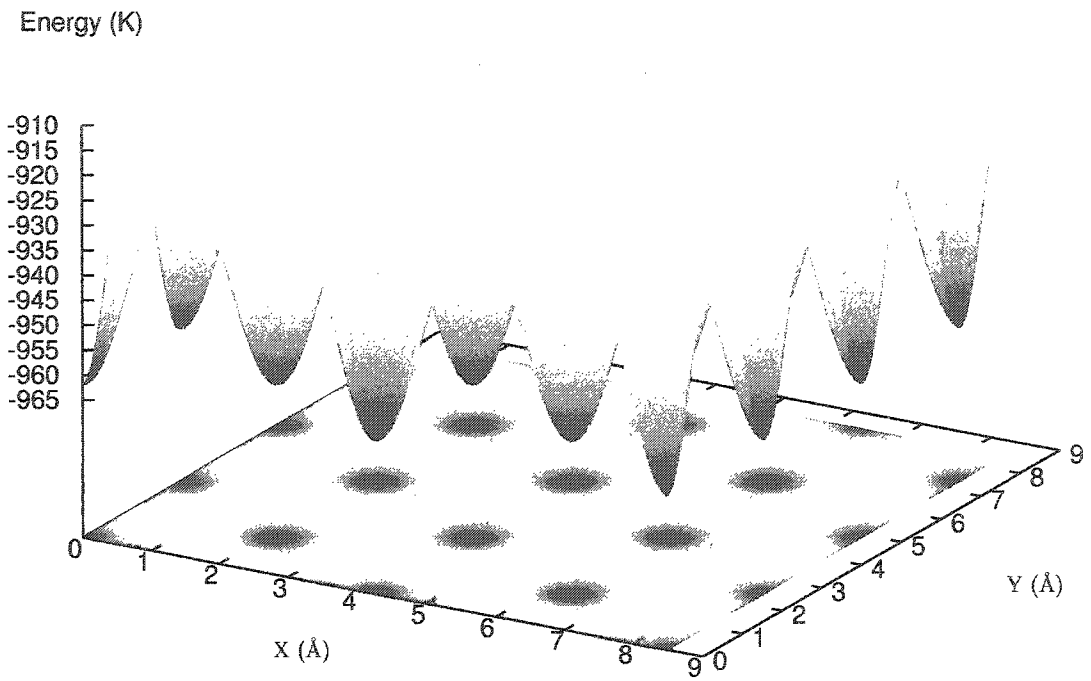

Figure 3.2: Argon-Graphite potential. The peaks of the potential are above the carbon atoms, and the minima are above the center of the graphite hexagons.

the substrate. Only the E_0 and the E_1 terms are kept for the Monte Carlo simulation. All higher order terms contribute less than 1% corrugation energy. A plot of the argon-substrate potential is shown in figure 3.2.

The substrate mediated interaction, given in equation 3.5, is due to induced image charges in the graphite substrate.

$$V_{SM} = C_{S1}\left(\frac{2+3\cos(2\phi)+3\cos(2\theta)}{6(r_{ij}r'_{ij})^3}\right) - C_{S2}\left(\frac{1}{(r'_{ij})^6}\right) \tag{3.5}$$

The angles and distances in the substrate mediated potential are shown in figure 3.3.

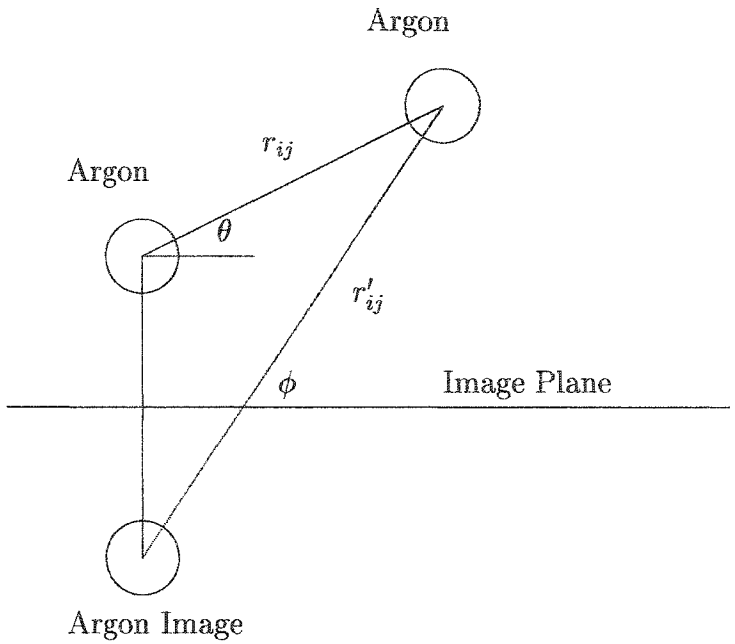

Figure 3.3: The distances and angles for the substrate mediated interaction. The image plane is 1.6785 Å above the center of the carbon atoms.

The distance r'_{ij} is the distance between an argon atom j and the image of argon atom i. The position of the image of an argon atom is defined with respect to an image plane. The distance from the center of the carbon atoms to the image plane is equal to one half the distance between graphite basal planes. The substrate mediated interaction is repulsive if atoms are in the same layer, but attractive if particles are in different layers. It was determined that three body interactions are less than 3% of the dispersion energy, and thus they were ignored. The parameters for the potentials are listed in Table 3.1.

The potential chosen for the calculation is the most accurate available, but the

Table 3.1: Potential Parameters

Potential Parameters		
Argon	A	226210.71
Argon	α	10.778874743
Potential	β	-1.8122004 1/Å
	C_6	1.10785163
	C_8	0.56072459
	C_{10}	0.34602794
	D	1.36 Å
	ϵ	143.224 K
	R_m	3.7565 Å
Substrate	C_{S1}	175123.81 KÅ^6
Mediated	C_{S2}	103777.07 KÅ^6
Argon	ϵ	49.13 K
Graphite	σ	3.4 Å
Potential	γ_R	-0.54
	γ_A	0.4

uncertainty in the substrate mediated and the argon graphite potential is around 25%[36]. The anisotropic argon-carbon potential produced a well depth of approximately 1.5 times the value of Lennard-Jones potential. While the well depth of the argon-graphite system has never been probed directly, the well depth of the other rare gas-graphite systems have been examined[37]. The results indicate that the anisotropic Lennard-Jones potential may produce a well depth that is too large, and the standard Lennard-Jones potential produces a well depth that is too small.

The Argon-Argon potential parameters listed in table 3.1 are taken directly from the papers of Aziz and Slamen[33] and Aziz and Chen[32]. The parameters for the substrate mediated and the argon-graphite potentials were changed slightly from the values in the literature. In previous work of Flenner and Etters[38], the substrate mediated parameters were obtained from Bruch[39], and the (ϵ, σ) parameters for the argon-substrate potential was from Steele[35]. In the previous work, the calculated specific heat was similar to the experimental results of Migone. Specifically, there were two peaks in the calculated specific heat, a broad peak at around 49.5K and a narrow peak around 43.7K. The height and the width of both of the peaks were similar to the height and width of the peaks observed in the experiments of Migone's. The main difference is that the two peaks in the specific heat in Migone's experiments were separated by 2.2K, while the two calculated specific heat peaks were separated by 5.8K. There was concern that the proximity of the phase transitions occurring at the two peaks could influence the results. The details of those phase

transitions can be found in the previous work[38], and they are very similar to the phase transitions reported in this work. The broad peak was associated with melting of the two-dimensional solid, and the narrow peak signaled a rotational transition. To provide better agreement with experiment, and to determine if the proximity of the phase transitions influenced the results, C_{S1}, C_{S2} in the substrate mediated potential, and the ϵ parameter in the argon-graphite potential were adjusted in several sets of simulations.

Changing the strength of the parameters in the potentials influenced the temperature in which the phase transitions occurred. If the substrate mediated interaction was removed, melting occurred around 54K instead of 49K, and there was no rotational transition, i.e. the argon solid was rotated for all temperatures below melting. If the substrate mediated interaction was increased by 25%, then there was a decrease of 1.5K in the melting temperature and the rotational transition occurred between 44K and 45K. If the argon-substrate interaction was decreased by 25%, then the rotational transition occurred at some temperature between 46K and 47K, and melting occurred between 49K and 50K. If the argon-substrate interaction was increased by 25%, then the rotational transition occurred somewhere between 35K and 40K, and melting occurred between 49K and 50K. A summary of how the changes in the potential parameters affected the transition temperatures is given in table 3.1. A simulation was performed where the substrate mediated interaction and the argon-substrate interaction were both reduced by 15%, and the rotational transition occurred at 47.3K,

ϵ	C_{S1}	C_{S2}	T_m	T_R
72.25 K	206028.009 KÅ^6	122090.672 KÅ^6	49K-50K	35K-40K
49.13 K	206028.009 KÅ^6	122090.672 KÅ^6	49K-50K	46K-47K
57.8 K	0 KÅ^6	0 KÅ^6	53K-55K	
57.8 K	257535 KÅ^6	152613 KÅ^6	47K-49K	44K-45K

Table 3.2: Changes in melting temperature (T_m) and the rotational transition temperature (T_R) when the potential was varied. The ϵ parameter controls the strength of the argon-substrate interaction.

and the melting temperature was between 49K and 50K. These values of the phase transitions are very close to the experimental values, and the potential parameters were fixed at those values for the rest of the simulations. The potential parameters in table 3.1 represents the 15% decrease in the strength of the argon-graphite interaction and the substrate mediated interaction.

3.2 Calculated Quantities

A large canonical ensemble Monte Carlo simulation was conducted. Periodic boundary conditions were used. The Monte Carlo simulations in this work utilized the well known Metropolis algorithm, which is described in many books[40]. To understand the behavior of the system, many different quantities were calculated. Care was taken to be sure that thermodynamic equilibrium was reached, and equilibrium averages were calculated. Various indicators were used to determine if the system

was in thermodynamic equilibrium. A running average of the energy, and the energy per 100 steps were examined. One step represents one attempted Monte Carlo move per particle. The simulations were run until the energy appeared to be fluctuating around an average value and not drifting up or down. Also, the specific heat was examined versus the number of steps used in the calculation. Since the specific heat is calculated using the fluctuations in the energy, see equation 3.6 below, it is sensitive to small changes in the system. A small change in the system can result in large and unexpected changes in the calculated specific heat.

For densities of $\rho = 1.00, 1.07, 1.14, 1.22$, and 1.31 the simulations can be divided into two categories, a heating set of simulations and a cooling set of simulations. Around the phase transitions all the odd temperature runs were begun from the last configuration of a simulation two degrees lower, and the even temperature simulations were started from the last configuration of temperature two degrees higher. The simulations were run until the results were consistant, and there was no evidence of hysteresis. Several runs were also conducted at various temperatures with various initial conditions to make sure that equilibrium values were determined. Also, simulations were conducted with varying number of particles in the simulation cell to determine if there were notable size effects. All the size effects, and any observations of hysteresis will be discussed in the results.

Because of the excellent experimental specific heat data, the specific heat provides an important link between these simulations and experimental results. The specific

heat per absorbed atom was calculated using energy fluctuations by

$$C_V = \frac{\langle E^2 \rangle - \langle E \rangle^2}{N k_B T^2} \tag{3.6}$$

The brackets indicate thermal averages, E is the internal energy, N is the number of argon atoms, and T is the temperature.

The lattice constants can be calculated by Fourier transforming the pair distribution function $g(\vec{x})$, the probability density that a particle is at $\vec{x}$ given that a particle is at $\vec{x} = \vec{0}$.

$$\hat{g}(\vec{q}) = \int g(\vec{x}) e^{i\vec{q}\cdot\vec{x}} d\vec{x} \tag{3.7}$$

For a triangular solid in which the x axis is along an average nearest neighbor bond, there are peaks in $\hat{g}(\vec{q})$ at the reciprocal lattice vectors of the triangular argon solid. The pair distribution function was calculated with the x axis of the coordinate system along a $\sqrt{3} \times \sqrt{3}$ symmetry direction, thus the positions of the peaks in $\hat{g}(\vec{q})$ are also rotated from the values given above depending on the rotation angle of the argon solid. In practice, only the peak at $\vec{q} = (0, \frac{4\pi}{a\sqrt{3}})$ was calculated, then the lattice constant is given by $a = 4\pi/|\vec{q}\,|\sqrt{3}$.

The above strategy worked well if the argon solid was only rotated in one direction with respect to the substrate throughout the simulation. If the rotation angle changed throughout the calculation, then $\hat{g}(\vec{q})$ might have two or more closely spaced peaks. For example, there might be a peak corresponding to a rotation of $-\Theta$ and Θ. The two overlapping peaks can cause the apparent peak position to be at a different rotation angle and correspond to a different lattice constant that would be calculated from

either one of the two peaks. The change in the lattice constant is small, but the change in rotation angle can be significant. The lattice constant can also be found by integrating over the angle in equation 3.7, i.e.

$$\begin{aligned} \int g(\vec{x}) e^{i\vec{q}\cdot\vec{x}} d\vec{x} &= \int g(r) e^{iqr\cos\theta} r dr d\theta \\ &= \int g(r) J_0(qr) 2\pi r dr \end{aligned} \tag{3.8}$$

where $J_0(qr)$ is the Bessel function of order 0 and $g(r)$ is the radial pair distribution function. The radial distribution function is proportional to the probability that an argon atom is a distance r away from an atom at $r = 0$. Comparison was made between the lattice constants calculated using 3.7 and 3.8 when the solid argon was rotated at one direction with respect to the substrate for the densities of 0.71 and 0.39. In every case the lattice constant agreed to within the accuracy of the calculation. The uncertainty was 0.002Å, which is around 0.05% of the lattice constant. Since equation 3.7 and equation 3.8 produced the same value of the lattice constant, and using equation 3.8 is around 10 times faster, equation 3.8 was used to calculate the lattice constant for all densities.

The lattice constant for $\rho = 0.71$ was also calculated by finding the first moment of the first peak of the radial pair distribution function. It is difficult to determine where the first peak ends and the second peak begins since $g(r)$ does not go to zero between the two peaks. The integral over the first peak in the radial pair distribution

function resulted in a lattice constant that was around 0.02Å larger than using the equation 3.8, an increase of about 0.5% versus using equation 3.8.

The rotation angle proved to be difficult to calculate accurately. The bond angles fluctuate around the rotation angle, but the average bond angle should give the rotation angle for a large enough system. Since a rotation of the whole system from $+\theta$ to $-\theta$ corresponds to the same state, then it is expected to see the system at a $+\theta$ and $-\theta$ rotation angle throughout the simulation. This is not always observed for a simulation with a finite number of steps. There is an energy barrier that must be crossed to go from $+\theta$ to $-\theta$, and the system may stay within the local minimum at $+\theta$ or $-\theta$ for a long time before crossing the energy barrier. As the temperature is increased, there is an increased chance of crossing the energy barrier between the two states.

To calculate the rotation angle, the angle each bond makes from a $\sqrt{3} \times \sqrt{3}$ symmetry axis of the substrate was found. Then the average bond angle for one configuration was calculated, and a probability distribution of the average bond angles was constructed. From this distribution, the rotation angle was determined from the peak position of a gaussian fit to the dominant peak of the probability distribution. The periodic boundary conditions can influence the rotation of the argon solid for a small MC cell. Simulations were conducted with no substrate corrugation to determine the effects of the periodic boundary conditions. A solid was determined to be rotated if its behavior was different than the simulations with no substrate cor-

rugation. Specifically, if the value of the rotation angle did not depend on initial conditions, and if there was only one peak around Θ or two peaks around $\pm\Theta$.

Simulations with different numbers of particles were performed to make sure that the calculated rotation angle and lattice constant was accurate. A series simulations at $\rho \approx 0.7$ and T = 35K were conducted with 144, 256, 289, 324, 400, 529, 625, and 1024 particles in the Monte Carlo cell. It was found that for simulations with 256 or more particles in the simulation cell, the value of the rotation angle varied between 2.4° and 2.95° at 35K, but the system was always rotated and the rotation angle did not depend on the initial conditions for a fixed number of particles. The effect of changing the number of particles in the system on the lattice constant will be discussed in the results.

To look at melting the order parameter Ψ_6 was calculated

$$\Psi_6 = \frac{1}{N_B}\left\langle \sum_{i,j=1}^{N} \exp\left(6i\theta_{ij}\right)\right\rangle \tag{3.9}$$

The sum over j is over all nearest neighbors of i, and θ_{ij} is the angle the nearest neighbor bonds make with an arbitrary axis. The factor N_B is the number of bonds used in the calculation. The order parameter is one for a perfect triangular lattice, and zero for an isotropic fluid. Since the susceptibility of the order parameter should peak at the melting transition, we also look at the susceptibility of Ψ_6,

$$\chi_6 = \frac{\langle \Psi_6^2 \rangle - \langle \Psi_6 \rangle^2}{T} \tag{3.10}$$

The fourth order reduced cumulant of the rotation angle of the system was also examined. The fourth order reduced cumulant is given below, and was calculated by

using the probability distribution of the rotational angle described above.

$$C_4 = 1 - \frac{\langle \Theta^4 \rangle}{3 \langle \Theta^2 \rangle^2} \tag{3.11}$$

The reduced cumulant gives information about the shape and position of a probability distribution. If the probability distribution is a delta function, or if it is a gaussian an infinite distance away from zero, then it is 2/3. The second possibility is impossible in this case since the rotation angle is bounded between -30 degrees and 30 degrees. If the probability distribution is a gaussian centered at zero, then it is zero. For a low temperature rotated state the probability distribution of rotation angles should be a gaussian centered around Θ or $\pm\Theta$, thus we expect C_4 to be around 2/3. For a state in which the argon solid is aligned with the substrate, C_4 should be zero. Also, if Θ is the order parameter for a continuous phase transition, C_4 takes on a specific value at the critical point that depends on the universality class of the transition[41].

The fourth order reduced cumulant can also provide insight into the order of the phase transition[41, 42, 43]. Around a first order phase transition, phase coexistence is often observed. This results in more than one peak in the probability distributions of the order parameter and the energy. The relative heights of the peaks depends on the size of the system and the proximity of the phase transition. This typically causes the reduced cumulant of the order parameter to take on values that differ from the high temperature limit, the low temperature limit, or any value which would be obtained at the critical point. Commonly, the reduced cumulant will be negative

at temperatures right above a first order phase transition because of the low, but nonzero probability of finding the system in the low temperature state.

Chapter 4

Results

A series of Monte Carlo simulations were performed as described in Chapter 3. The densities studied were $\rho = 0.71, 1.00, 1.07, 1.14, 1.22$, and 1.31 with 256 particles in the simulation cell, and $\rho = 0.39$ with 625 particles in the simulation cell. The densities are given in units of $\rho_0 = 0.0636$ atoms/Å^2, which is the density of the $\sqrt{3} \times \sqrt{3}$ structure. Densities were chosen so that the simulation cell was a unit multiple of the substrate unit cell. The results are divided into five sections. The first section describes the calculated specific heat, and compares the results to experiment. The next two sections describe the observed phase transitions. The fourth section describes second layer promotion, which is an important part of the melting of complete monolayers. The last section is composed of plots of the different energy terms as a function of temperature for all the densities studied.

4.1 Specific Heat

A comparison of the calculated specific heat for all densities are shown in figure 4.1. For densities of $\rho = 1.00, 0.71$, and 0.39, there is a sharp specific heat peak of width 0.3 C/Nk_B centered around 47.4K, and a broad peak centered around 50K, figures 4.4, 4.3, and 4.2. The sharp peak is shown in figures 4.9, 4.10, and 4.11 for the densities of 0.39, 0.71, and 1.00 respectively. There appears to be a shoulder for $\rho = 0.39$ at 54K, which we identify as being associated with the liquid vapor transition. For $\rho = 1.07$, there is only one specific heat peak at 49K, figure 4.5. For densities greater than $\rho = 1.07$, the peak position shifts to higher temperatures for higher densities, figures 4.6, 4.7, and 4.8. Also, the full width at half maximum (FWHM) of the peak decreases for $\rho = 1.31$. The FWHM is around 10K for $\rho = 1.22$ and 3K for $\rho = 1.31$. The simulations were run for at least 12 million Monte Carlo steps around the specific heat peaks, with the last 4 million Monte Carlo steps used for equilibrium averages. Around the narrow specific heat peak, the simulations were run for 20 million Monte Carlo steps, and the last six to eight million Monte Carlo steps were used for equilibrium averages. The uncertainty in the specific heat is less than or equal to ± 0.5 C/Nk_B, and is the greatest around the peaks. Table 4.1 lists the position of all the specific heat peaks. The narrow peak is associated with a rotational transition, and the broad peak is associated with melting, as will be discussed in sections 4.3 and 4.2 respectively.

Another feature of the specific heat is that the peak height at the broad specific

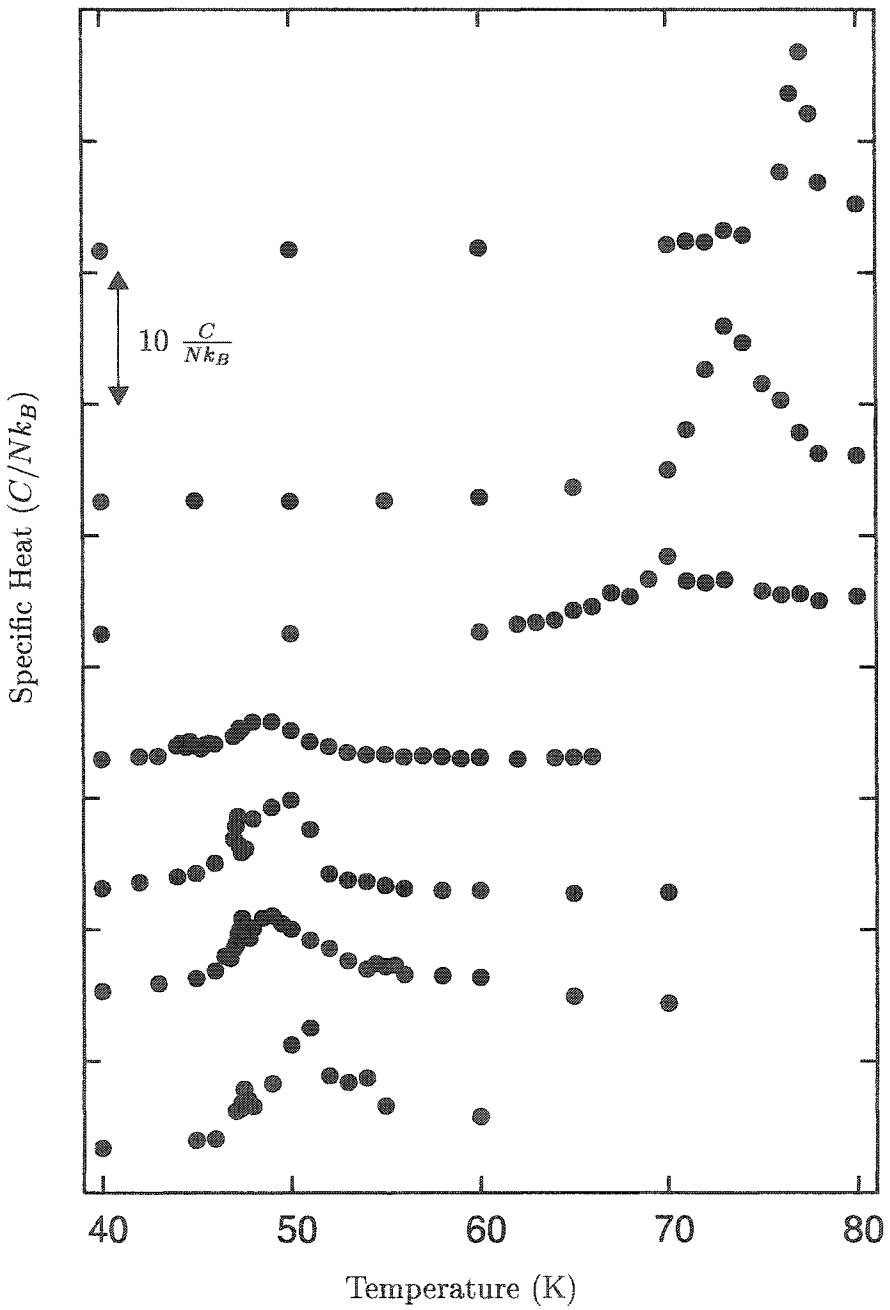

Figure 4.1: Specific heat for $\rho = 0.39, 0.71, 1.00, 1.07, 1.14, 1.22$ and 1.31 listed from the bottom to top.

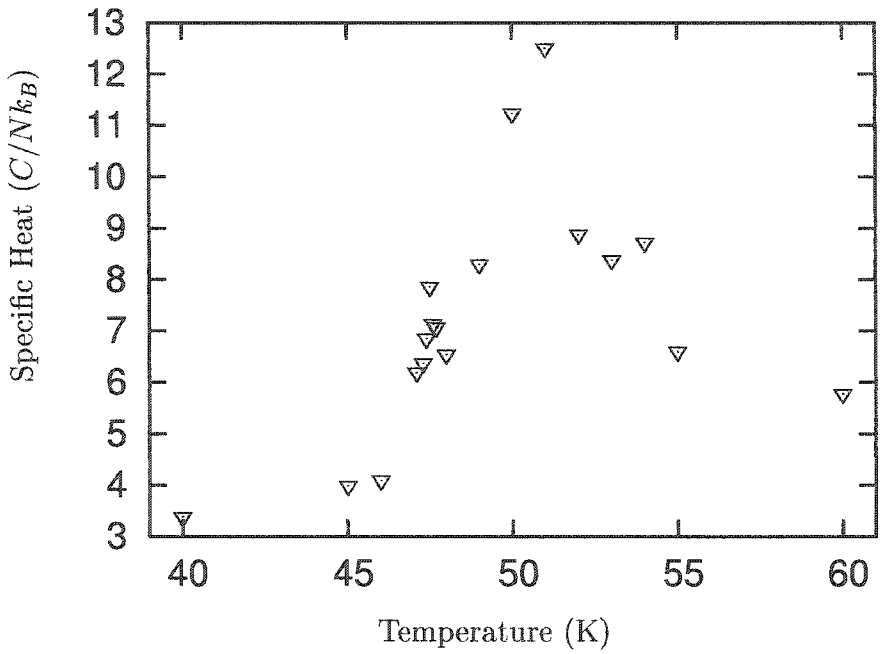

Figure 4.2: Specific heat for $\rho = 0.39$.

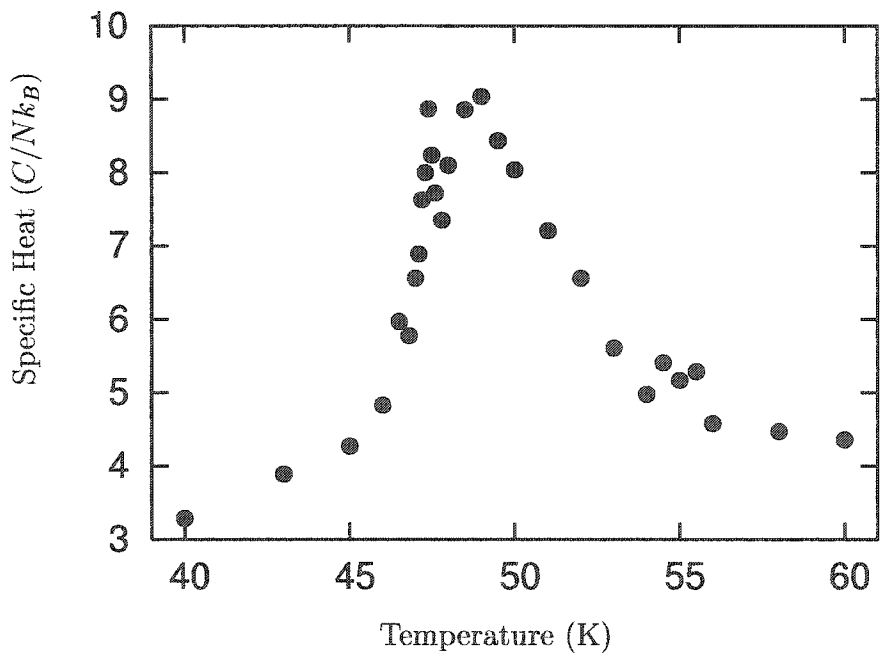

Figure 4.3: Specific heat for $\rho = 0.71$.

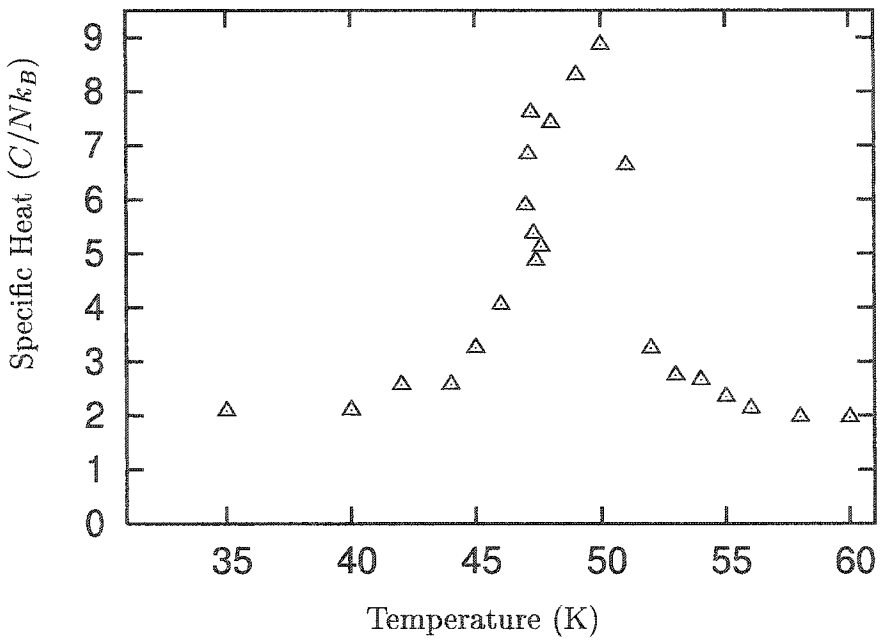

Figure 4.4: Specific heat for $\rho = 1.00$.

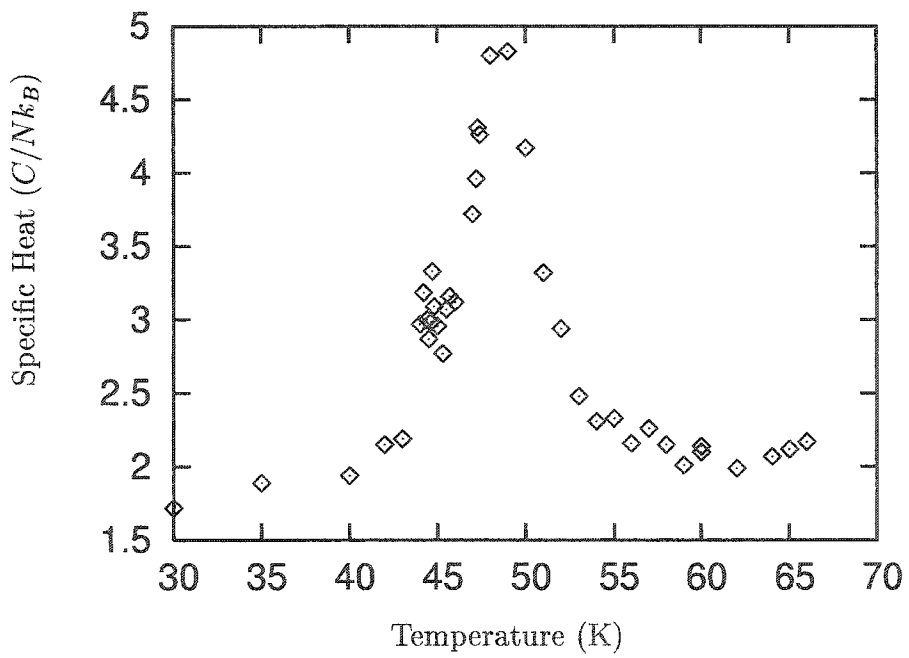

Figure 4.5: Specific heat for $\rho = 1.07$.

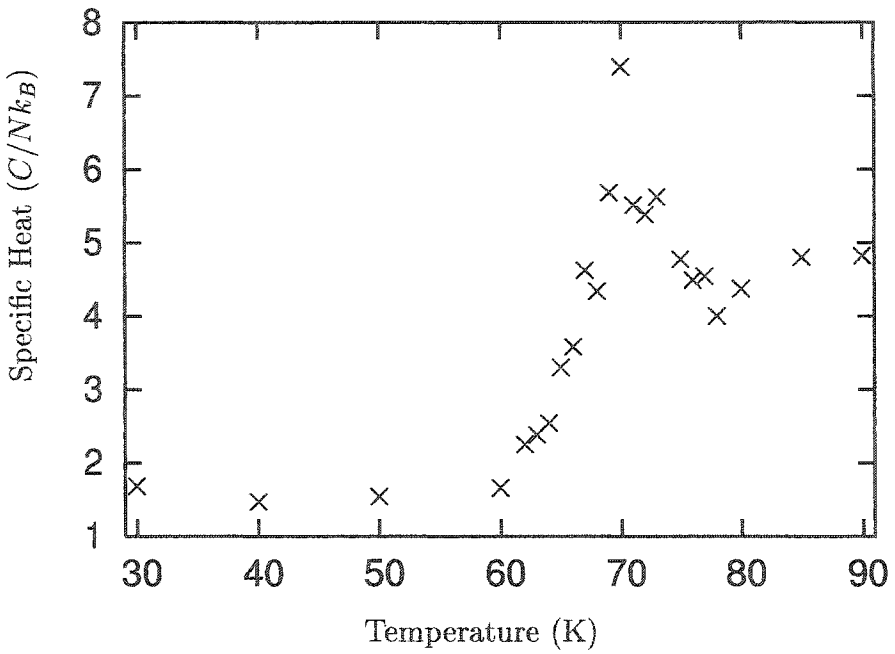

Figure 4.6: Specific heat for $\rho = 1.14$.

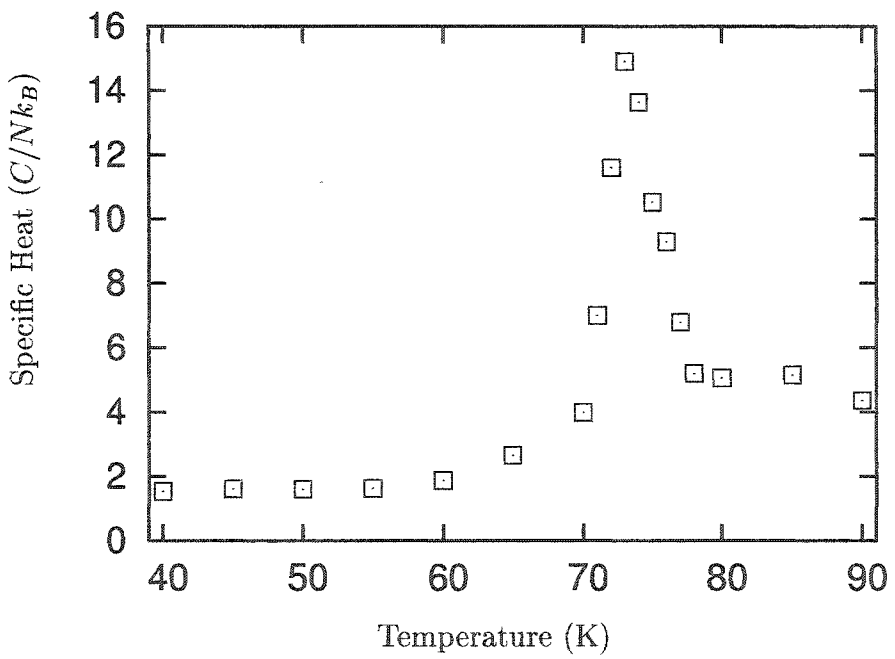

Figure 4.7: Specific heat for $\rho = 1.22$.

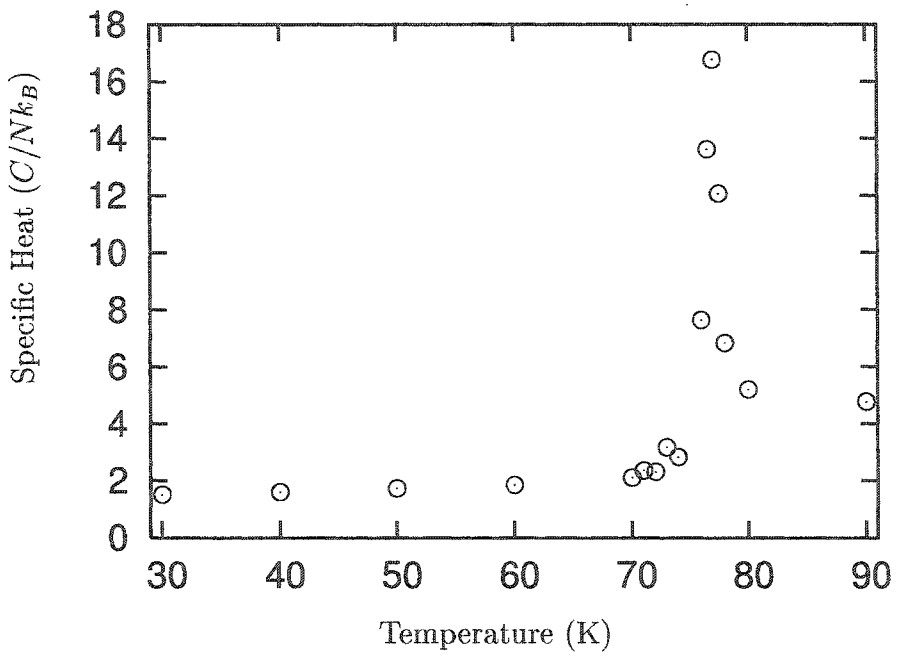

Figure 4.8: Specific heat for $\rho = 1.31$.

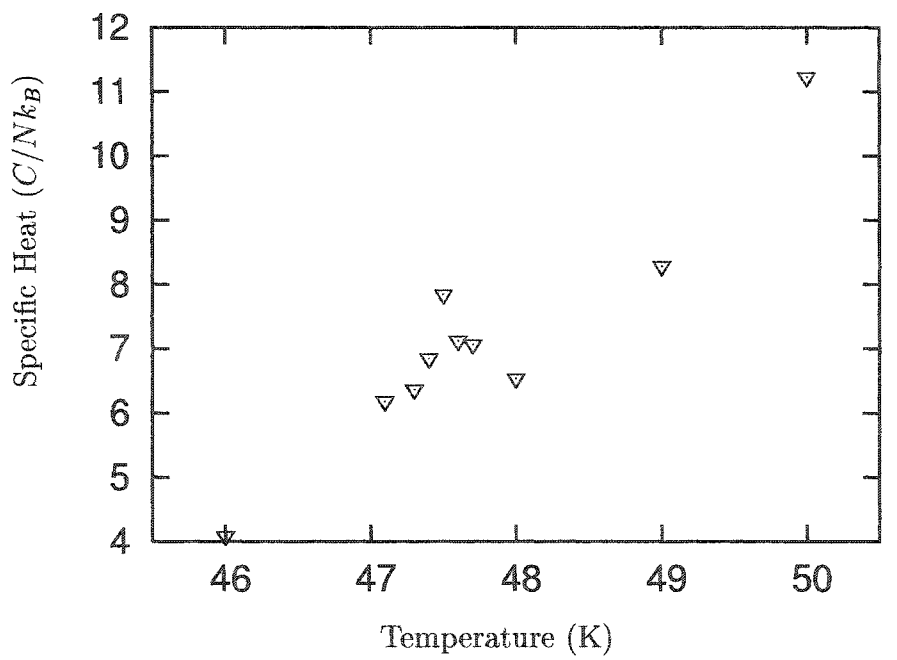

Figure 4.9: Specific heat for $\rho = 0.39$ around the narrow peak.

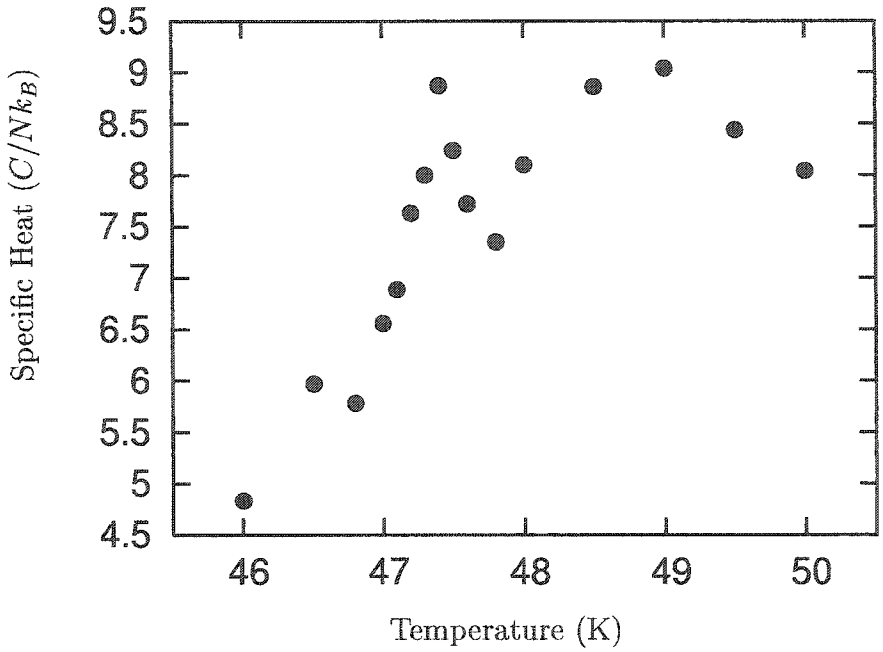

Figure 4.10: Specific heat for $\rho = 0.71$ around the narrow peak.

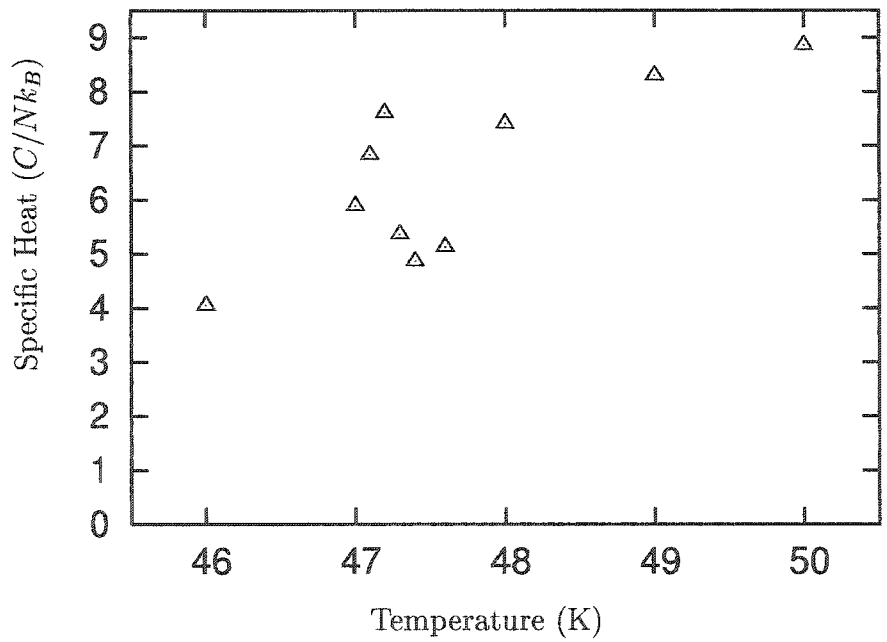

Figure 4.11: Specific heat for $\rho = 1.00$ around the narrow peak.

ρ	Narrow Peak	Broad Peak
0.39	47.5K	51K
0.71	47.4K	49K
1.00	47.2K	50K
1.07		49K
1.14		70K
1.22		73K
1.31		77K

Table 4.1: The peak position of the specific heat.

heat peak changes with density. The density dependence of the specific heat peak height at melting is compared to the experimental results of Migone in figure 4.12, and table 4.2 lists the peak height for these results. It can be seen that around $\rho \sim 1.00$, the peak height decreases until $\rho \sim 1.14$ where it reaches a minimum, and then starts to increase again. The density in which the peak height decreases corresponds to the same density in which the peak position shifts to higher temperatures. The calculated values for the specific heat peak height are around $9Nk_B$ for densities below $\rho = 1.00$, and are close to the $11Nk_B$ value obtained by Migone. The values for $\rho > 1.00$ are in excellent agreement with the values of Migone. Moreover, the behavior versus density is the same.

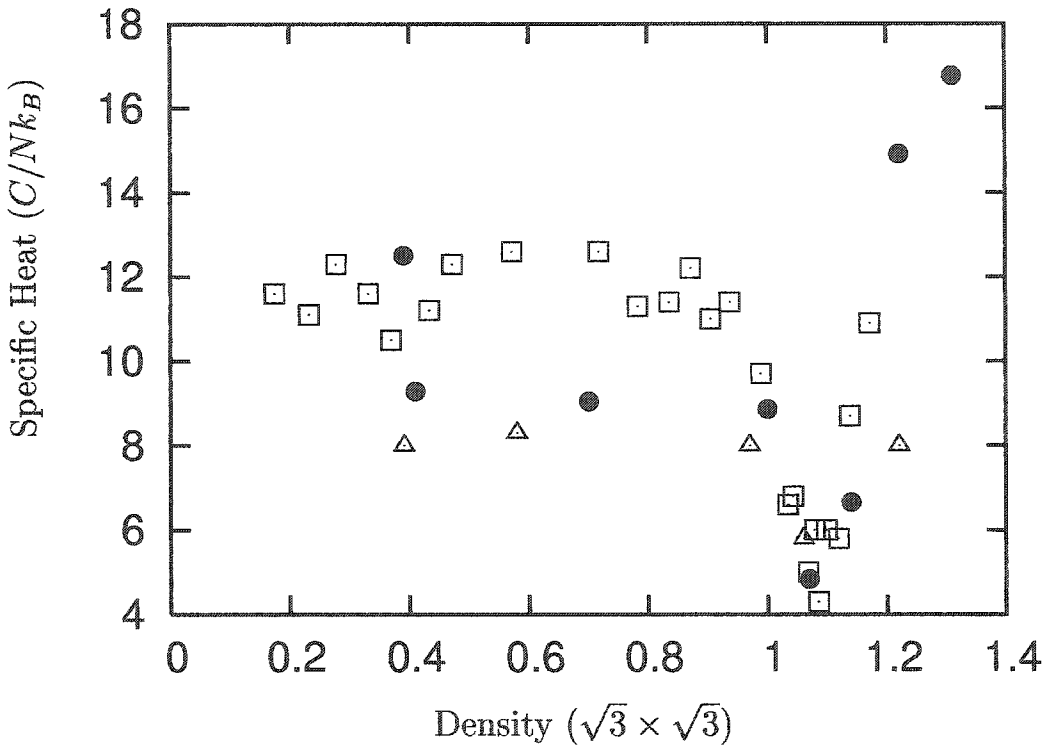

Figure 4.12: Specific heat peak height versus density for these simulations (•) compared to the experimental results of Migone (□) and Chung (△). The calculation was performed with 625 particles at $\rho = 0.39$, the lowest density, and 256 particles for the other densities.

ρ	Peak Height
0.39	12.51
0.41	9.28
0.71	9.04
1.00	8.89
1.07	3.97
1.14	6.66
1.22	14.91
1.31	16.77

Table 4.2: Specific heat peak height for the densities studied in these simulations. All the simulations were conducted with 256 particles except for $\rho = 0.39$, which was conducted with 625 particles.

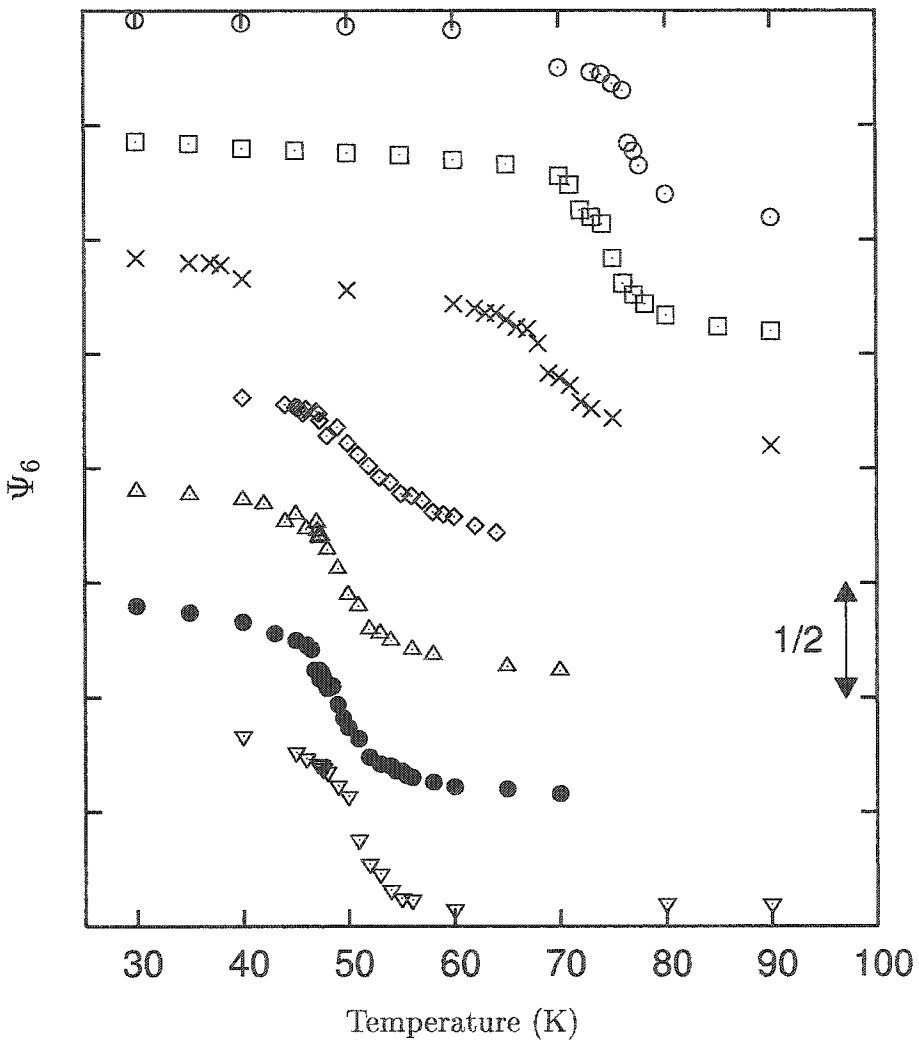

Figure 4.13: Order Parameter Ψ_6 for $\rho = 0.39$ (∇), 0.71 ($\bullet$), 1.00 ($\triangle$), 1.07 ($\Diamond$), 1.14 ($\times$), 1.22 ($\square$) and 1.31 ($\circ$).

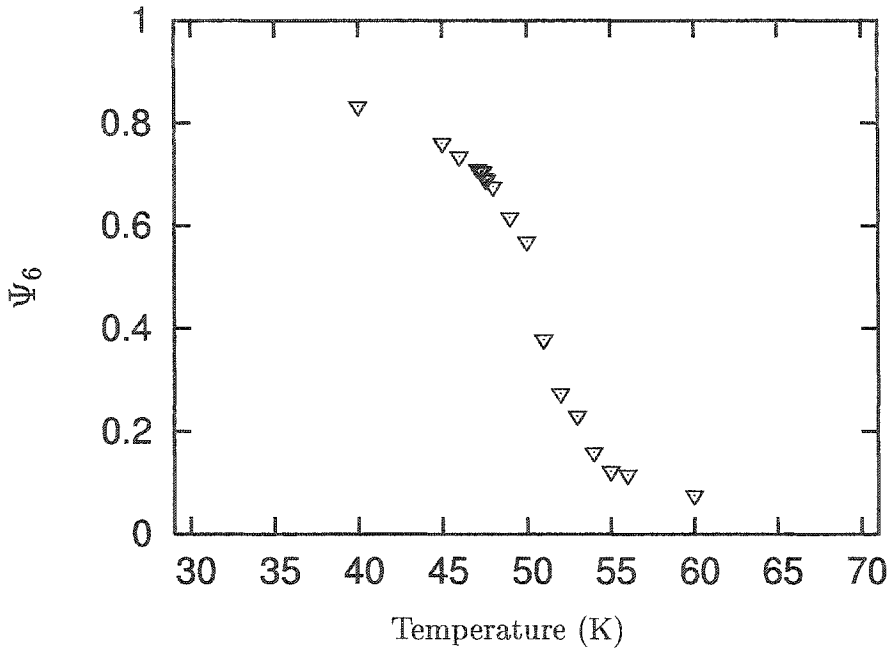

Figure 4.14: Ψ_6 for $\rho = 0.39$.

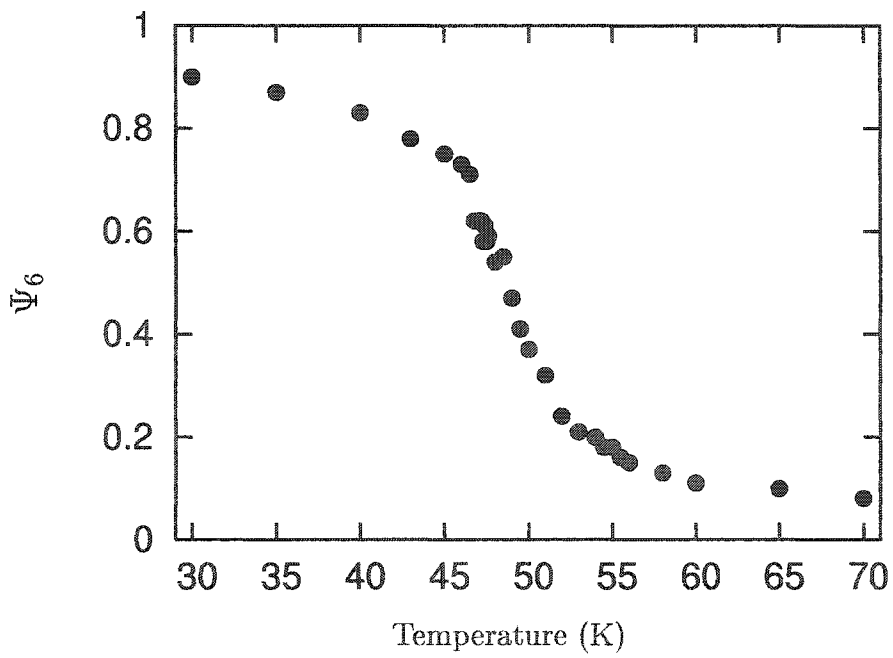

Figure 4.15: Ψ_6 for $\rho = 0.71$.

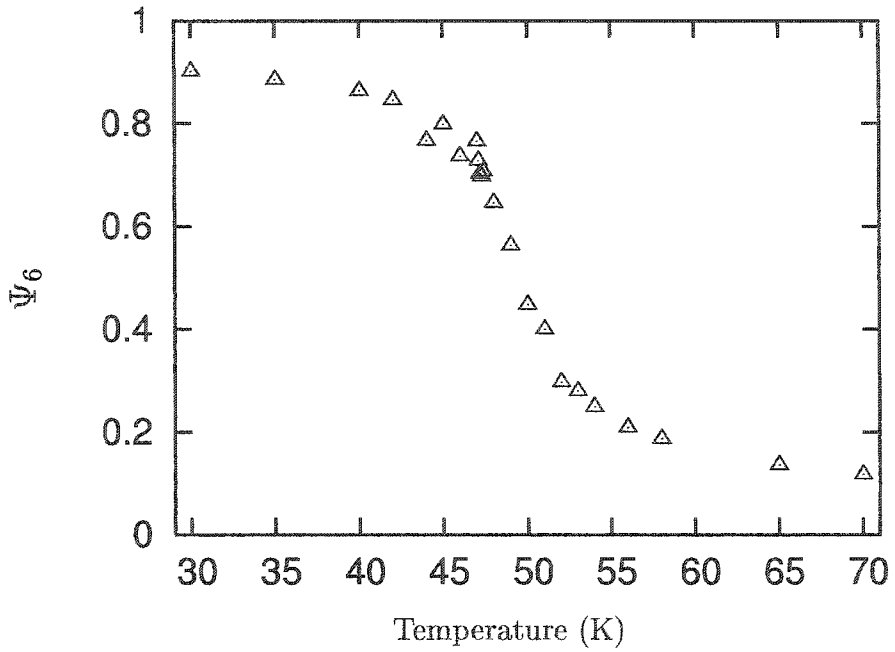

Figure 4.16: Ψ_6 for $\rho = 1.00$.

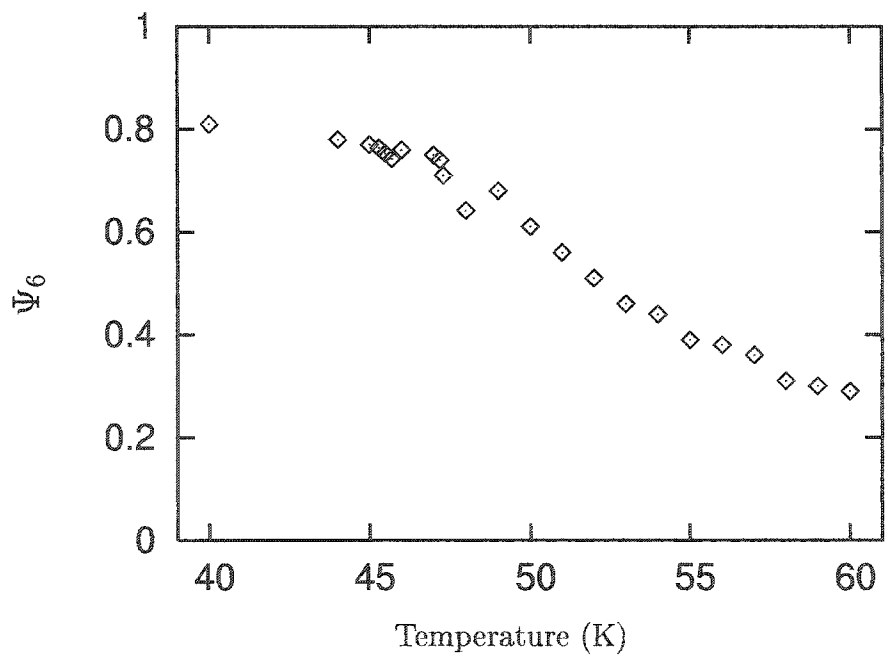

Figure 4.17: Ψ_6 for $\rho = 1.07$.

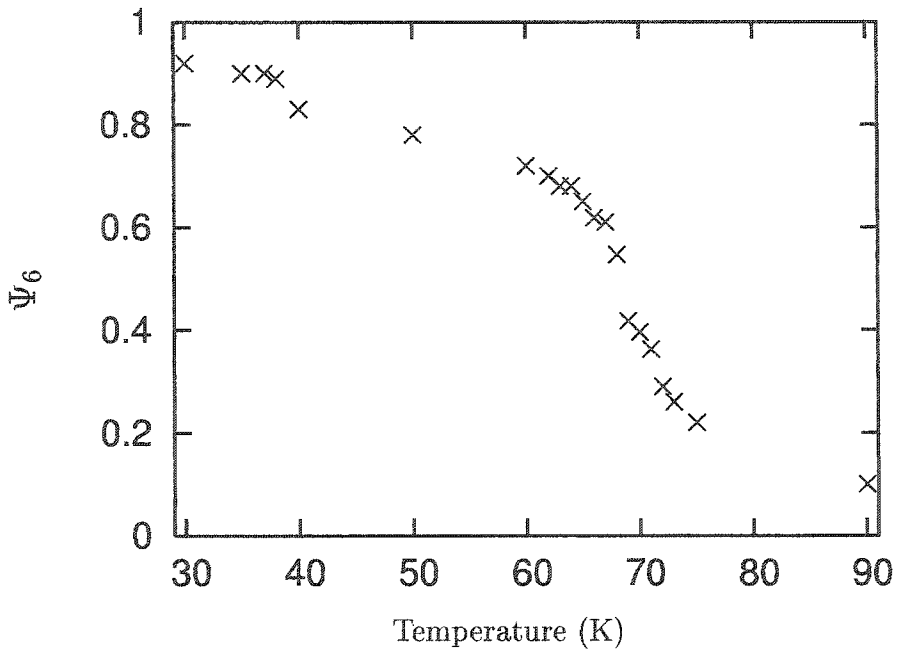

Figure 4.18: Ψ_6 for $\rho = 1.14$.

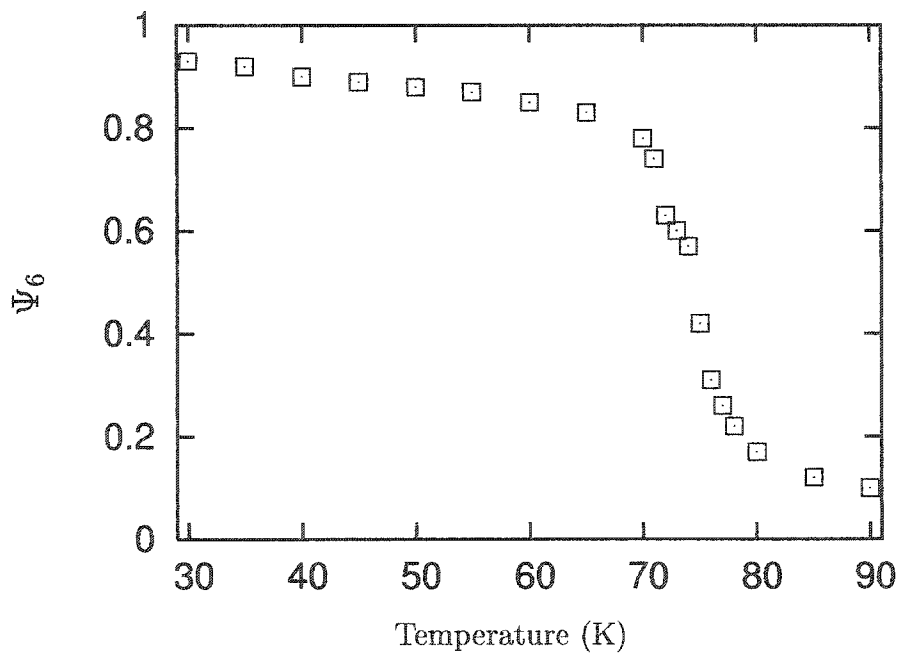

Figure 4.19: Ψ_6 for $\rho = 1.22$.

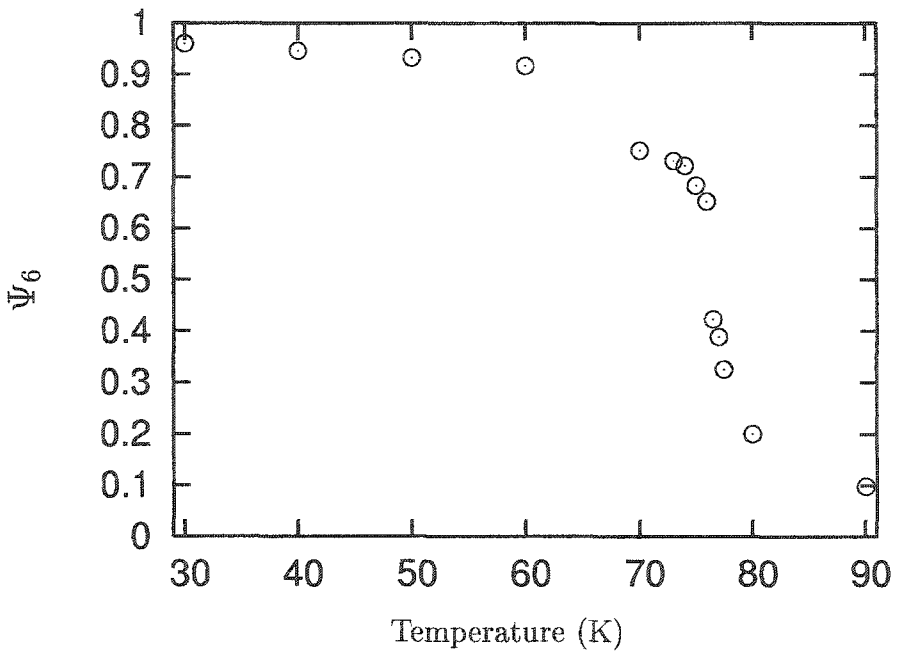

Figure 4.20: Ψ_6 for $\rho = 1.31$.

4.2 Melting

Melting is identified with the loss of six-fold bond orientational order of the solid, and occurs at the same temperature as the broad specific heat peak. This is observed by examining the order parameter Ψ_6. The behavior of Ψ_6 is similar for all the densities studied, figure 4.13. It approaches the low temperature value of one and the high temperature value of zero. The order parameter Ψ_6 is shown separately for $\rho = 0.39, 0.71, 1.00, 1.14, 1.22$, and 1.31 in figures 4.14, 4.15, 4.16, 4.18, and 4.20 respectively. For densities less than and equal to 1.07, the values of Ψ_6 are close, and their behavior versus temperature is similar. The argon atoms lose bond orientational order between 45K and 55K for all densities less than or equal to 1.07. The melting temperature changes rapidly for densities greater than 1.07, and melts at a higher temperature for densities greater than 1.07.

To help identify the melting temperature, the susceptibility of Ψ_6, χ_6, was calculated. The peak position of χ_6 is identified with the melting temperature of the solid. The susceptibility χ_6 is shown in figures 4.21, 4.22, 4.23, 4.24, 4.25, 4.26, and 4.27 for densities of 0.39, 0.71, 1.00, 1.07, 1.14, 1.22, and 1.31 respectively. The melting temperature for $\rho = 1.07$ is 51K while the melting temperature for $\rho = 1.14$ is 70K, an increase of 19K with a density change of 0.07. The peak position of χ_6 is always within 1K of the peak position of the broad specific heat peak. There is no peak in χ_6 at the same temperature as the sharp specific heat peak for $\rho = 0.39$ and 1.00. The FWHM of χ_6 has a similar density dependence as the FWHM of the broad spe-

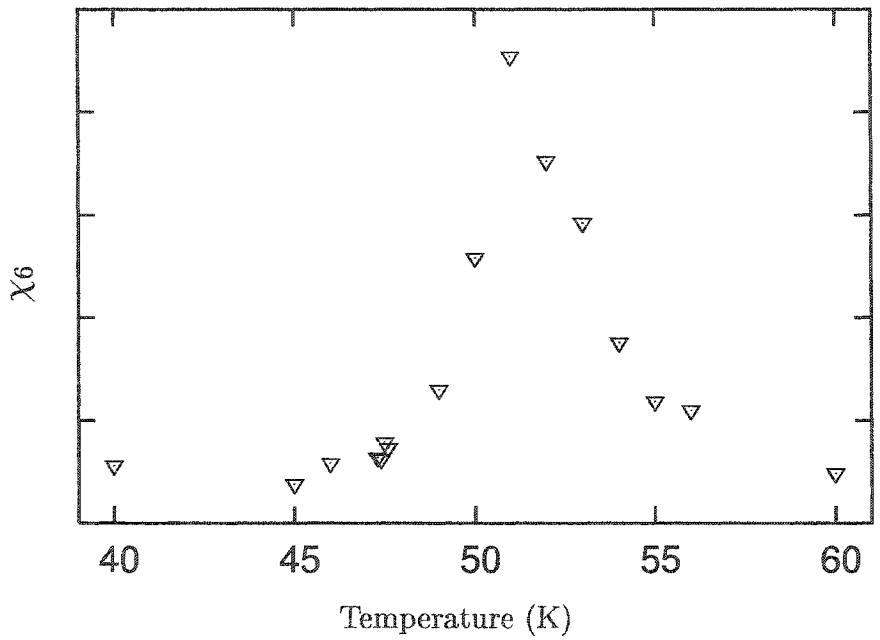

Figure 4.21: Order parameter susceptibility χ_6 for $\rho = 0.39$.

cific heat peak. Therefore the broad specific heat peak is associated with the loss of six-fold bond orientational order, i.e. melting. There appears to be a small peak in χ_6 for $\rho = 0.71$, but the peak is not outside the uncertainty of the calculation. Visual examination of the configurations and the radial pair distribution function also confirms that melting occurs around the broad specific heat peak.

In figure 4.28 the melting curve is shown along with the experimental results of Migone[44] and Chung[10], and table 4.3 lists the calculated melting temperature for each density. Some simulations were performed at densities of 1.08 and 1.09 to find the melting temperature, but were only examined around melting. Therefore, simulations were not conducted for a wide range of temperatures, thus the densities of 1.08 and 1.09 are not included in the rest of the results.

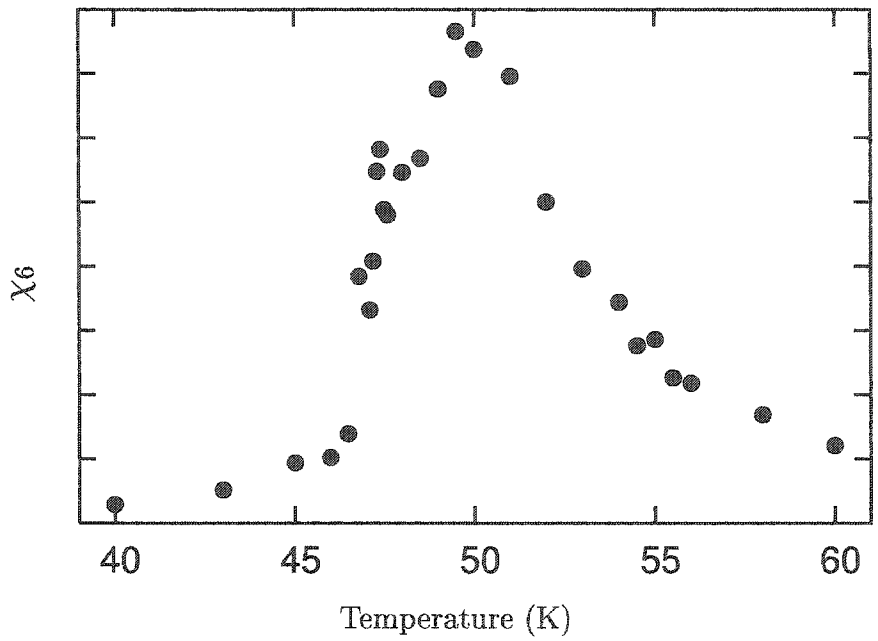

Figure 4.22: Order parameter susceptibility χ_6 for $\rho = 0.7$.

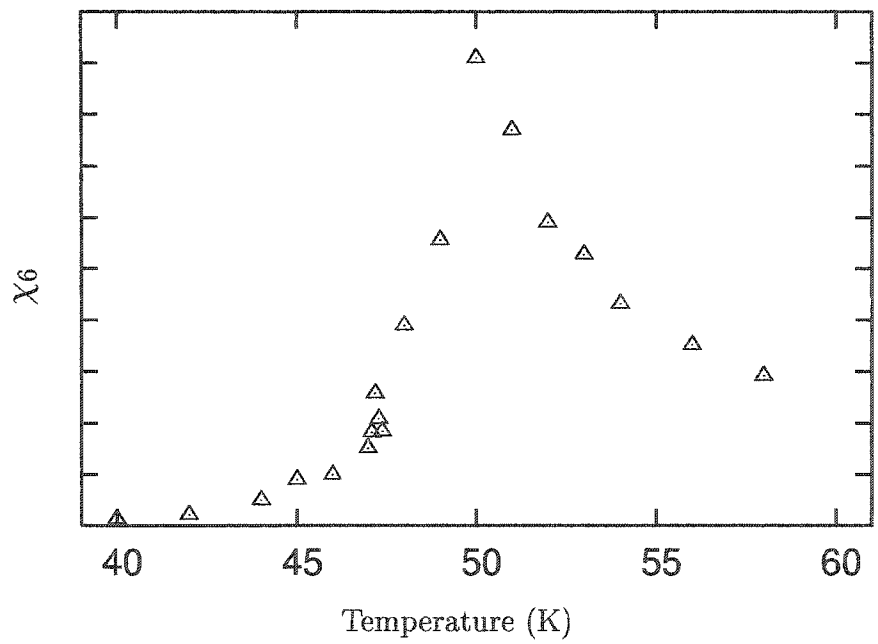

Figure 4.23: Order parameter susceptibility χ_6 for $\rho = 1.00$.

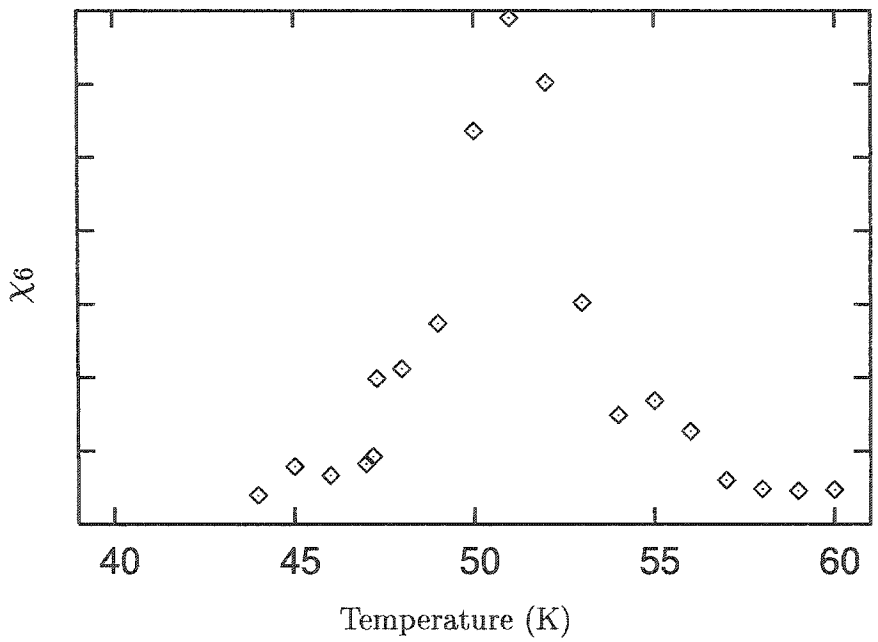

Figure 4.24: Order parameter susceptibility χ_6 for $\rho = 1.07$.

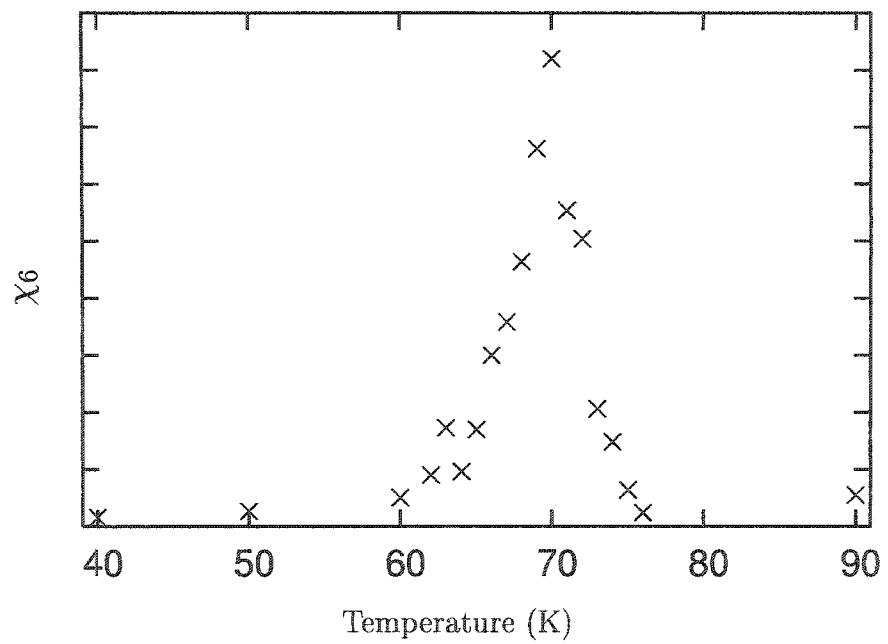

Figure 4.25: Order parameter susceptibility χ_6 for $\rho = 1.14$.

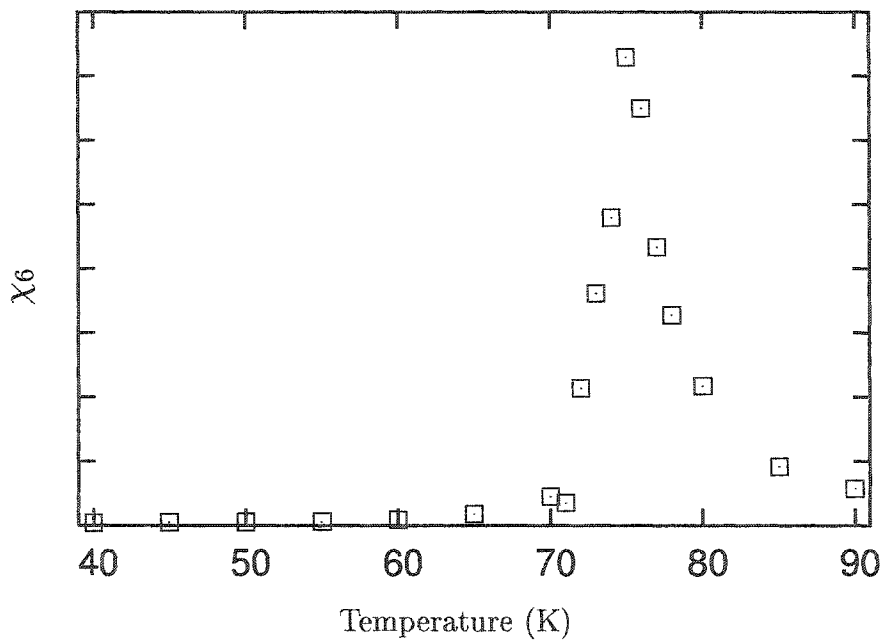

Figure 4.26: Order parameter susceptibility χ_6 for $\rho = 1.22$.

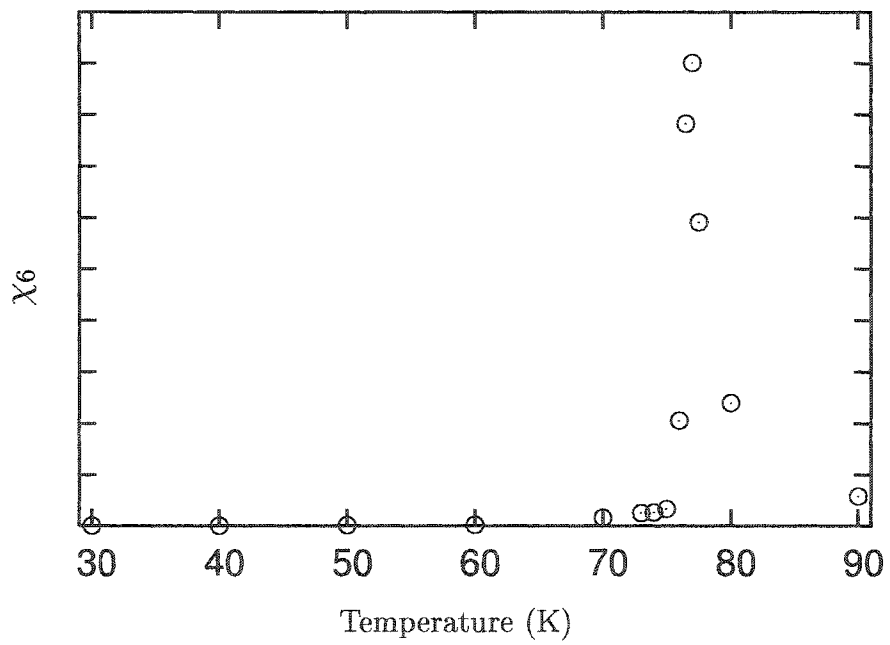

Figure 4.27: Order parameter susceptibility χ_6 for $\rho = 1.31$.

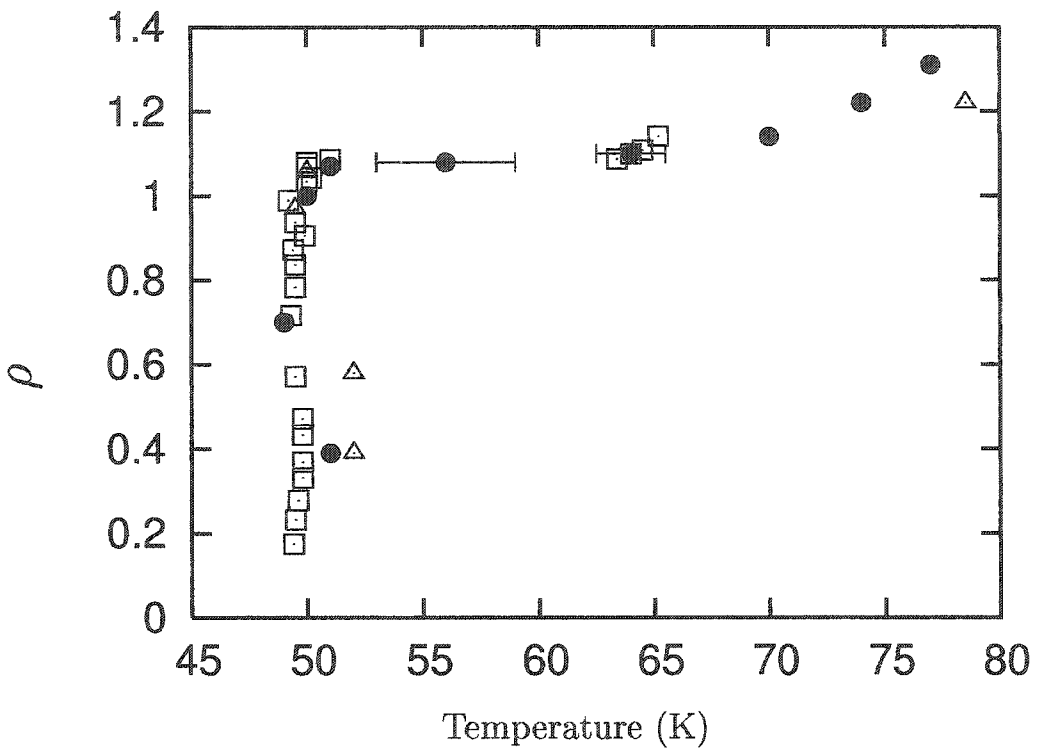

Figure 4.28: Melting Curve. The squares are from the specific heat data of Migone[44], the triangles are from the experiments of Chung[10], and the filled circles are the results from these simulations. The melting temperature at densities of 1.08, and 1.09 are approximate, and the uncertainty in the melting temperature for those densities is given by the error bars.

ρ	Calculated T_m
0.39	51
0.71	49
1.00	50
1.07	51
1.08	56
1.10	64
1.14	70
1.22	74
1.31	77

Table 4.3: The melting temperature for each density.

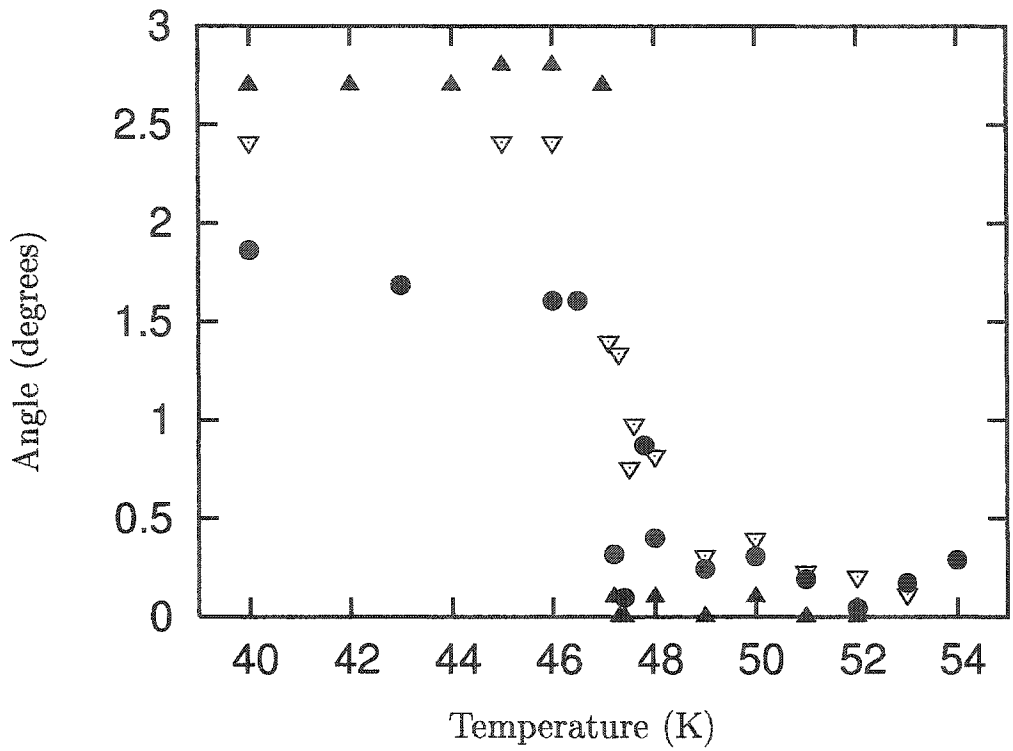

Figure 4.29: Rotation angle versus temperature for $\rho = 0.39$ (∇), $\rho = 0.71$ ($\bullet$) and $\rho = 1.00$ ($\blacktriangle$).

4.3 Rotational Transition

The calculated narrow specific heat peak is associated with a rotational transition. At 47.4K, the same temperature as the narrow specific heat peak, the solid argon goes from a state that is rotated with respect to a $\sqrt{3} \times \sqrt{3}$ symmetry direction, to a state that is aligned with a $\sqrt{3} \times \sqrt{3}$ symmetry direction, figure 4.29.

The rotation angle was found by examining the distribution of rotation angles, which is described in chapter 3. Below 46K there is one peak in the distribution of rotation angles at an angle $\Theta = 1.8$ degrees for $\rho = 0.71$ and 2.4 degrees for $\rho = 0.39$, figure 4.30. At 46.5K, two symmetric peaks are present at Θ and $-\Theta$, figure 4.31.

This persists until $T = 47.2$K, then a broad, third peak starts to emerge at $\Theta = 0$, but two symmetric peaks around $\Theta = 0$ are still present, figure 4.32. Between 47.2K and 48K, the peaks on either side of $\Theta = 0$ become shoulders and at 48K, there is only one broad peak at $\Theta = 0$, figure 4.33. The argon atoms are going from a rotated state to a state that is aligned with the substrate. To find the rotation angles, first the dominant peak in the distribution of rotation angles was determined. Then the dominant peak was fit to a gaussian distribution, and the absolute value of the peak position was identified with the rotation angle. If there were two peaks at $\pm\Theta$, see figure 4.31, then a gaussian was fit to each peak separately, and the rotation angle was the average of the absolute value of the position of each peak. For some temperatures between 47K and 47.4K, it was impossible to determine the dominant peak since there were three peaks of the same height, and those temperatures are not included in figure 4.29.

For $\rho = 1.00$, the rotational transition was more abrupt. There was always only one dominant peak in the distribution of rotation angles, and that peak position was around $\pm 2.7°$ for temperatures below 47.2K, or around $0°$ for temperatures above 47.2K. For temperatures close to but above the rotational transition, there would be two small peaks at $\pm 2.7°$ at either side of the dominant peak at $\Theta = 0$.

Hysteresis was observed around the rotational transition for $\rho = 1.00$. The simulations of the odd temperatures were started from the final configuration of a simulation run at 2K higher temperature, and the even temperatures were started from the final

configuration of a simulation run at 2K lower temperature. Thus, the odd temperature simulations corresponded to cooling the argon atoms, and the even temperatures is equivalent to heating the atoms. When the argon atoms were cooled, the argon solid stayed aligned with the substrate at 43K and 45K for over 16 million Monte Carlo steps, then the atoms rotated to 2.7°, and the lattice constant decreased suddenly. The rotational behavior of the argon atoms and the lattice constant did not change for eight million more Monte Carlo steps.

For $\rho = 1.07$ and higher, the rotation angle behaved differently than for the lower densities. For $\rho = 1.07$, there was only one peak in the distribution of rotation angles for temperatures below 45K around $\pm 2.8°$. Between 45K and 51K, several peaks were present in the distribution of rotation angles. The argon solid melts at 51K. The peaks would be around $\pm 2.8°$, $\pm 7°$, and at 0°. Also, there was a nonzero probability of finding the argon solid at any rotation angle between 7° and $-7°$. The argon solid would be rotated at one rotation angle for two million or more steps, and then rotate to another angle and stay around that angle for another two million steps. Several simulations were conducted with different initial conditions and the behavior of the rotation angle of the argon solid was always the same. While these simulations do not rule out a rotational transition, it is also not clear that there is a rotational transition for $\rho = 1.07$.

The rotation angle for temperatures 5K or more below melting was 2.9° for $\rho = 1.14$ and 3.0° for $\rho = 1.22$. Starting at about 5K below melting, multiple peaks would

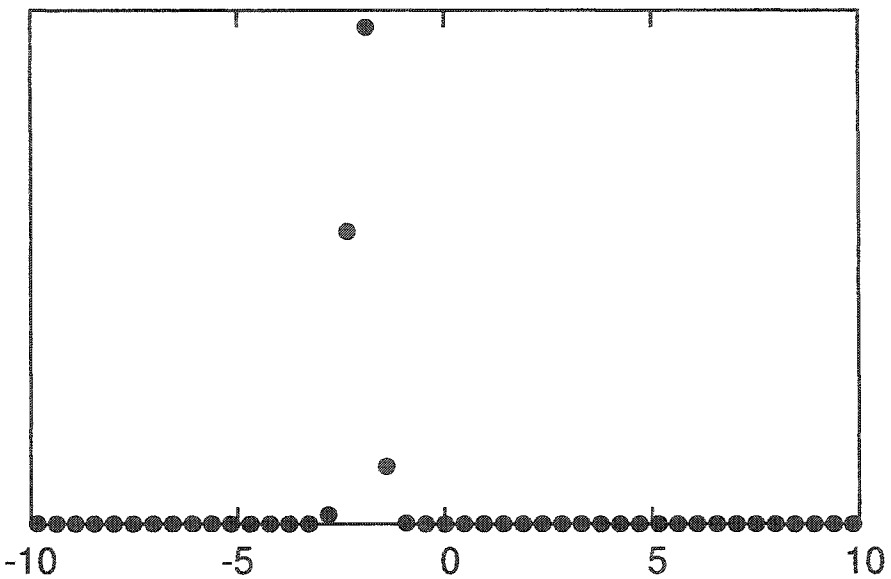

Figure 4.30: Distribution of rotation angle for $\rho = 0.71$ at 35K.

emerge in the distribution of rotation angles. The peaks would not be very high, and there would be a nonzero probability of finding the argon solid rotated at all angles between $\sim 15°$ and $\sim -15°$. The argon solid would not be at one rotation angle for more than half a million steps before it would rotate to a different angle. This behavior did not change when the initial conditions were varied. For the density of 1.31, the argon solid was aligned with the substrate below 70K. At 70K, the argon solid rotated to an angle of 2.7° and stayed at that angle until melting.

Since Θ and $-\Theta$ are equivalent states, the argon atoms may be well described by a double well orientational potential. This suggests that the Ising model may provide a good description of the orientational transition. To provide information on the shape of the probability distributions of the rotation angles, and for a connection to the

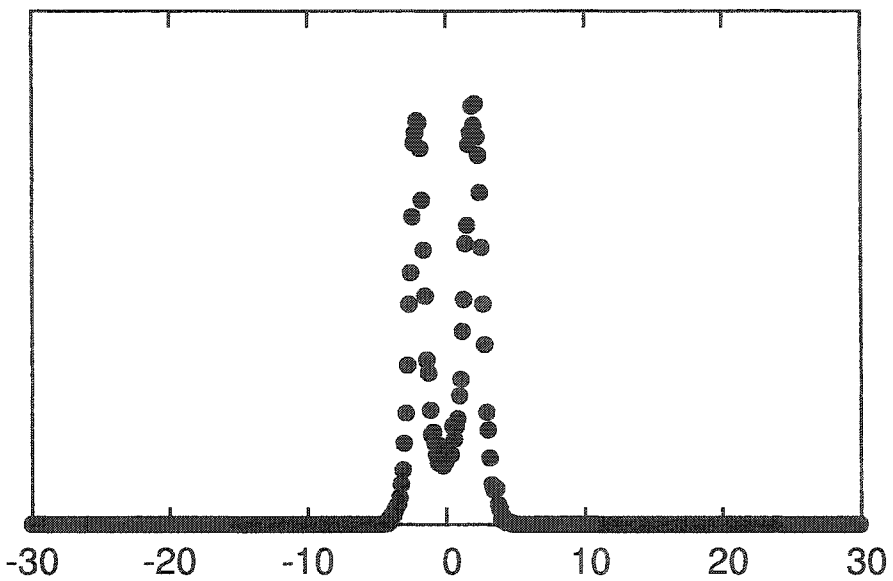

Figure 4.31: Distribution of rotation angle for $\rho = 0.71$ at 46.5K.

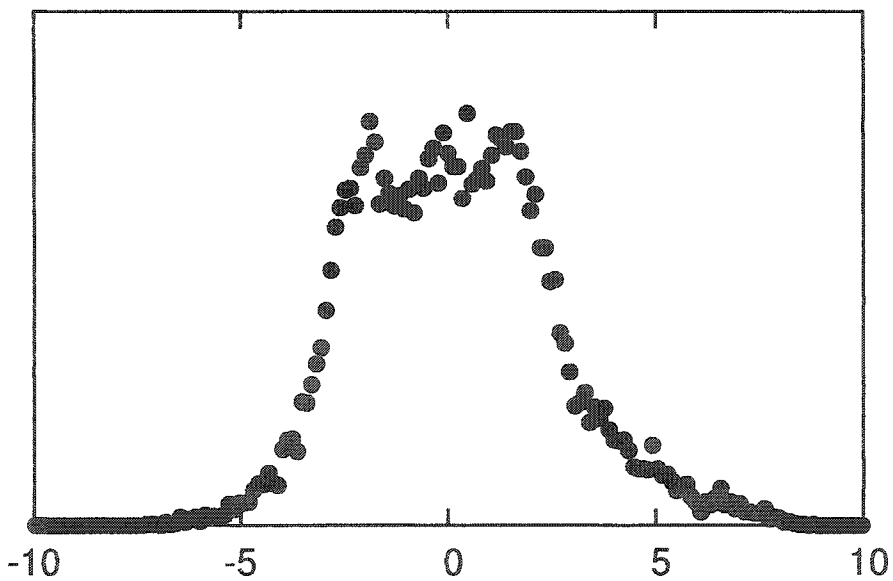

Figure 4.32: Distribution of rotation angles for $\rho = 0.71$ at 47K.

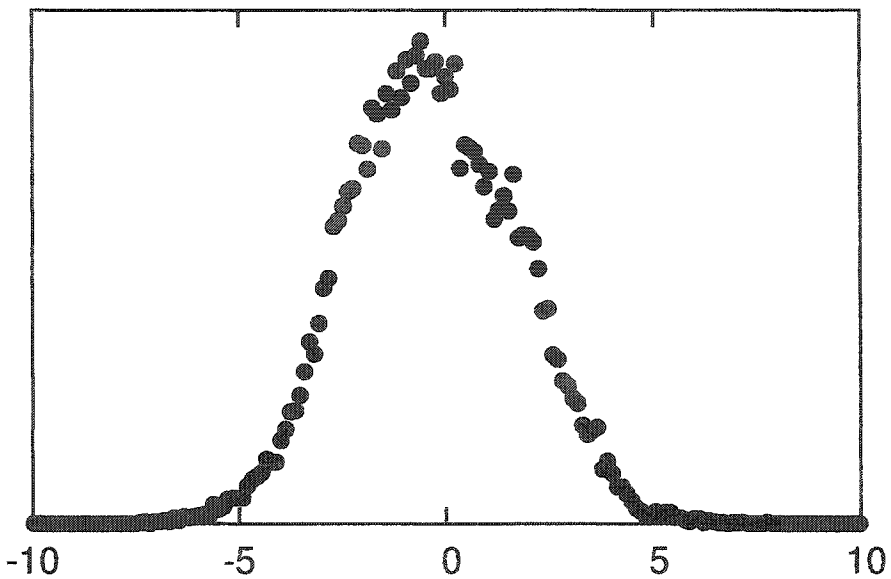

Figure 4.33: Distribution of rotation angles for $\rho = 0.71$ at 48K.

Ising model, the fourth order reduced cumulant was calculated, figures 4.34 and 4.35. For a rotated state, it is expected that the distribution of rotation angles is one or two Gaussians centered at the rotation angle of the solid, and the reduced cumulant would be close to 2/3. For a state aligned with the substrate the distribution of rotation angles should be a gaussian centered at zero, and in this case the reduced cumulant would be zero. At the critical point, the distribution of rotation angles is no longer gaussian, and thus it does not have the value of 2/3 or zero, but rather has a value that depends on the universality class of the continuous phase transition[41].

The reduced cumulant is around 2/3 for temperatures below 46K, then it begins to decrease at 46K and goes to zero at the rotational transition, and is zero above the rotational transition into the isotropic liquid phase. The circle with the cross is the

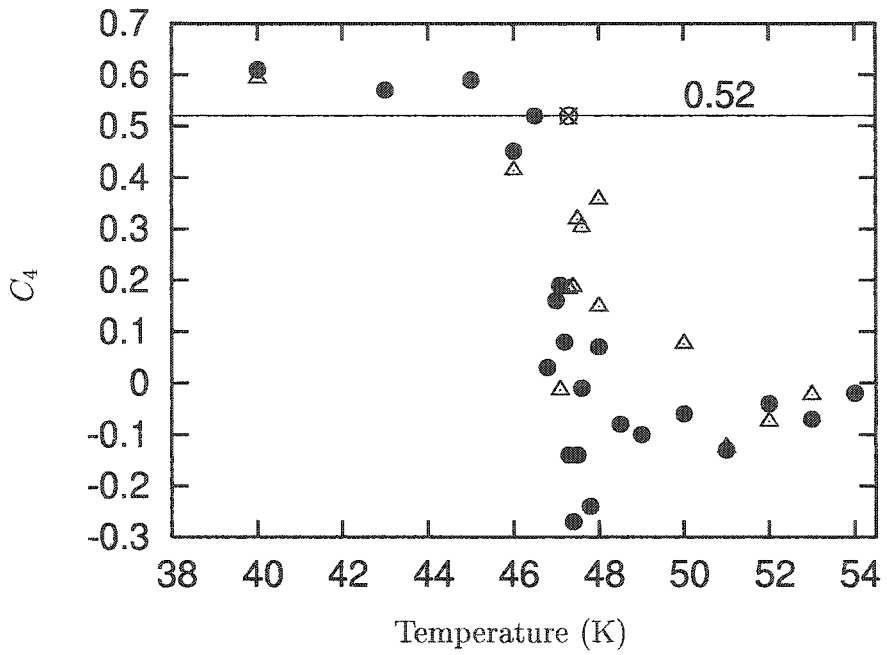

Figure 4.34: Fourth order reduced cumulant for $\rho = 0.39$ (∇) and $\rho = 0.71$ ($\bullet$). The horizontal line is the 2D Ising critical point value of the reduced cumulant. The cross in the circle is placed at the position of the sharp specific heat peak.

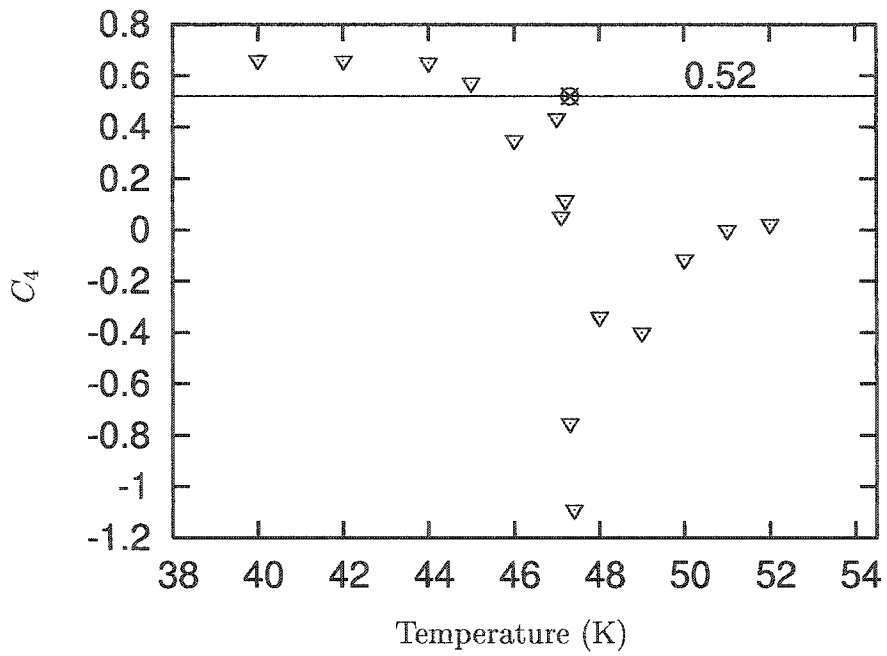

Figure 4.35: Fourth order reduced cumulant for $\rho = 1.00$. The horizontal line is the 2D Ising critical point value of the reduced cumulant. The cross with the circle is placed at the position of the sharp specific heat peak.

critical point value given by the Ising model, and is placed at the same temperature as the narrow specific heat peak. The horizontal line corresponds to 0.52. For this set of potential parameters, the cumulant is close to the 0.52 value corresponding to the Ising universality class. In the previous calculations for densities of $\rho = 0.71$ and 0.89 of Flenner and Etters[38], where the argon-carbon potential and the substrate mediated potential was 15% larger than in these simulations, the change in the cumulant was more abrupt and the cumulant had values closer to 0.52 at the same temperature that the rotation angle went to zero. Since the value of the reduced cumulant does not depend on system size at the critical point[41], simulations of different system sizes are typically conducted and the point at which the reduced cumulant crosses is identified with the critical point. In these simulations, when the system size is changed, the density also has to be changed slightly so that the simulation cell is always a unit multiple of the graphite unit cell. It is not clear how this would effect the value of the reduced cumulant so a finite size scaling analysis was not performed.

According to the theory of Novaco and McTague[11], the rotation angle is associated with the formation of mass density waves. A result of the mass density waves is that the argon atoms are displaced from the equilibrium position they would have if there was no substrate corrugation. The effect of this displacement is that the argon atoms spend more time in the center of the graphite hexagons than they do over the carbon atoms. Figure 4.37 shows the likelyhood of finding an argon atom at various points in the graphite unit cell at 35K for $\rho = 0.71$, and figure 4.36 is the unit cell

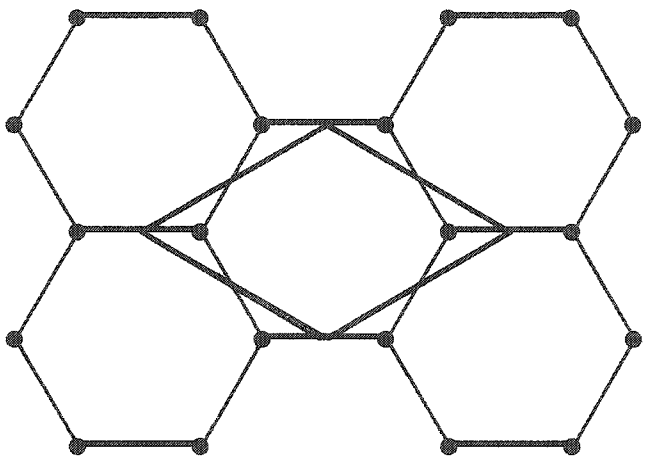

Figure 4.36: The unit cell for the calculation of the probability distribution. Each corner is a saddle point between two carbon atoms. The filled circles are carbon atoms. The center of a graphite hexagon is in the middle of the unit cell.

used for the calculation. The figure is normalized so that if the argon atoms are equally likely to be found anywhere above the substrate, then the distribution would be one for all points. The argon atoms are more than twice as likely to be found in the center of a graphite hexagon than they are over a carbon atom. Figure 4.38 shows the temperature dependence of the peak height of the distribution, which is always at the center of the graphite hexagon. At 47.4K, there is a sharp spike, then the peak height of the distribution begins to decrease rapidly after 50K. Notice that the peak height is not one even in the fluid phase. Therefore, the argon atoms are more likely to be found over the center of a carbon hexagon even in the fluid phase.

The increased likelyhood of the argon atoms to be in the center of the graphite hexagons influences the average value of E1. The average of the E1 energy is zero if the argon atoms are equally likely to be found anywhere over the graphite surface. But argon atoms are not evenly distributed above the graphite, and they are more likely to be found at a position above the substrate which decreases the average value of E1. The average of the E1 energy is almost constant for $T < 47$K, then there is a sharp decrease in the average E1 energy for $\rho = 0.39$, 0.71 and 1.00 between 47K and 47.5K, figures 4.39 and 4.40. This is the same temperature as the sharp specific heat peak. E1 obtains a minimum value, and is almost constant between 47.5K and 49K, then it begins to increase again at 49K for $\rho = 0.71$, 51K for $\rho = 0.39$, and 50K for $\rho = 1.00$, i.e. at melting. The well depth of the corrugation is -38K, thus the E1 energy is about 25% of the well depth.

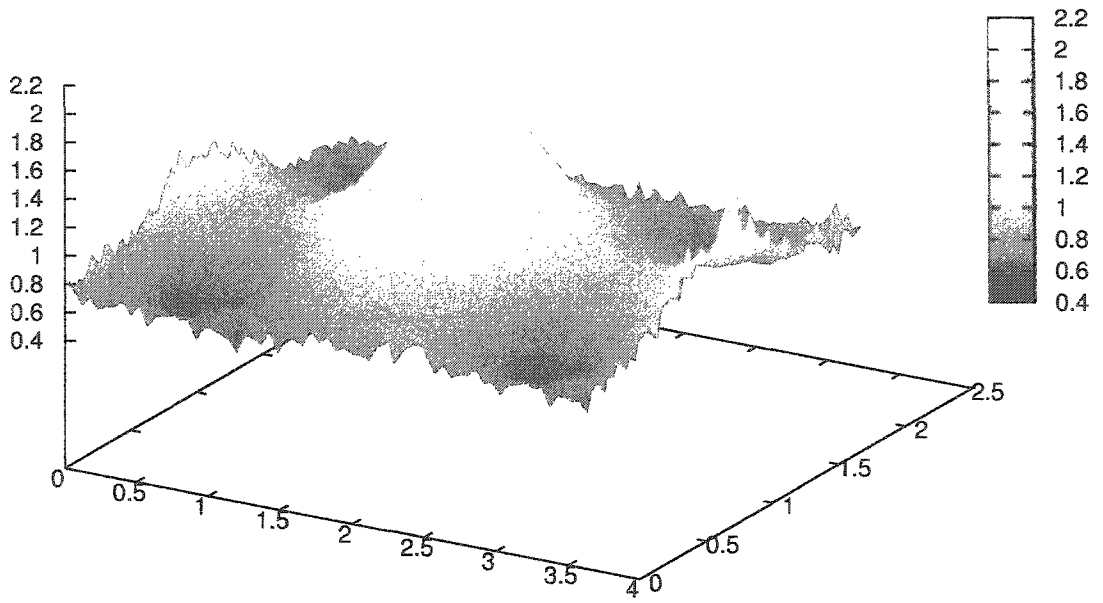

Figure 4.37: A normalized distribution of argon atoms in a graphite unit cell. The peak is the center of a graphite hexagon. The distribution has been normalized so that if there is an equal probability of finding an argon atom at any point over the graphite surface, then the distribution would be one at every point. The minimum of the distribution is 0.4, and over a carbon atom. The maximum in the distribution is 2.2, which is in the center of a graphite hexagon.

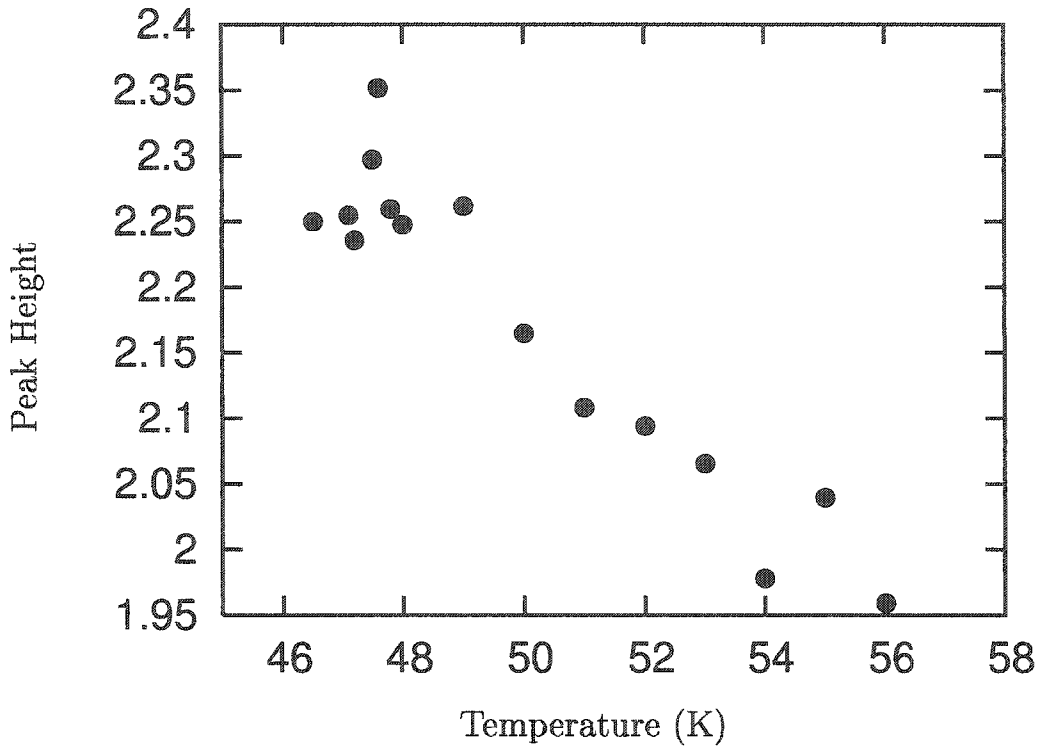

Figure 4.38: Peak height of the substrate distribution for $\rho = 0.71$.

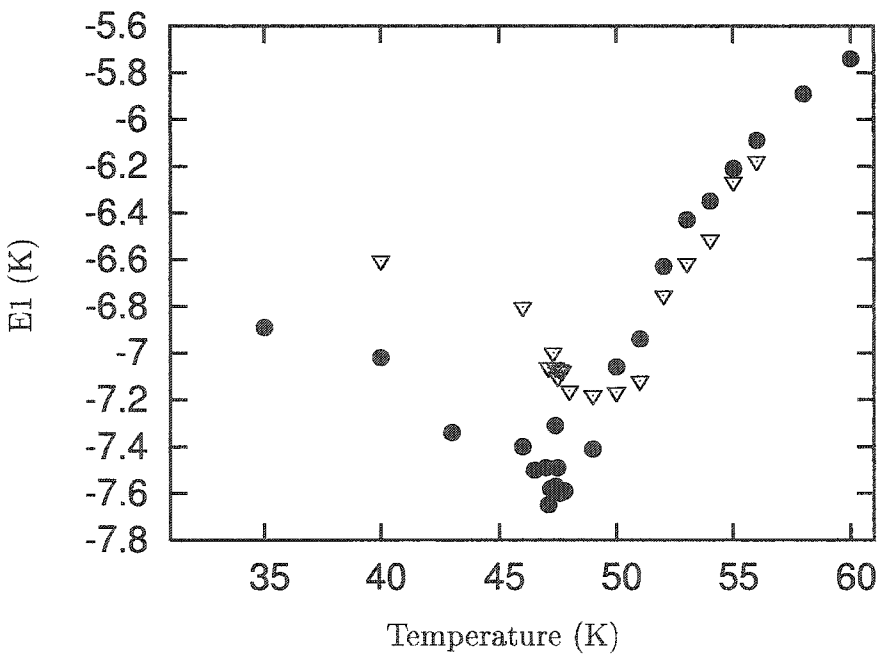

Figure 4.39: E1 energy for $\rho = 0.39$ (∇) and 0.71 ($\bullet$).

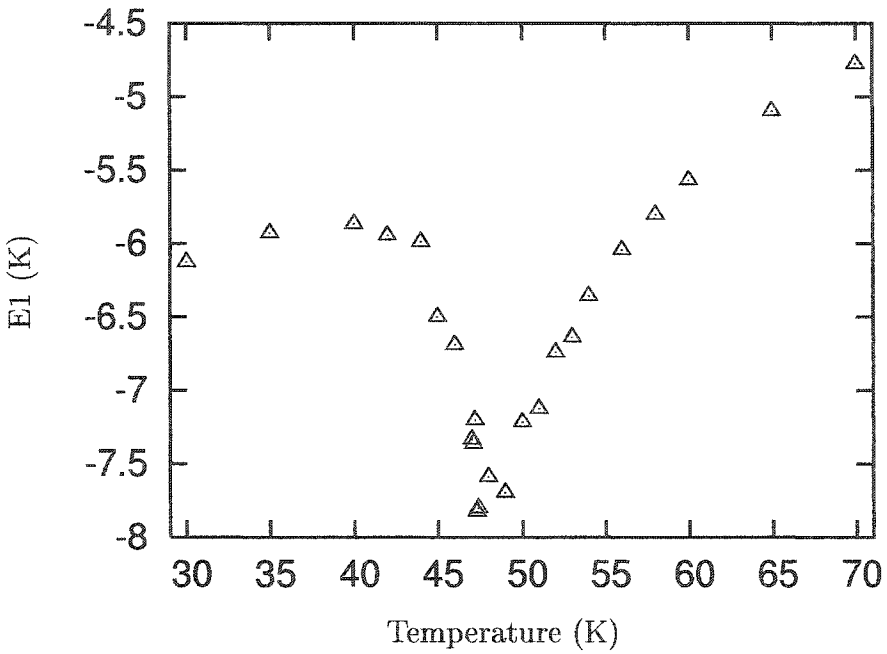

Figure 4.40: E1 energy for $\rho = 1.00$.

The other noticeable change in the system is a change in the rate of thermal expansion at the narrow specific heat peak. The change in the rate of thermal expansion is similar for $\rho = 0.39$ and 0.71, but slightly different for $\rho = 1.00$. The rate of thermal expansion is larger between the 47.5K and 50K than for temperatures below 47.5K as can be seen in the change in the slope of the lattice constant versus temperature, figure 4.41. The lattice constant evolves continuously through the rotational transition and through melting. The lattice constant was always smaller for $\rho = 0.39$, and this is due to a size effect which will be discussed later. For $\rho = 1.00$, there is an increase in the rate of thermal expansion at 45K, but the largest change in the lattice constant occurs between 46K and 47.4K where the lattice constant increases by 0.05Å, figure 4.42. After 47.4K, the rate of thermal expansion is not as large.

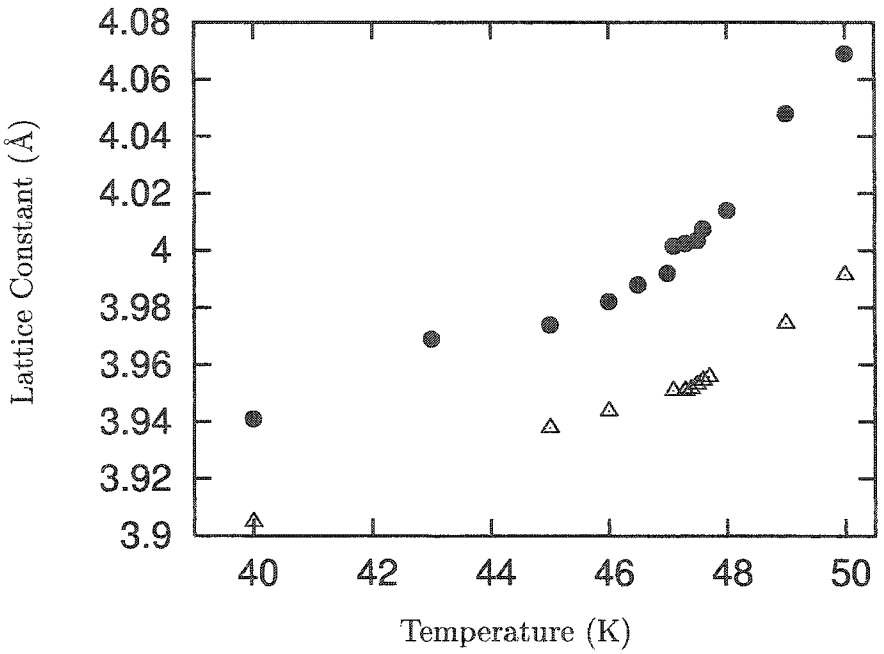

Figure 4.41: The lattice constant for $\rho = 0.39$ (∇) and 0.71 ($\bullet$).

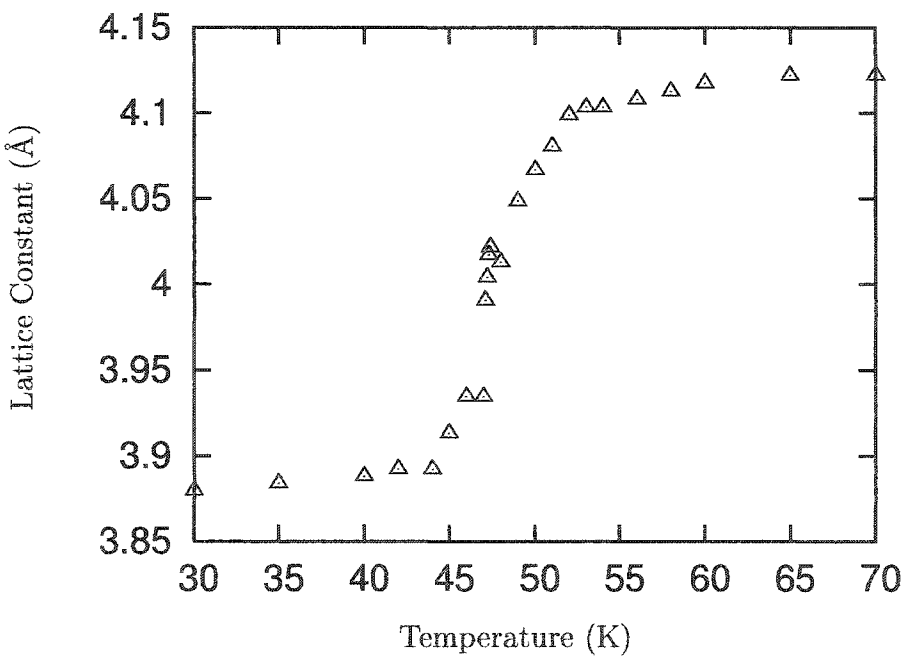

Figure 4.42: The lattice constant for $\rho = 1.00$.

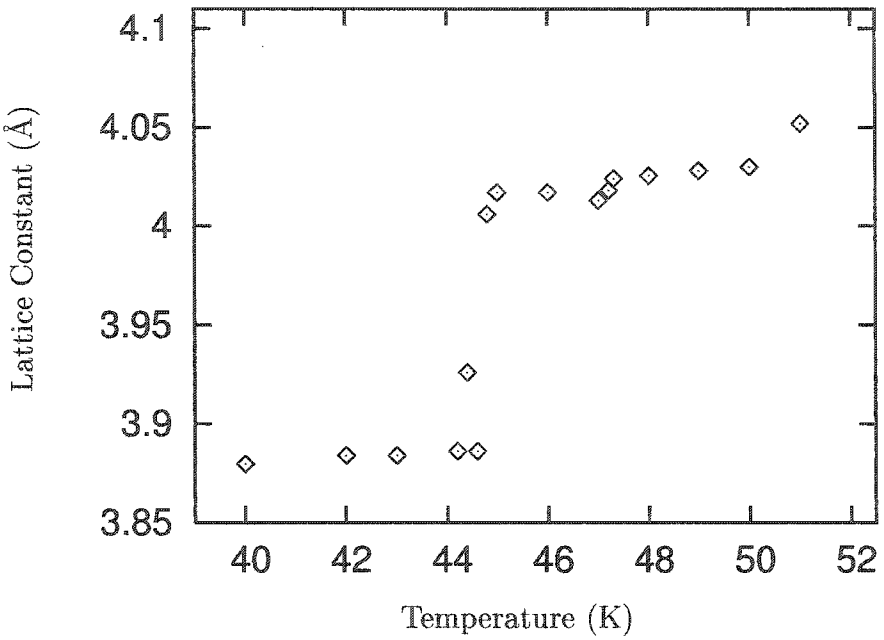

Figure 4.43: The lattice constant for $\rho = 1.07$.

For $\rho = 1.07$ there is no narrow specific heat peak, but there are similarities between the behavior of the argon atoms with the lower temperatures. Below 44K, there is not much change in the lattice constant, and between 45K and 50K there is not much change in the lattice constant. Most of the change in the lattice constant occurs between the interval of 44K and 45K, figure 4.43. Also, during the interval of the rapid change in the lattice constant, the E1 energy term also decreases, figure 4.44.

The simulations of $\rho = 0.39$ were conducted with 625 particles because of the difficulty which occurred in doing a simulation with 256 particles for $\rho = 0.41$, and to determine if there were size effects for low densities. The specific heat for $\rho = 0.41$ is shown in figure 4.45. The simulations were run for 24 million Monte Carlo steps

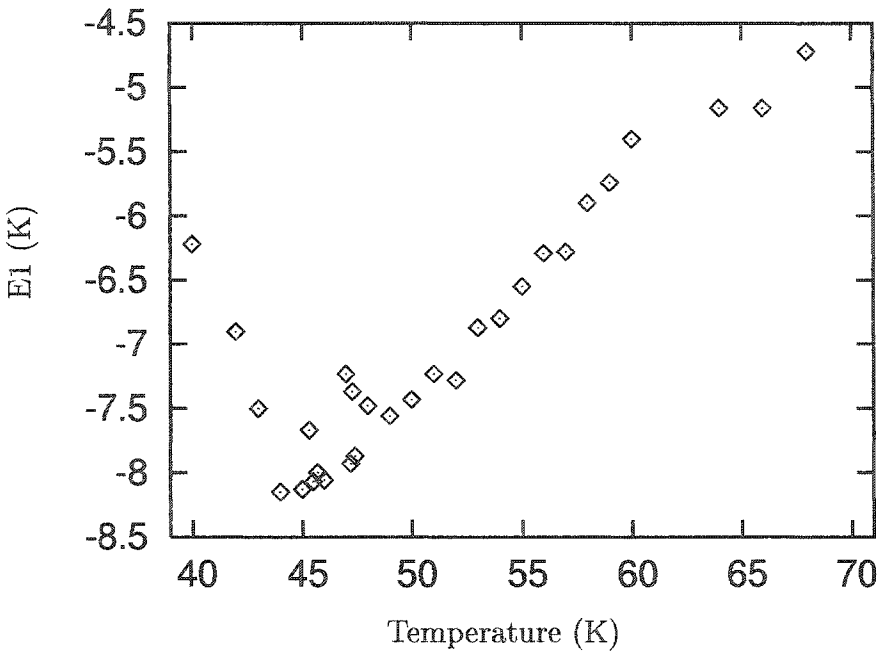

Figure 4.44: The average E1 energy for $\rho = 1.07$.

with averages taken over the last four to eight million steps. The main features of the specific heat appear to be present. There is a broad peak centered around 50K, but the narrow peak is not very well resolved, and it is impossible to determine at which temperature the peak occurs.

There was increased scatter for $\rho = 0.41$ around the sharp specific heat peak because of the large percentage of particles on the edge of the system. For most densities the periodic boundary conditions do a good job of simulating an infinite system, but for any density significantly less than monolayer completion, there are edges in the simulated system as well as the real system. The difference between the simulated system and the real system is that the percentage of atoms along the edge

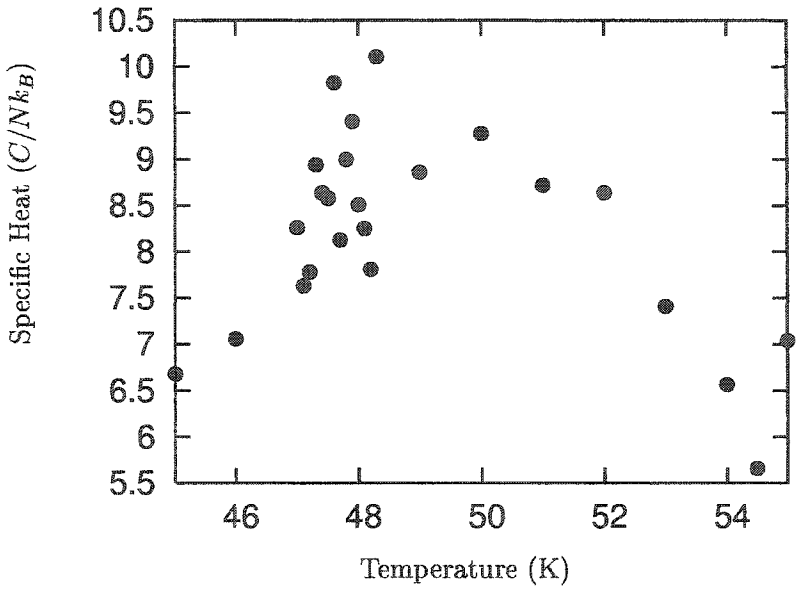

Figure 4.45: Specific Heat for $\rho = 0.41$

of the simulated system is much larger than in the real system. Monolayer completion is around 1.26 in these units, and depends weakly on temperature.

This affects the value of the lattice constant. The particles along the edge are not as tightly bound as argon atoms in the center of the solid patches, thus the calculation of the lattice constant is larger for the smaller system sizes. To determine the size of the effect, simulations were done at 35K, 45K, and 48K for different number of particles in the simulation cell. The density was kept around 0.7, but had to be adjusted slightly so that the simulation cell was an integer multiple of a graphite unit cell. At 35K, simulations were performed with 144, 256, 289, 324, 400, 625, 529, and 1024 particles in the simulation cell, and the results are shown in figure 4.46. The lattice constant with 256 particles in the simulation cell was approximately 0.033Å larger than the values obtained with 324 or more particles in the simulation cell.

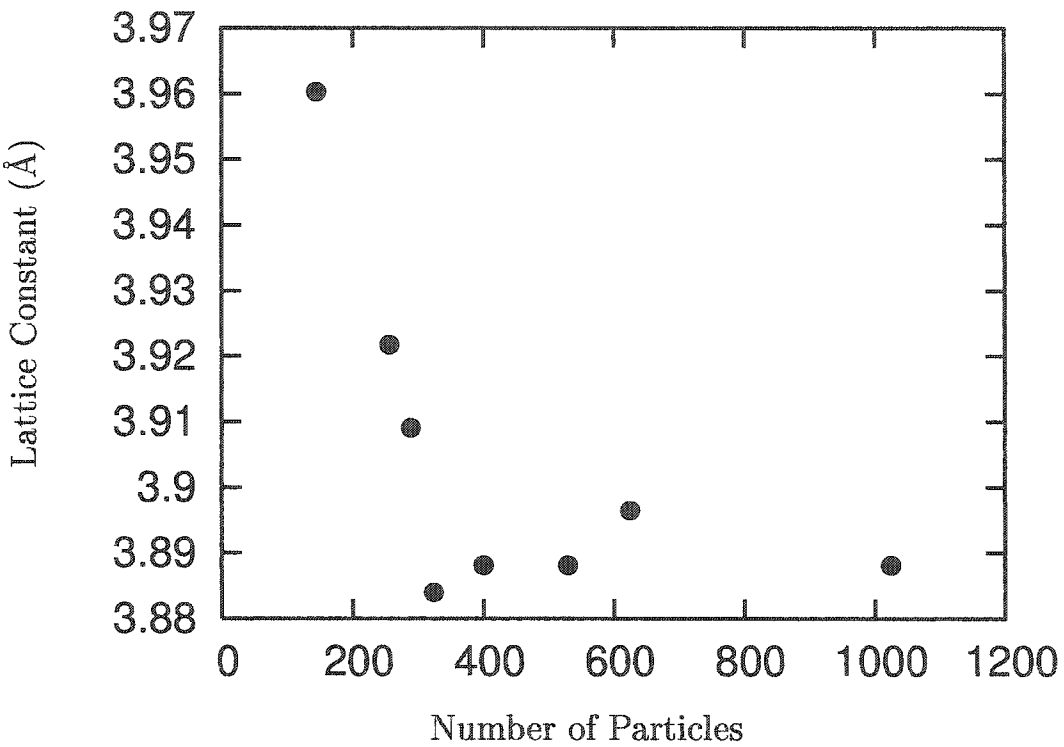

Figure 4.46: The lattice constant at 35K as the number of particles in the simulation cell is varied. The density was around 0.7.

Also, simulations with 1600 particles were performed at 45K, one with a random configuration of particles as the initial configuration, and one with a perfect triangular lattice as the initial configuration. The simulations were run until they gave the same results for all the calculated quantities. The lattice constant was 0.031Å larger for a simulation with 256 particles than for the simulations with 1600 particles. It appears that there is no temperature dependence for the edge correction to the lattice constant for the temperature range between 35K and 45K.

There is a temperature dependence on the correction to the lattice constant right below melting. To see if the size effect was larger at 48K, two simulations utilizing 1600 particles were performed at 48K. The same strategy was used at 48K as was used at 45K, but the two results never agreed after running for 6 million Monte Carlo steps. The simulation started from the triangular lattice was rotated and had a lattice constant of 3.9473 ± 0.006Å, and the simulation started with a random lattice was aligned with the substrate and had a lattice constant of 3.9646 ± 0.006Å. The actual lattice constant is probably given by a value somewhere between the value given by the simulations.

A correction was made assuming that the lattice constant was the average of the two values obtained from the two simulations with different initial conditions, figure 4.48. Therefore the lattice constant between 45K and 50K were given by $a_c = a_0 - (0.031 + 0.0150 * (T - 48))$ where a_c is the corrected lattice constant, a_0 is the lattice constant found in the simulation with 256 particles and T is the

temperature. Figure 4.47 compares lattice constant at $\rho = 0.39$ and the corrected lattice constant for $\rho = 0.71$ where the errorbars for $\rho = 0.71$ represents the range of values for the correction given by the two simulations. With the correction, both of the lattice constants fall within the range of the experimental values, figure 4.48.

4.4 Second Layer Promotion

For densities of 1.07 and higher, some atoms start to form a second layer. For $\rho = 1.07$, atoms start to populate a second layer at 60K, about 10K above melting, thus it does not influence melting. For $\rho = 1.14, 1.22$, and 1.31, the second layer begins to form below melting at some temperature between 50K and 60K. This is observed by looking at the distribution of the argon atoms perpendicular to the substrate, figures 4.49, 4.50, and 4.51. There are two distinct peaks in the distributions, thus the atoms are forming two layers. As the temperature increases, the number of atoms promoted to the second layer increases. Also, a greater percentage of the atoms are promoted to the second layer for the higher densities. This lowers the density in the first layer, figure 4.52. The average height of the first layer increases with increased temperature, figure 4.53 for all the densities. For temperatures below 60K, the average z position of the atoms depends on density and is higher for the higher density. For temperatures greater than 60K, when second layer promotion starts to occur, the average z position of the atoms in the first layer is the same for every density.

Once enough atoms are promoted to the second layer, there is an increase in

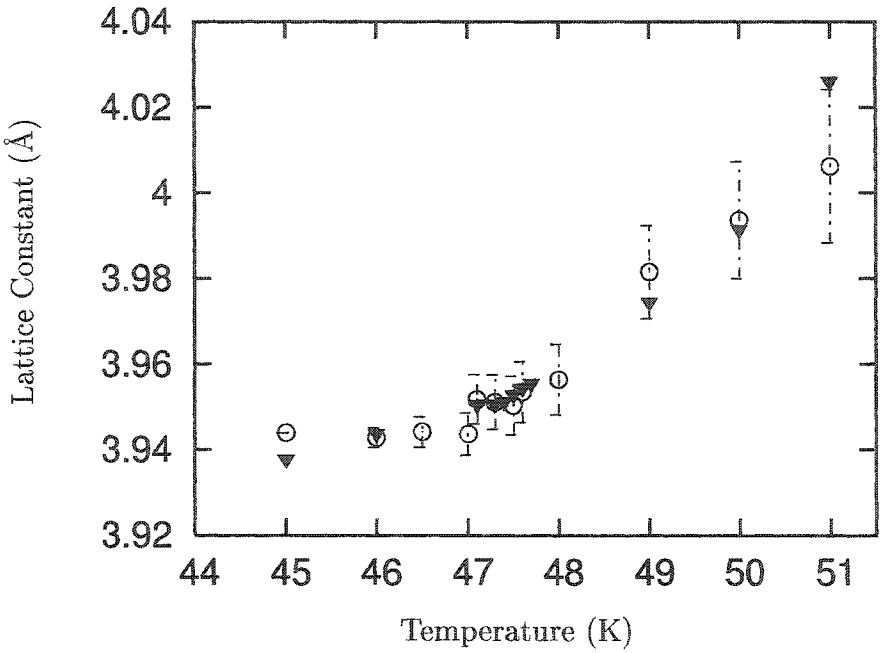

Figure 4.47: Lattice constant for $\rho = 0.39$ (▼) and $\rho = 0.71$ (○) with the correction discussed in the text for $\rho = 0.71$. The errorbars represent the uncertainty in the size of the correction.

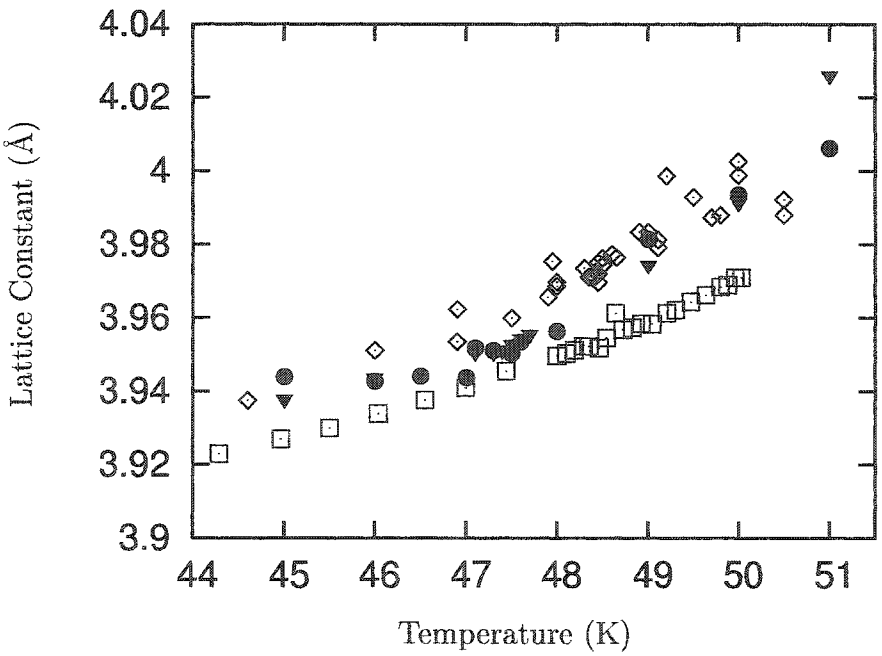

Figure 4.48: Lattice Constant for $\rho = 0.39$ (▼) and $\rho = 0.71$ (●) compared to the experimental values of Novaco (◇) and D'Amico (□). The lattice constant for $\rho = 0.71$ has a correction due to size effects which is discussed in the text.

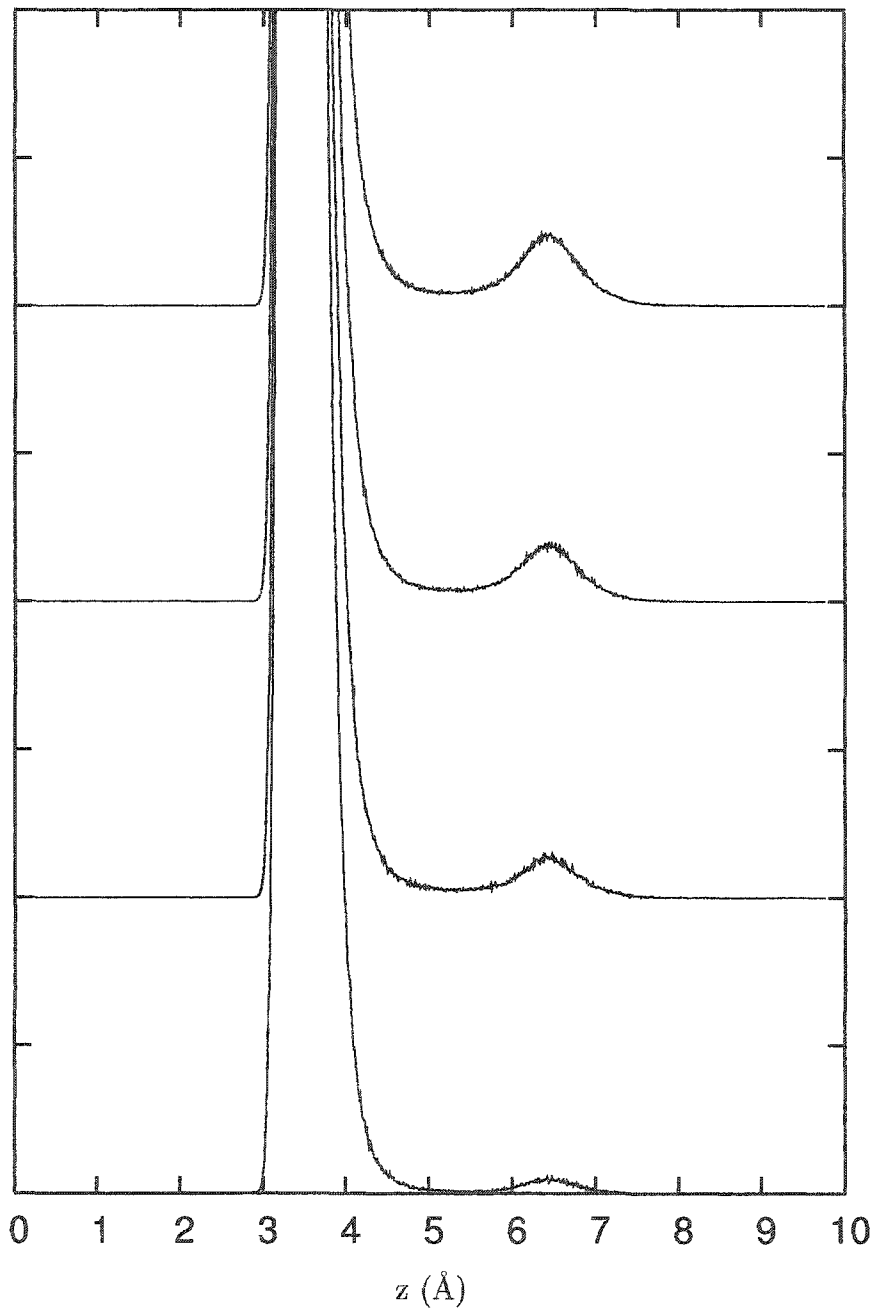

Figure 4.49: Distribution of atoms in the z direction for $\rho = 1.14$. The temperature from bottom to top is 66K, 70K, 72K, and 73K.

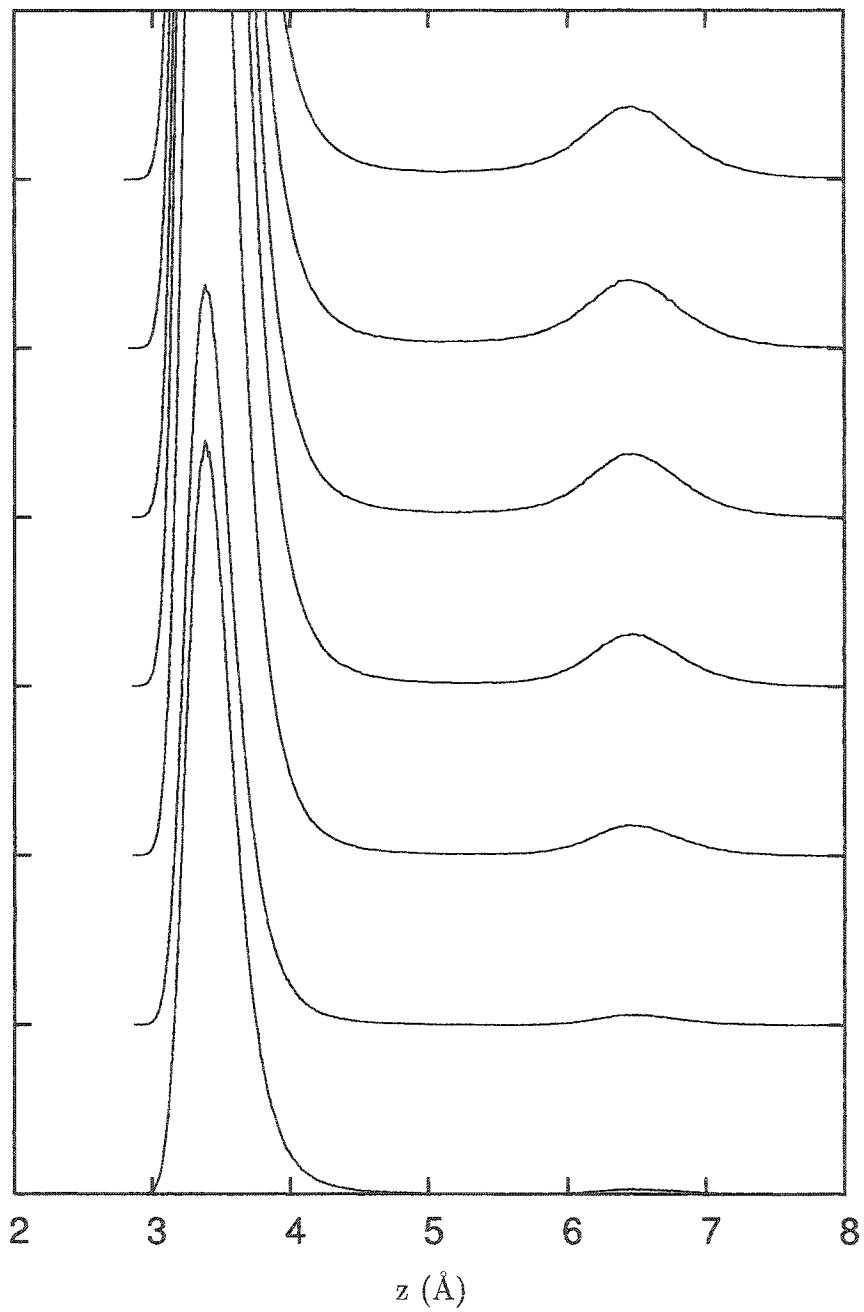

Figure 4.50: Distribution of atoms in the z direction for $\rho = 1.22$. The temperature from bottom to top is 70K, 71K, 72K, 74K, 75K, 76K, and 77K.

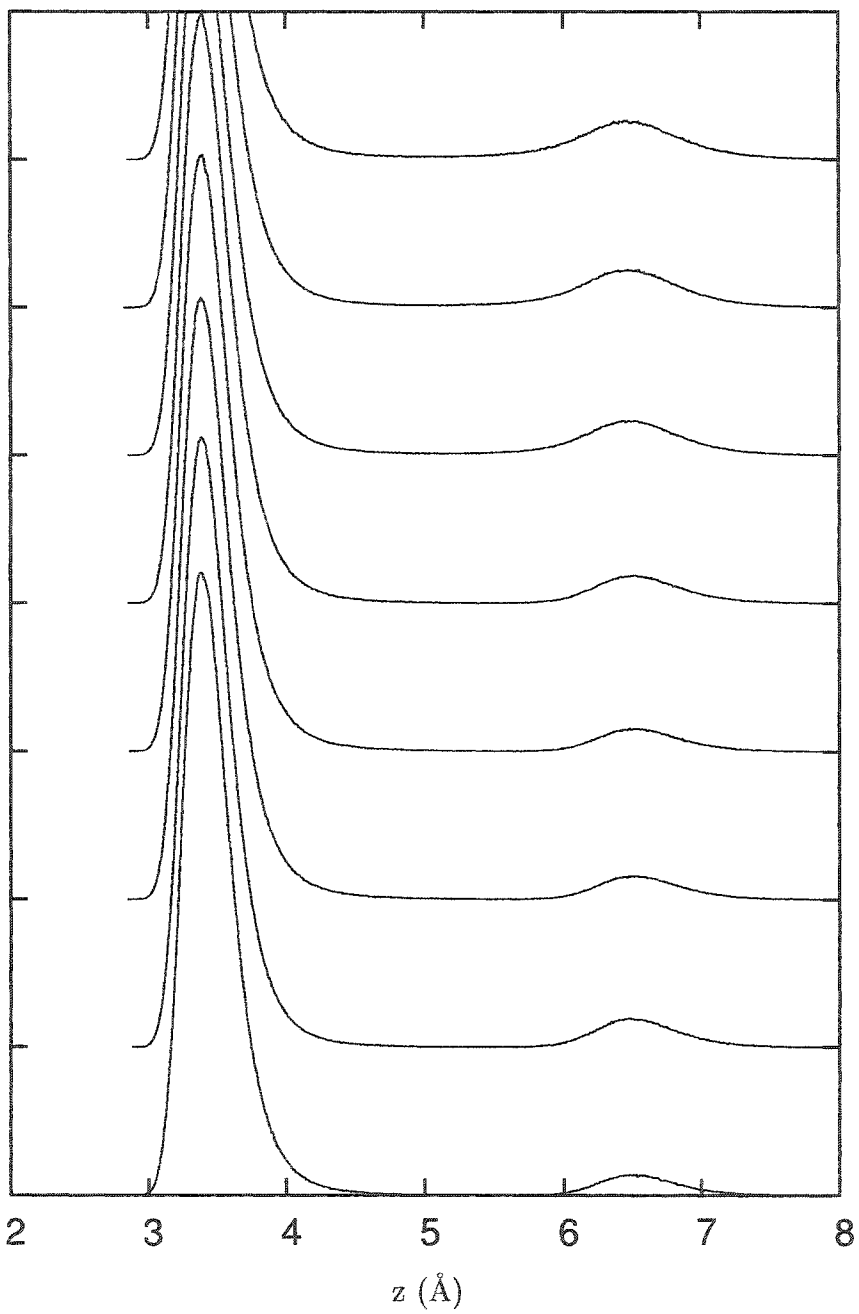

Figure 4.51: Distribution of atoms in the z direction for $\rho = 1.31$. The temperature from bottom to top is 70K, 71K, 73K, 74K, 75K, 77K, 78K, and 80K.

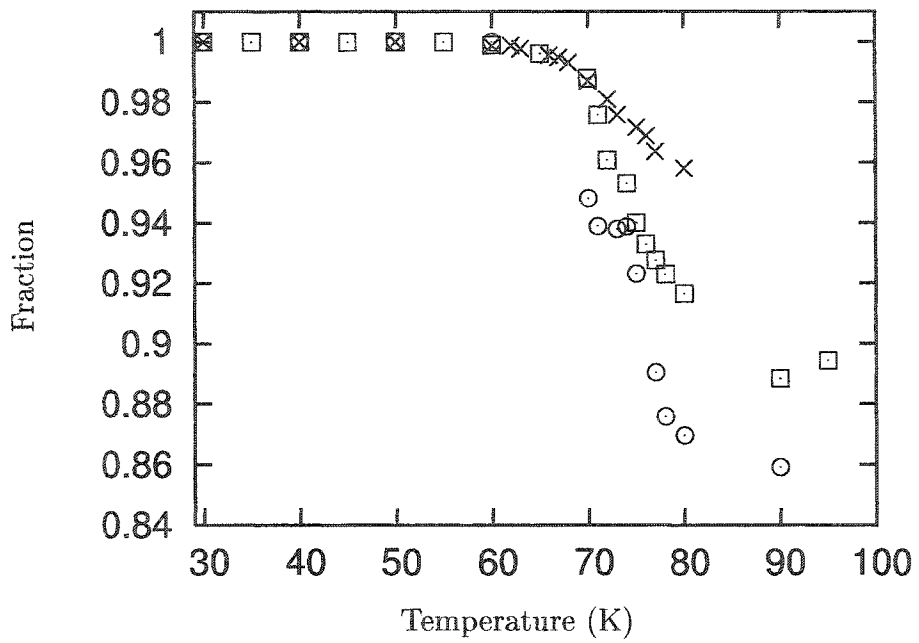

Figure 4.52: Fraction of the total number of atoms in the first layer for ρ = 1.14 (×), 1.22 (□), and 1.31 (○).

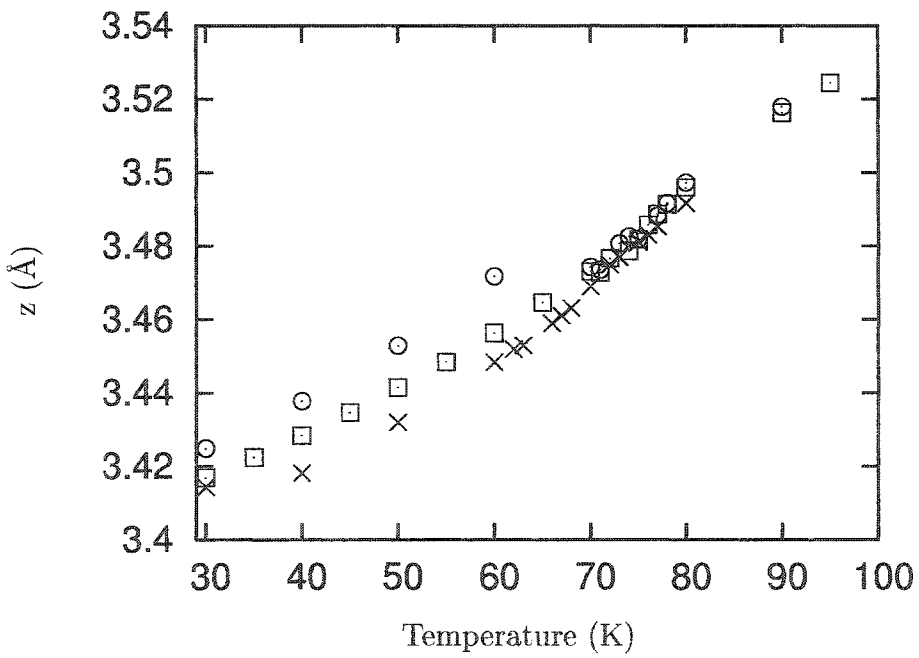

Figure 4.53: The average z position of the first layer for $\rho = 1.14$ (×), 1.22 (□), and 1.31 (○).

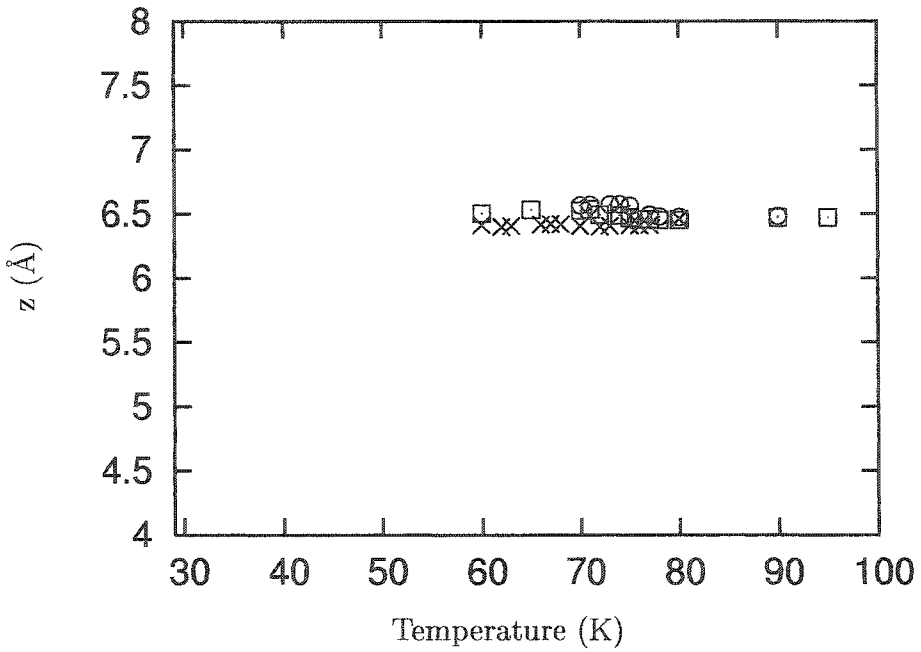

Figure 4.54: The average z position for the second layer for $\rho = 1.14$ (×), 1.22 (□), and 1.31 (○).

the lattice constant, figure 4.55. The lattice constant is almost constant for the temperatures below the onset of second layer promotion, but as more atoms are promoted into the second layer, the argon solid expands.

The promotion of the atoms to the second layer plays a large role in melting. Simulations were done with z fixed so that the atoms were not allowed to fluctuate in the z direction. The melting temperature increased in every case for the densities equal to and greater than 1.14, but for $\rho = 0.71$, the melting temperature remained constant, table 4.4. There is a remarkable density dependence of the melting temperature when z is fixed. While the increase in melting temperature was 15K for $\rho = 1.14$, and 18K for $\rho = 1.22$, it was 163K for $\rho = 1.31$. It is clear that the promotion of atoms into the second layer helps facilitate melting for complete monolayers.

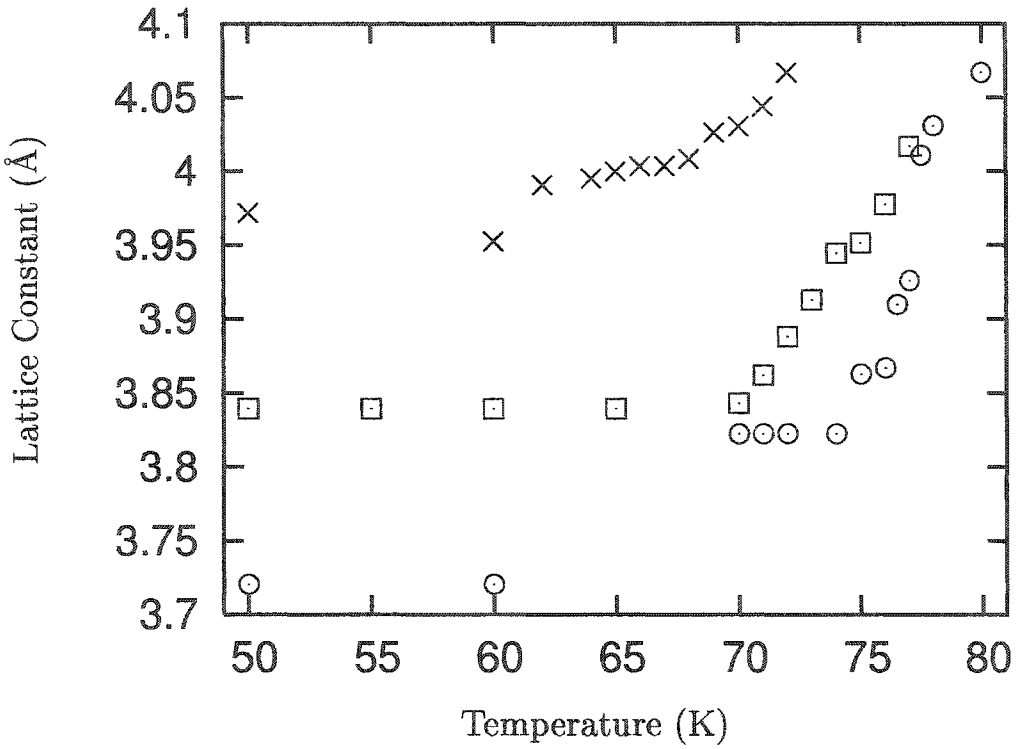

Figure 4.55: Lattice constant for $\rho = 1.14$ (×), 1.22 (□), and 1.31 (○).

Density	T_m	T_m z fixed
0.71	49K	49K
1.14	70K	85K
1.22	74K	92K
1.31	77K	240K

Table 4.4: The melting temperature for various densities with z fixed. The melting temperature increases for densities in which second layer promotion occurs.

4.5 Energy Terms

The temperature dependence of the energy gives clues about what is happening in the system. Since the specific heat is the temperature derivative of the average value of the internal energy, an inflection point in the average value of the internal energy occurs at a peak in the specific heat. Also, the average E1 energy can indicate a rotational transition since the average E1 energy decreases before the rotational transition and achieves a minimum value between the rotational transition and melting. The average value of E0 can indicate second layer promotion. For densities in which second layer promotion does not occur, the average value of E0 changes linearly with temperature, figure 4.57, 4.60, 4.63, 4.66. When second layer promotion does occur, the average value of E0 no longer changes linearly with temperature, figures 4.69, 4.72, 4.75. Because of the clues that the average value of the different energy terms gives about the argon graphite system, plots of the temperature dependence of all the different terms in the energy are shown in this section.

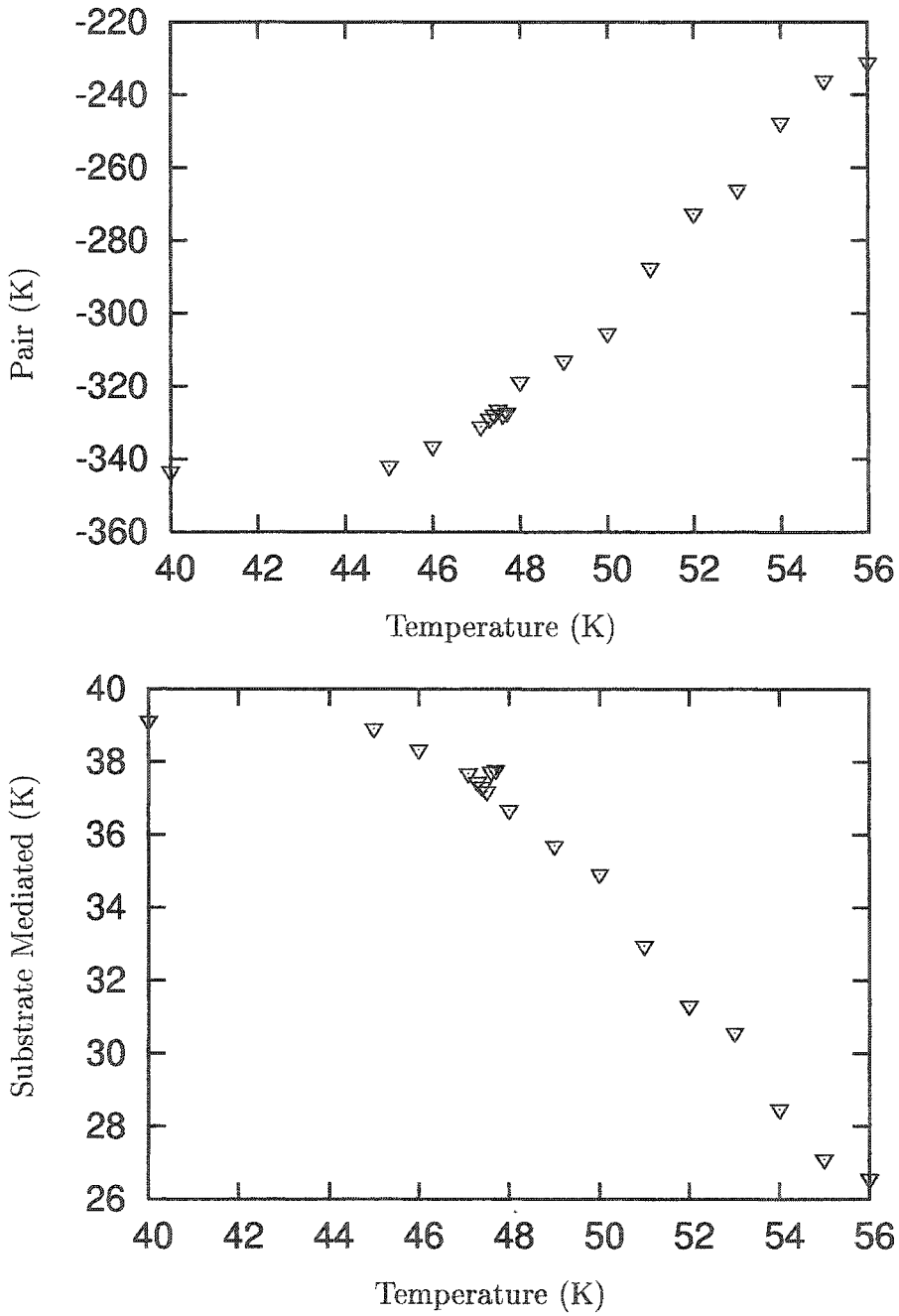

Figure 4.56: The average argon-argon energy (top) and the average substrate mediated energy (bottom) for $\rho = 0.39$.

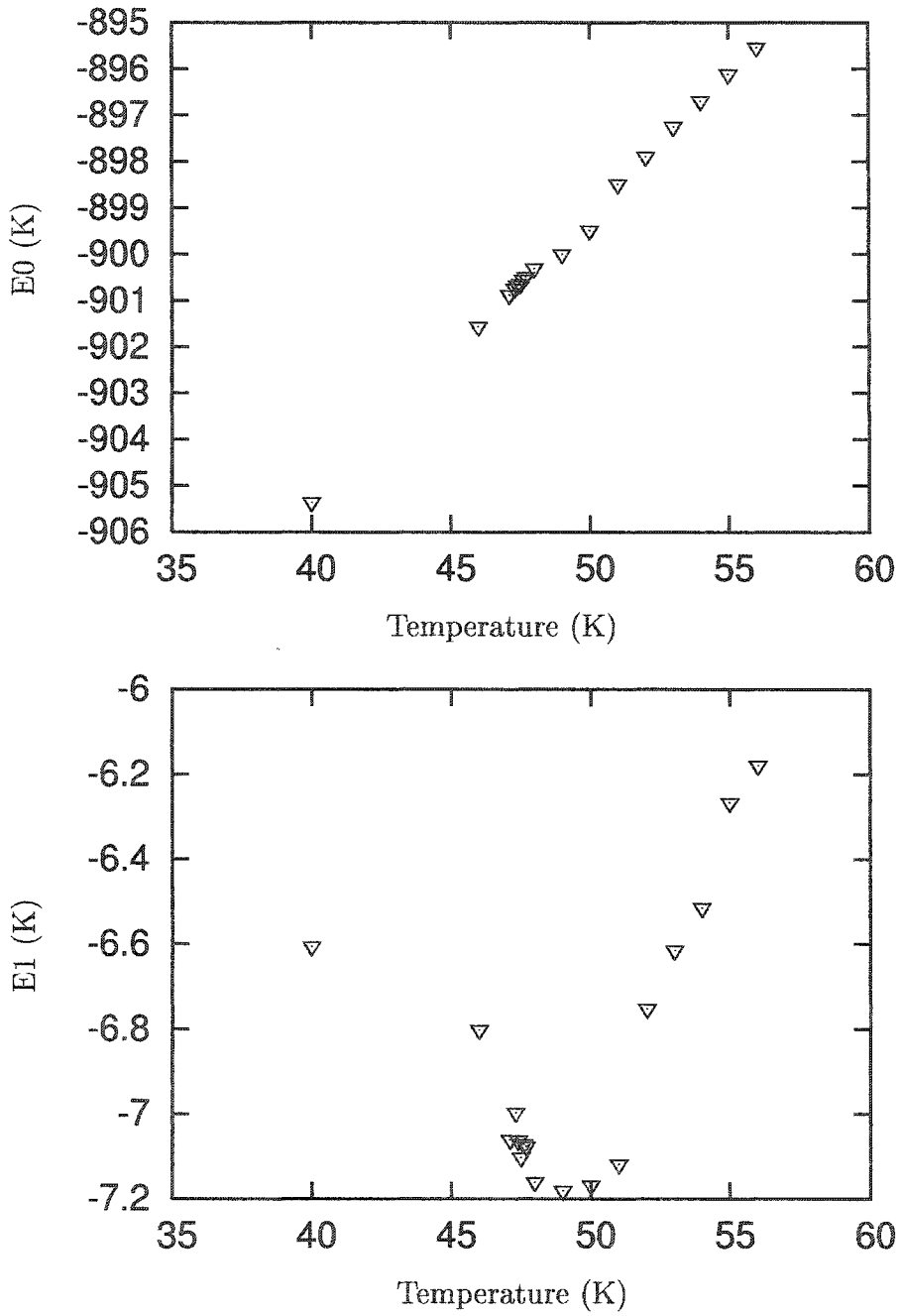

Figure 4.57: The average E0 energy (top) and the average E1 energy (bottom) for $\rho = 0.39$.

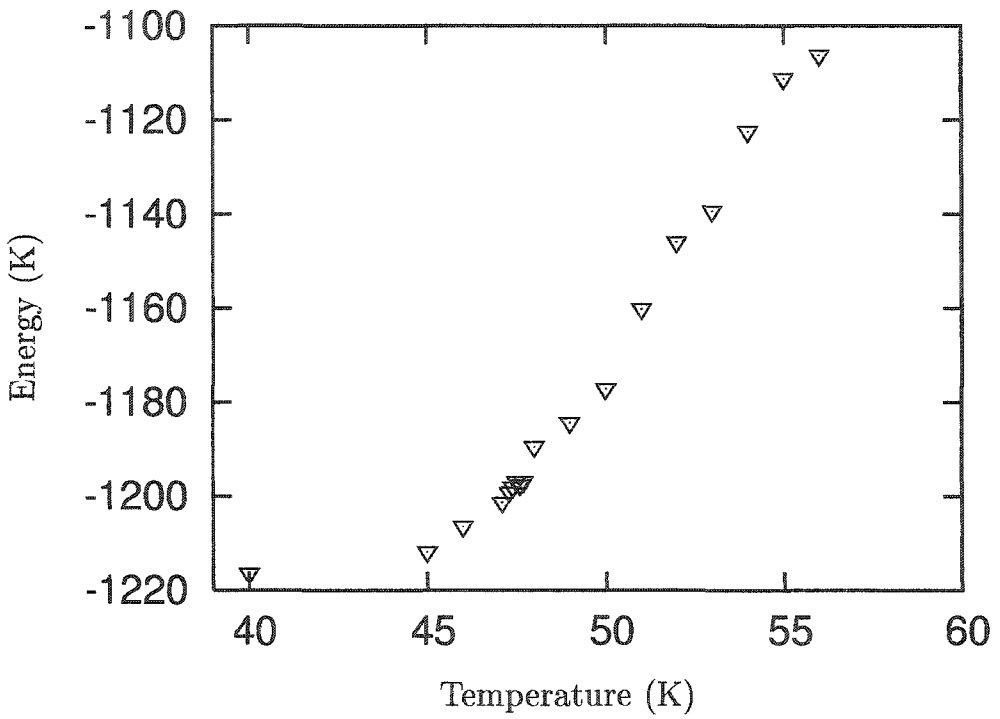

Figure 4.58: Sum of all the energy terms for $\rho = 0.39$.

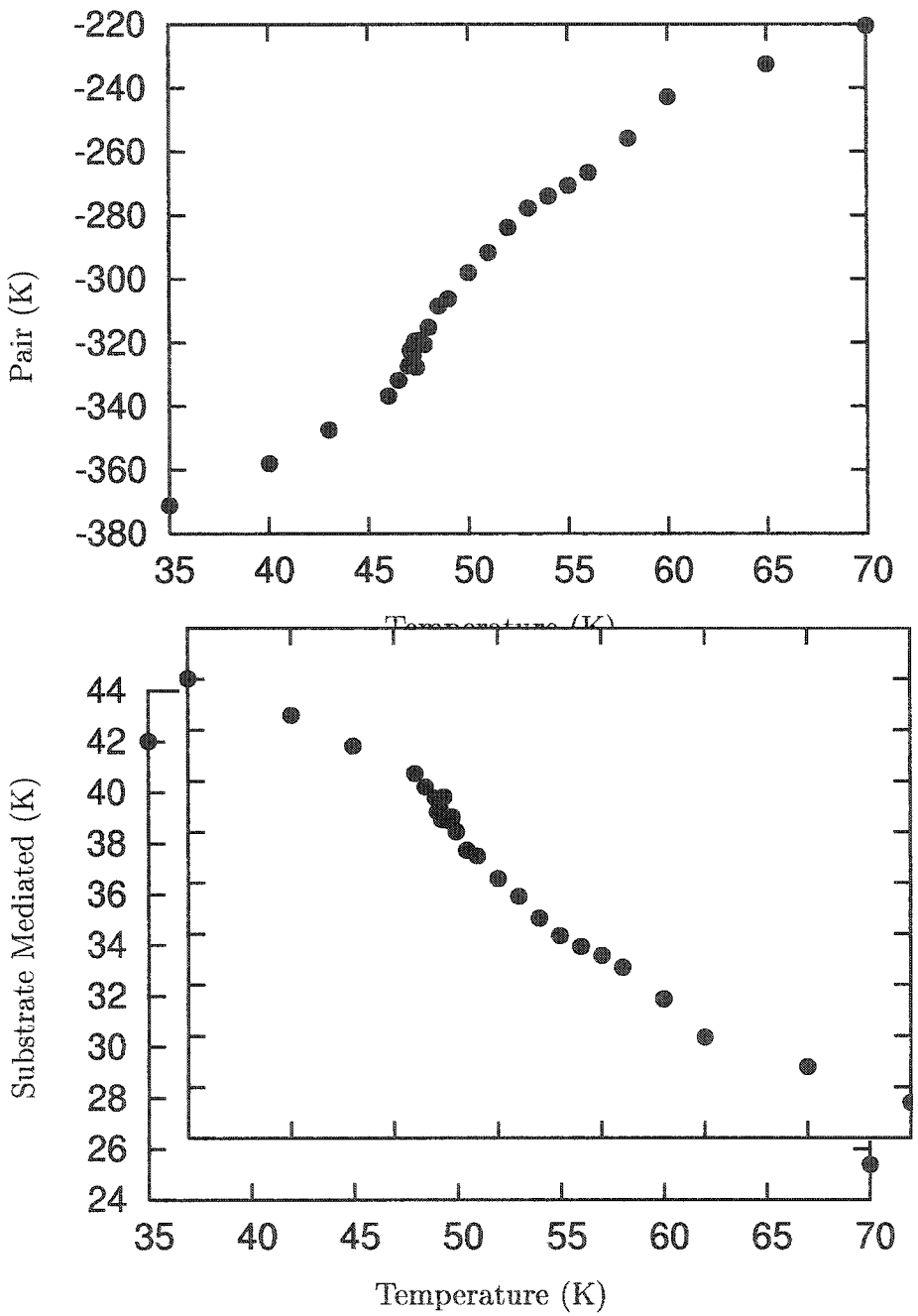

Figure 4.59: The average argon-argon energy (top) and the average substrate mediated energy (bottom) for $\rho = 0.71$.

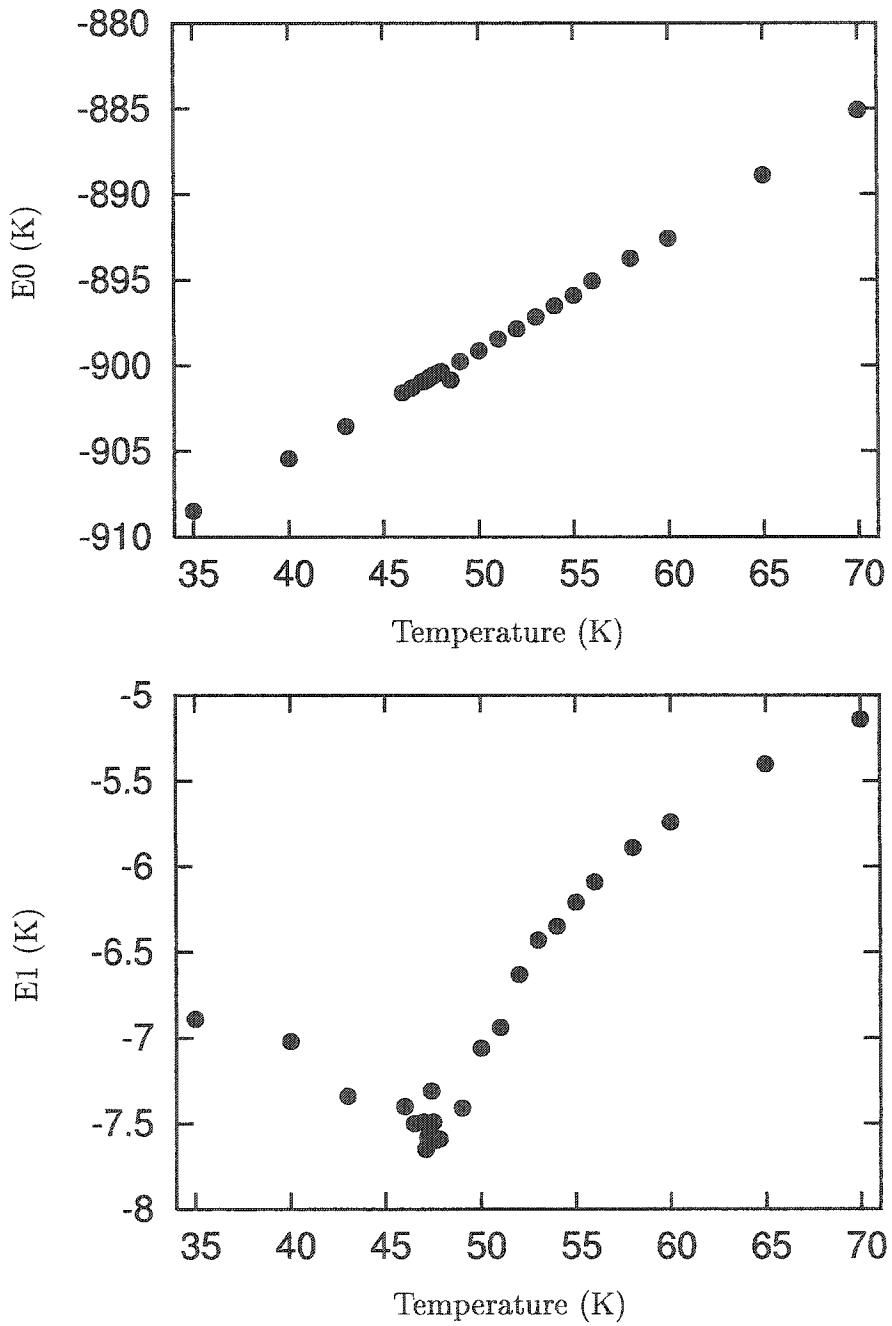

Figure 4.60: The average E0 energy (top) and the average E1 energy (bottom) for $\rho = 0.71$.

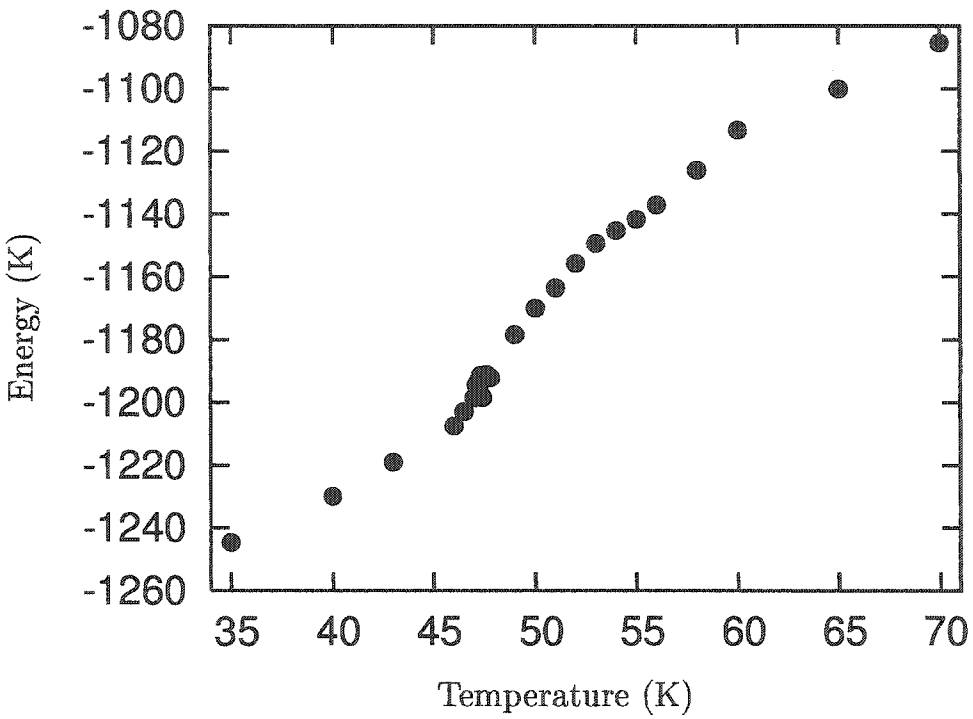

Figure 4.61: Sum of all the energy terms for $\rho = 0.71$.

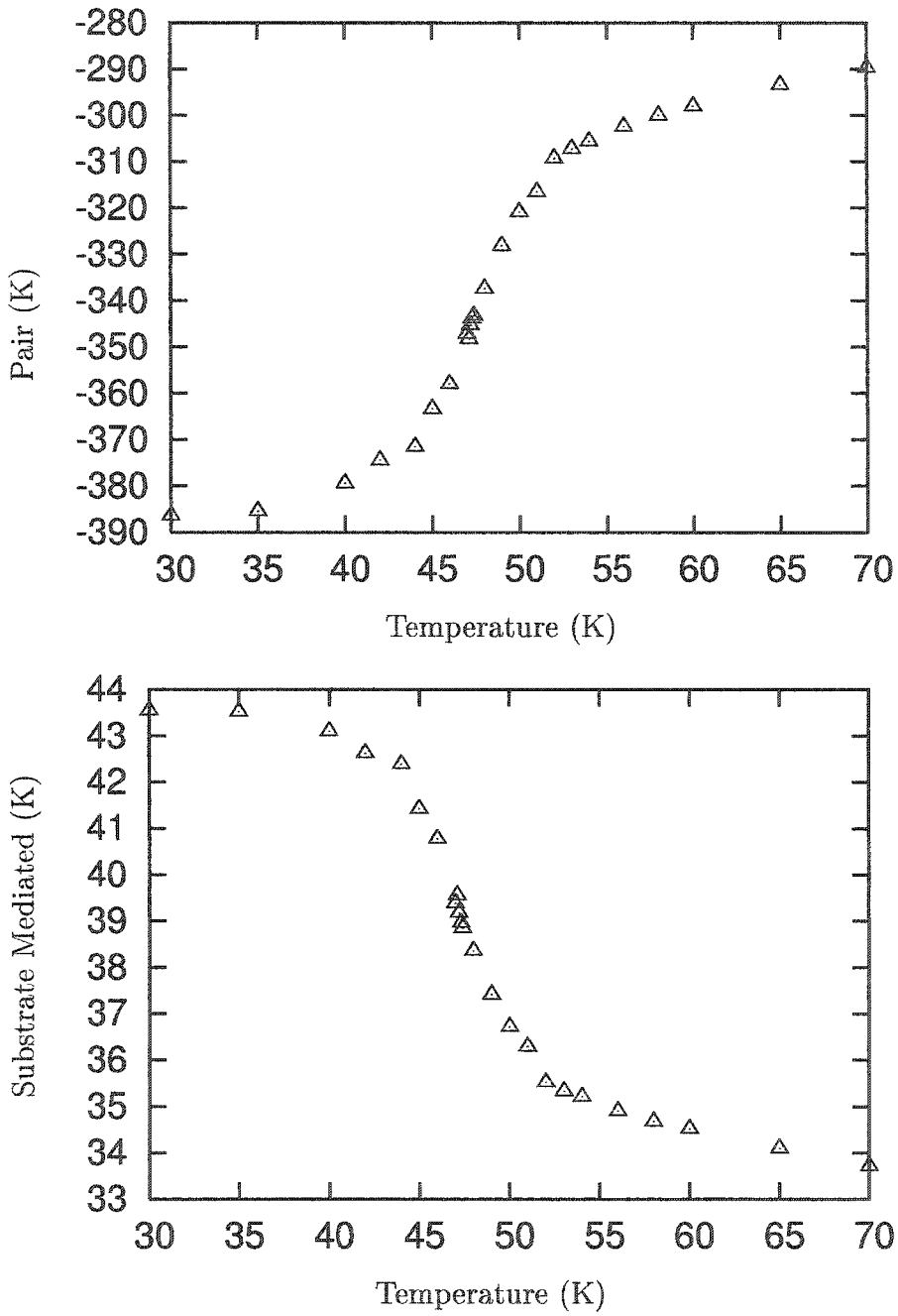

Figure 4.62: The average argon-argon energy (top) and the average substrate mediated energy (bottom) for $\rho = 1.00$.

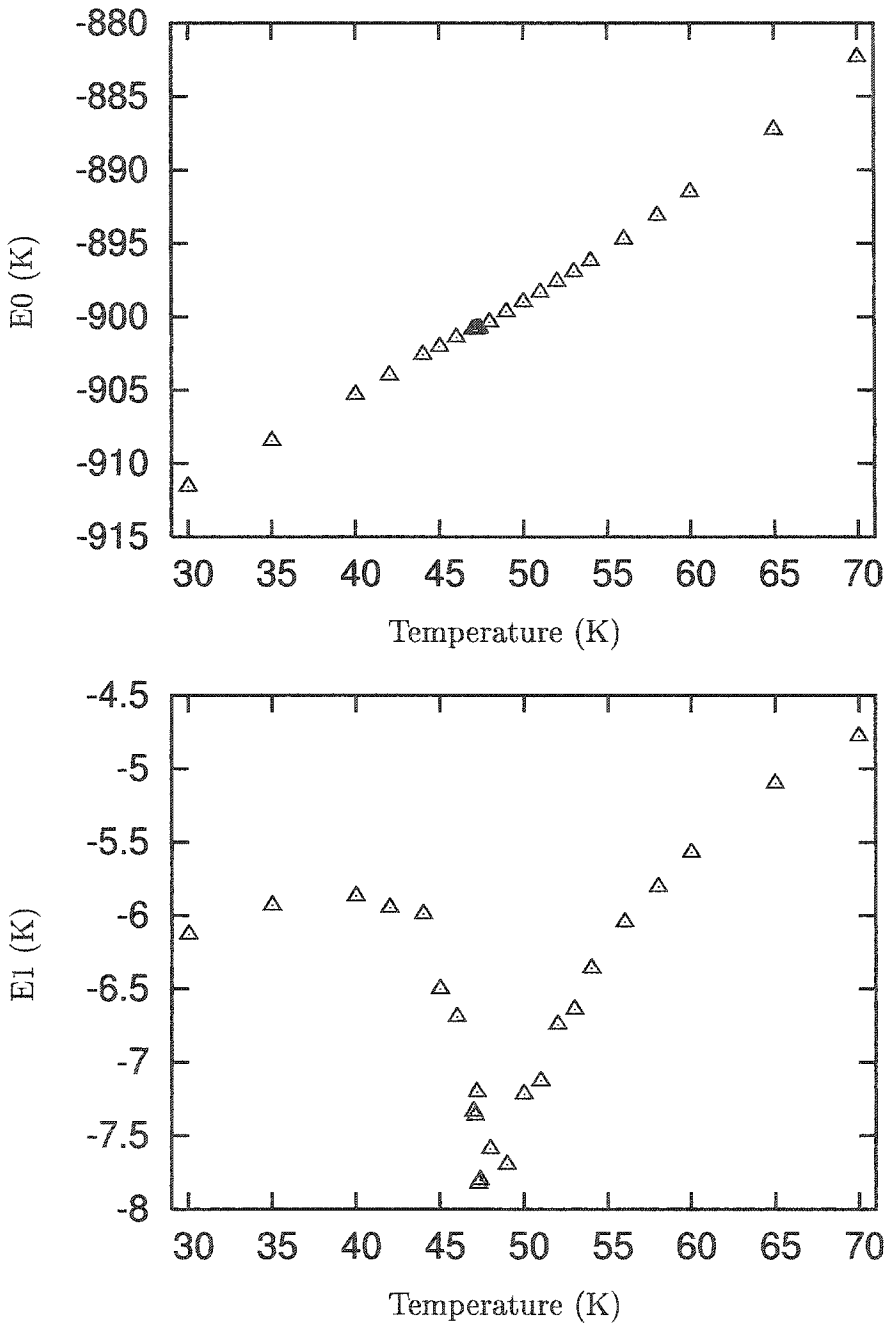

Figure 4.63: The average E0 energy (top) and the average E1 energy (bottom) for $\rho = 1.00$.

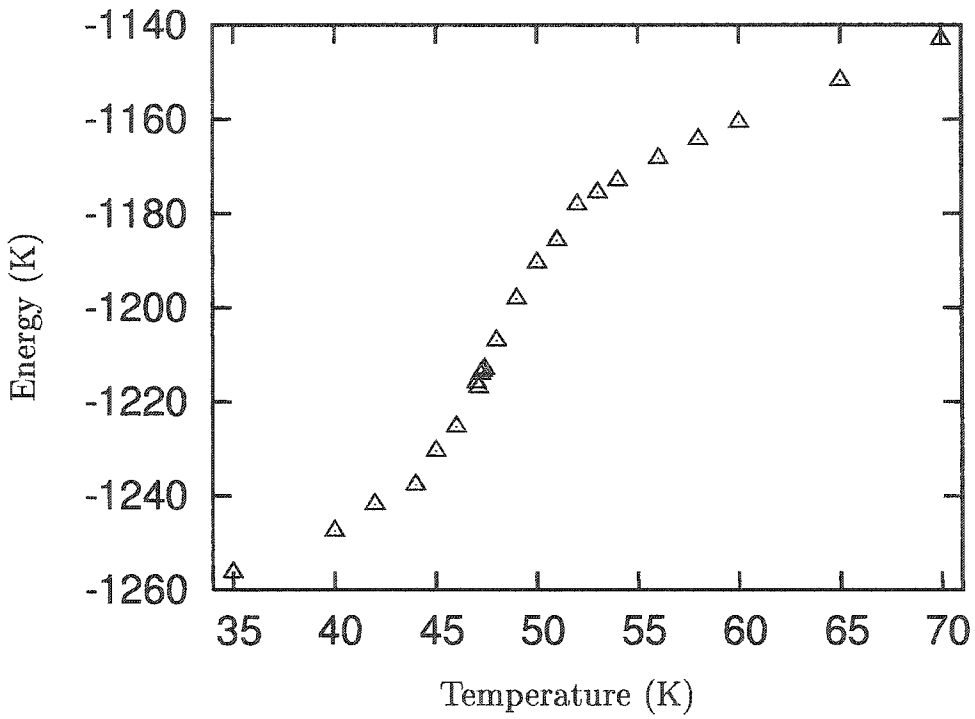

Figure 4.64: Sum of all the energy terms for $\rho = 1.00$.

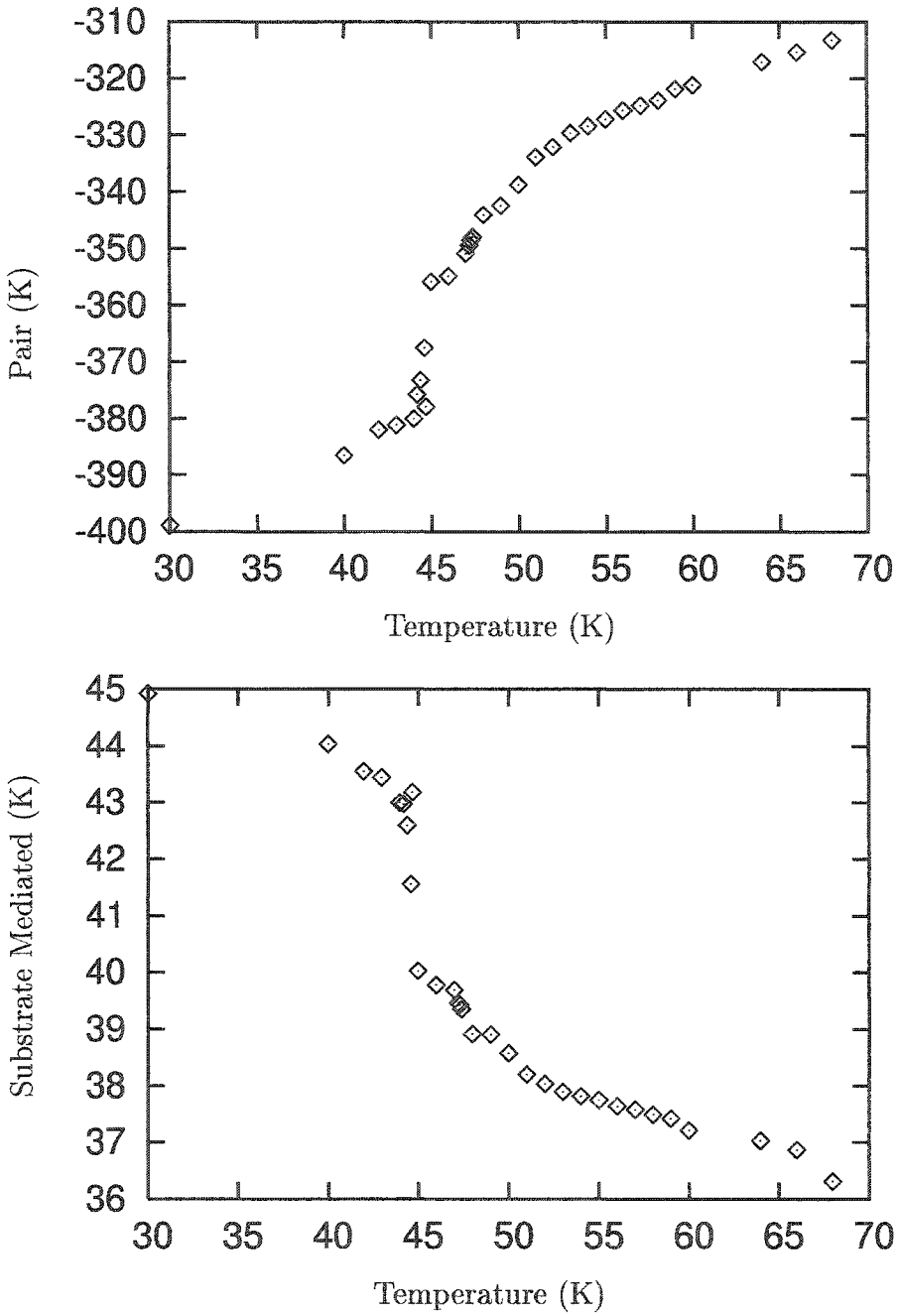

Figure 4.65: The average argon-argon energy (top) and the average substrate mediated energy (bottom) for $\rho = 1.07$.

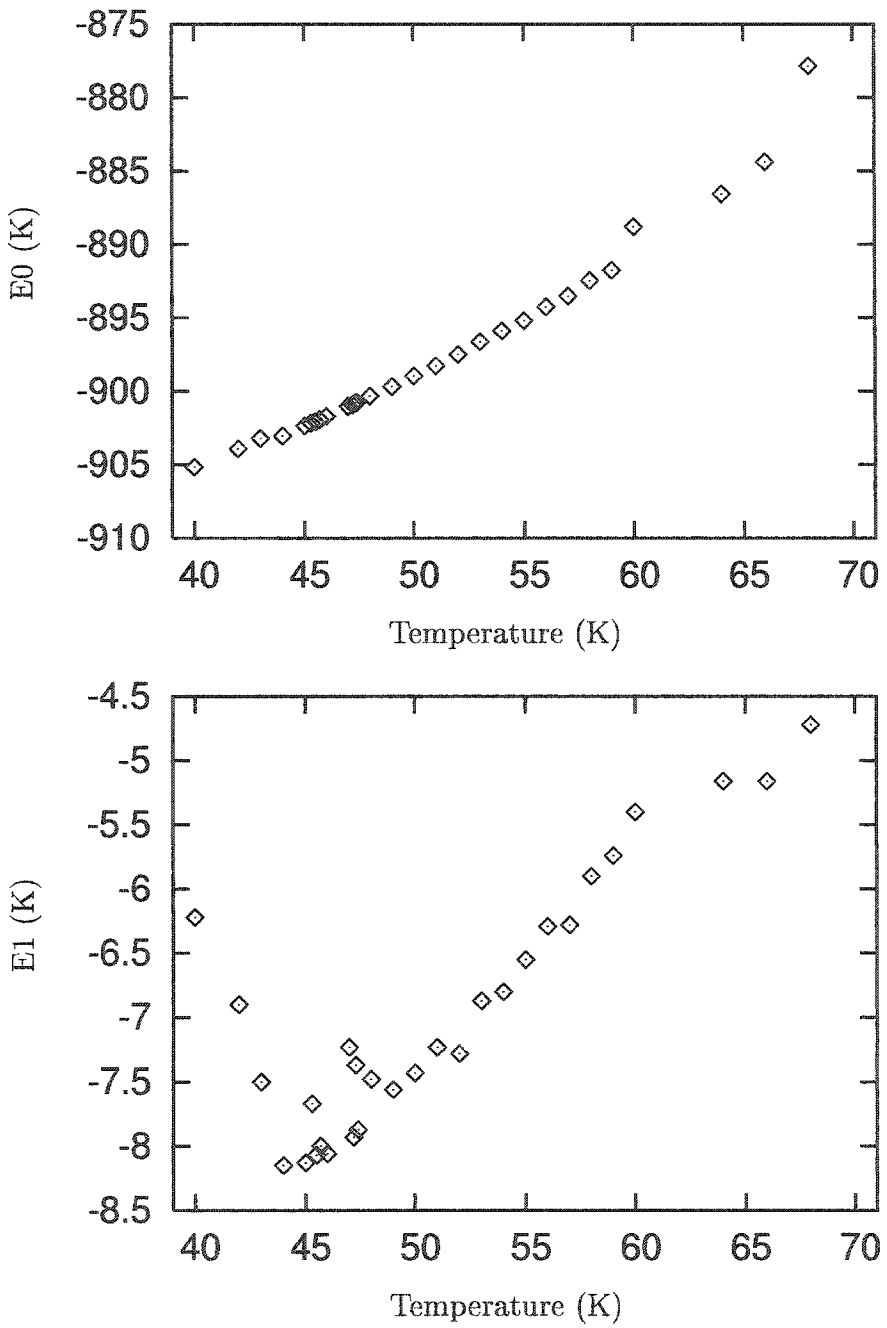

Figure 4.66: The average E0 energy (top) and the average E1 energy (bottom) for $\rho = 1.07$.

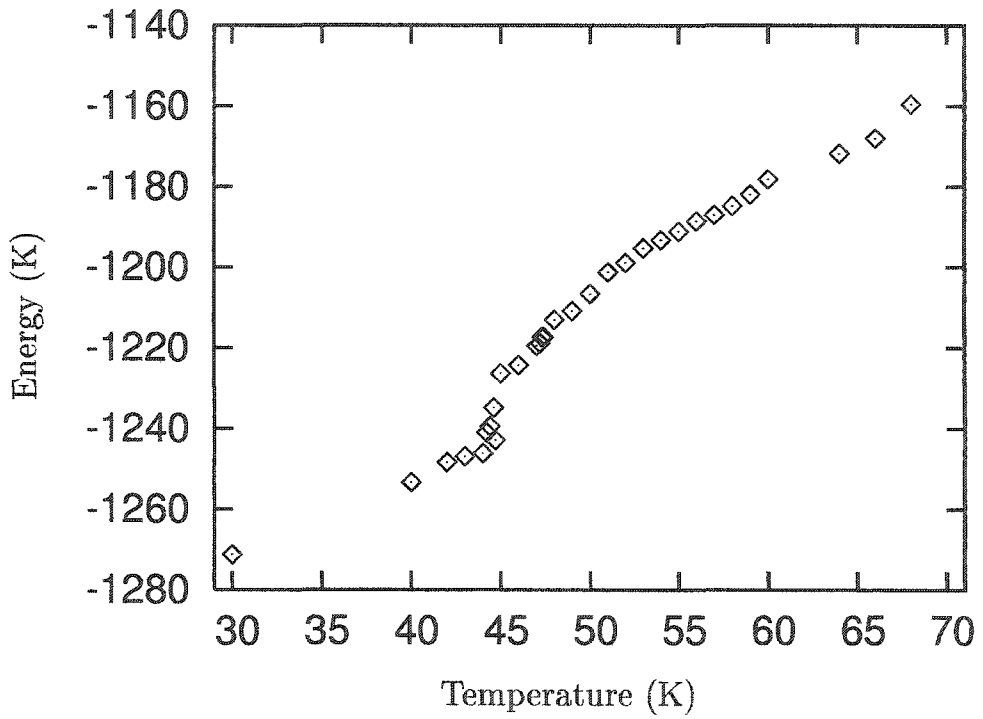

Figure 4.67: Sum of all the energy terms for $\rho = 1.07$.

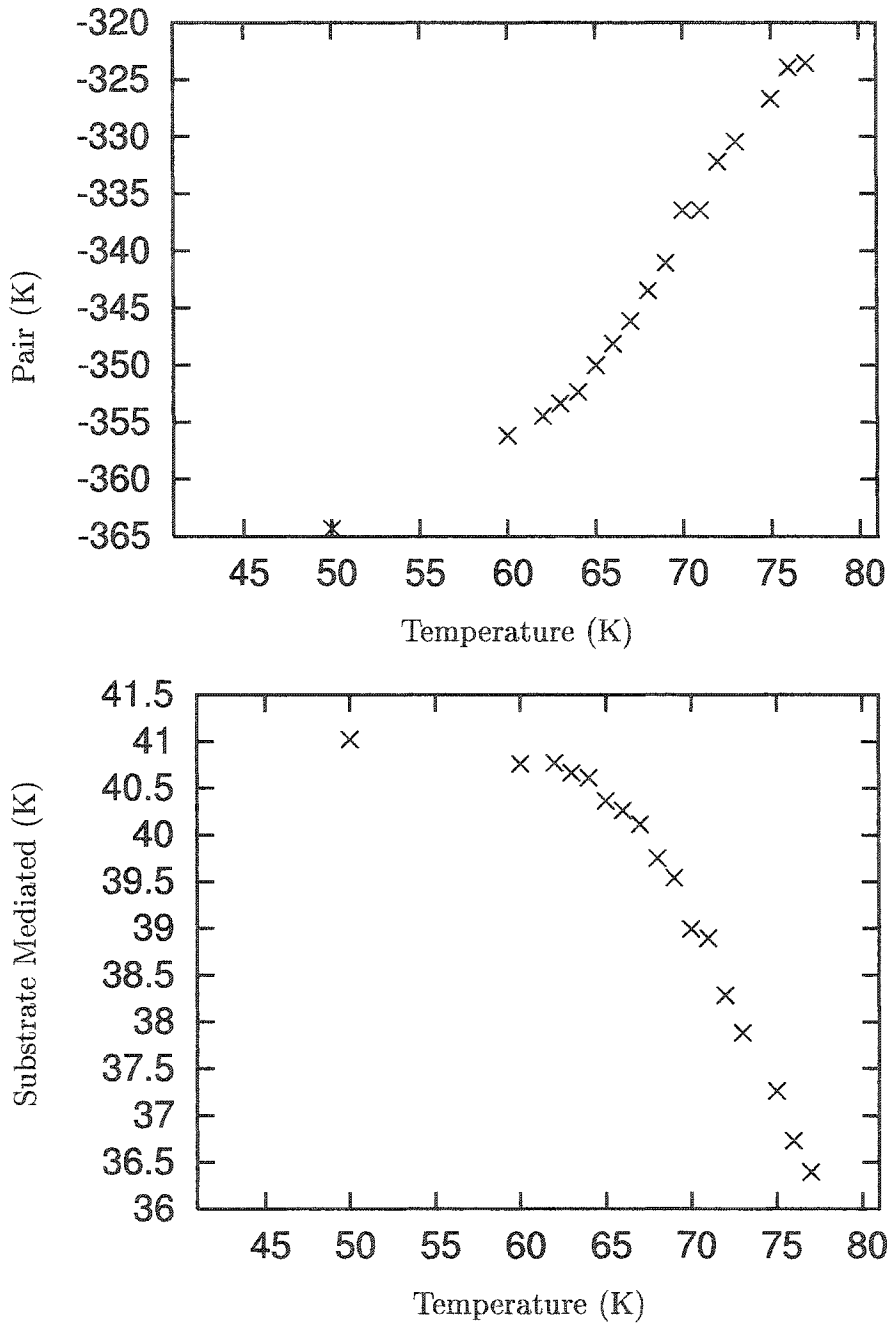

Figure 4.68: The average argon-argon energy (top) and the average substrate mediated energy (bottom) for $\rho = 1.14$.

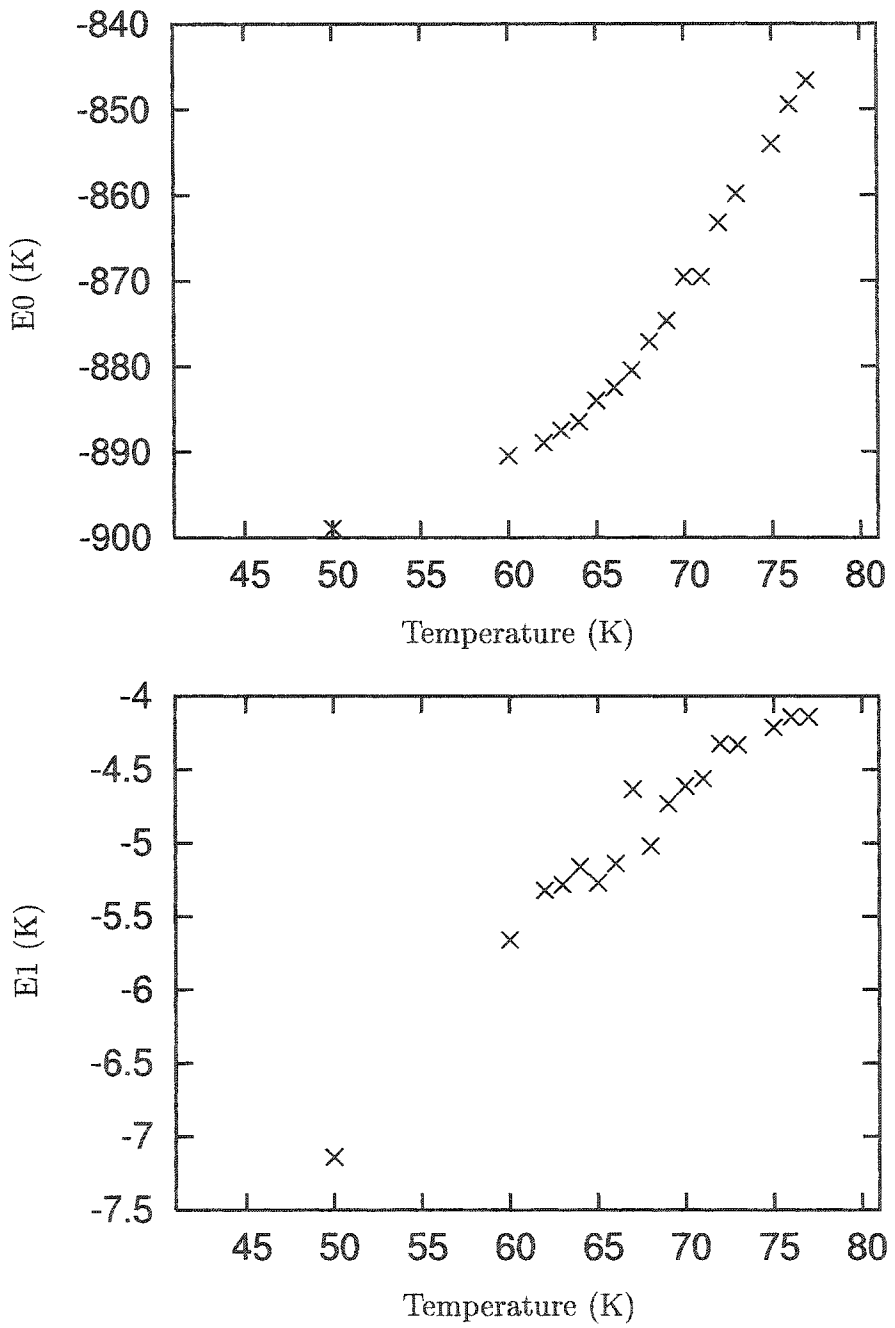

Figure 4.69: The average E0 energy (top) and the average E1 energy (bottom) for $\rho = 1.14$.

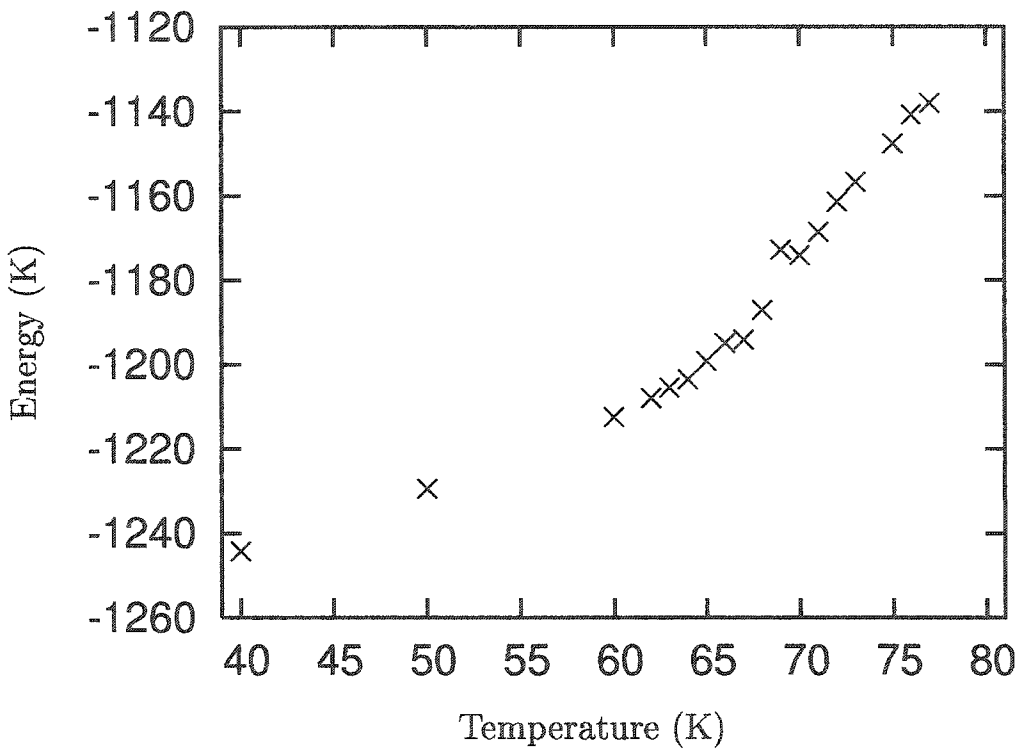

Figure 4.70: Sum of all the energy terms for $\rho = 1.14$.

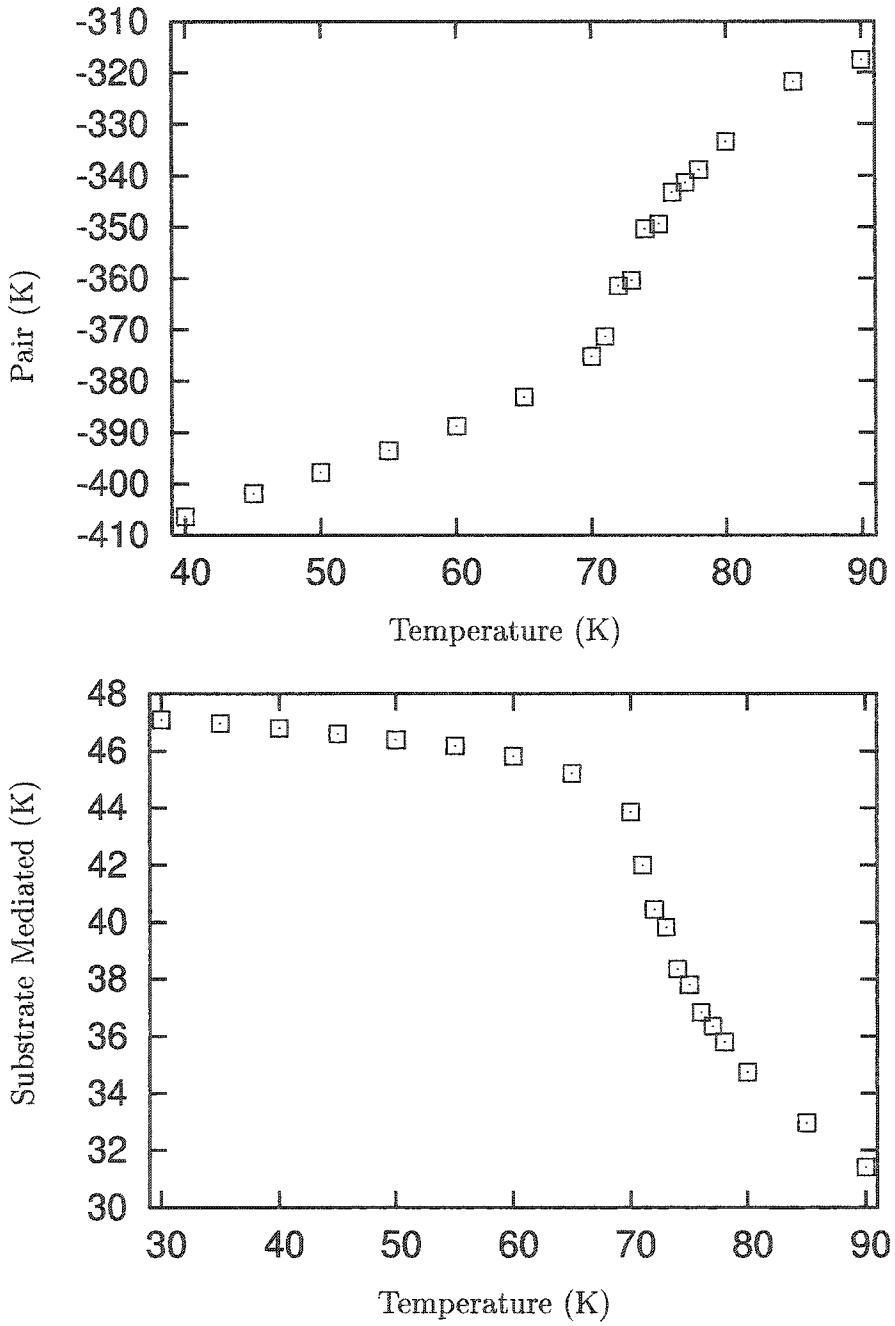

Figure 4.71: The average argon-argon energy (top) and the average substrate mediated energy (bottom) for $\rho = 1.22$.

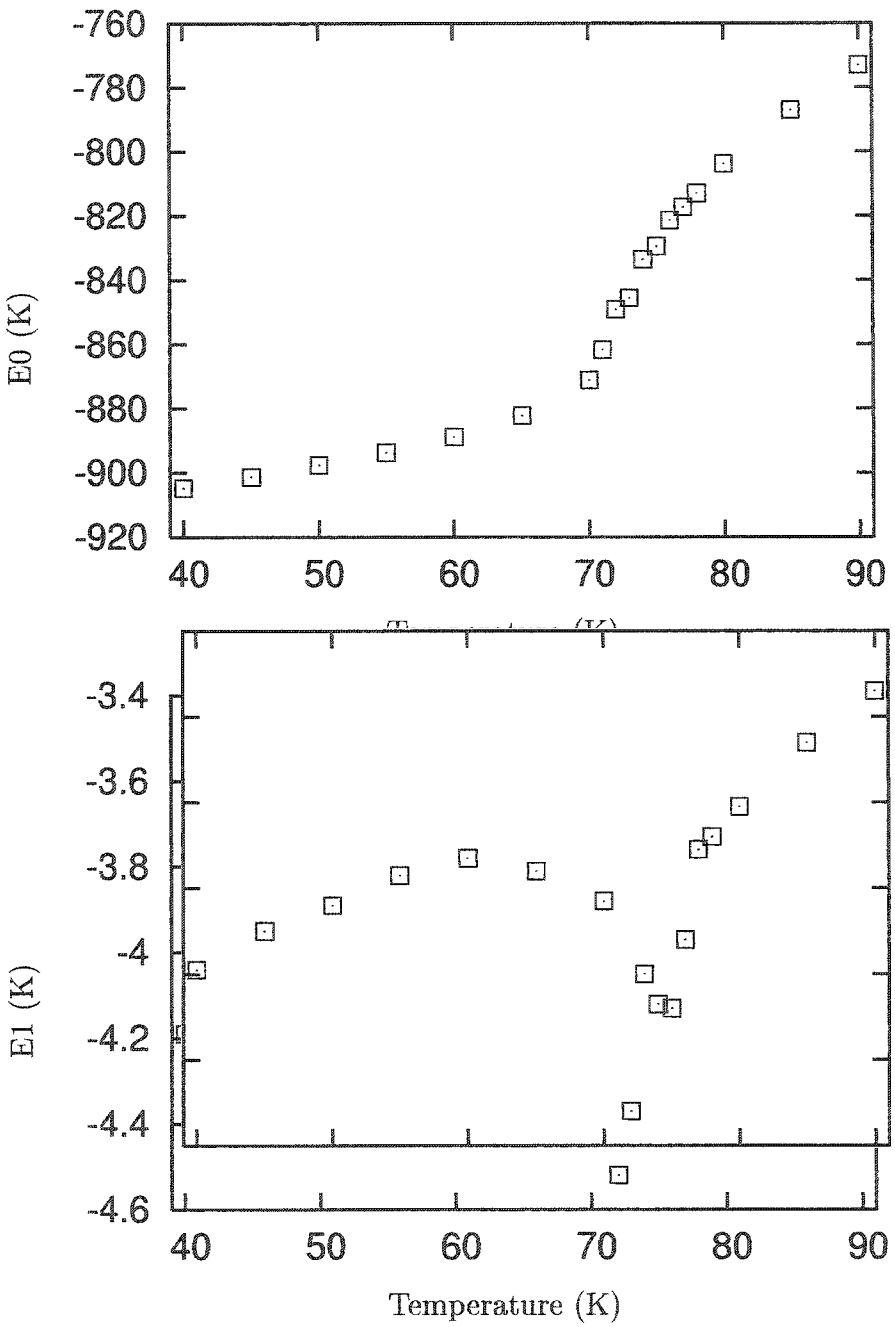

Figure 4.72: The average E0 energy (top) and the average E1 energy (bottom) for $\rho = 1.22$.

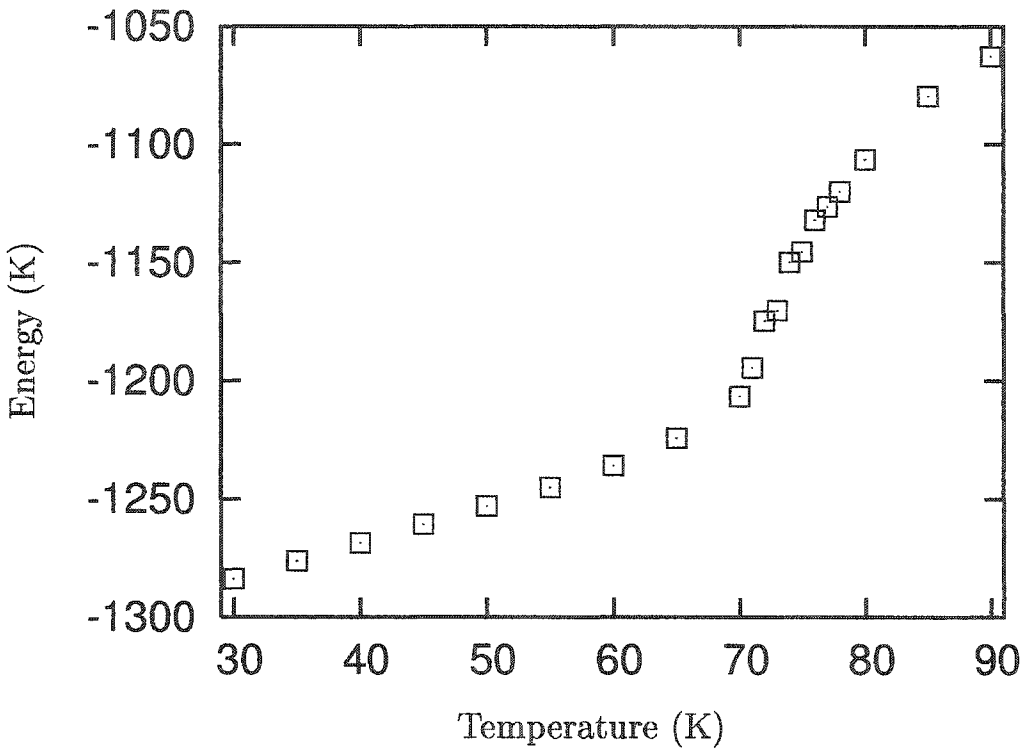

Figure 4.73: Sum of all the energy terms for $\rho = 1.22$..

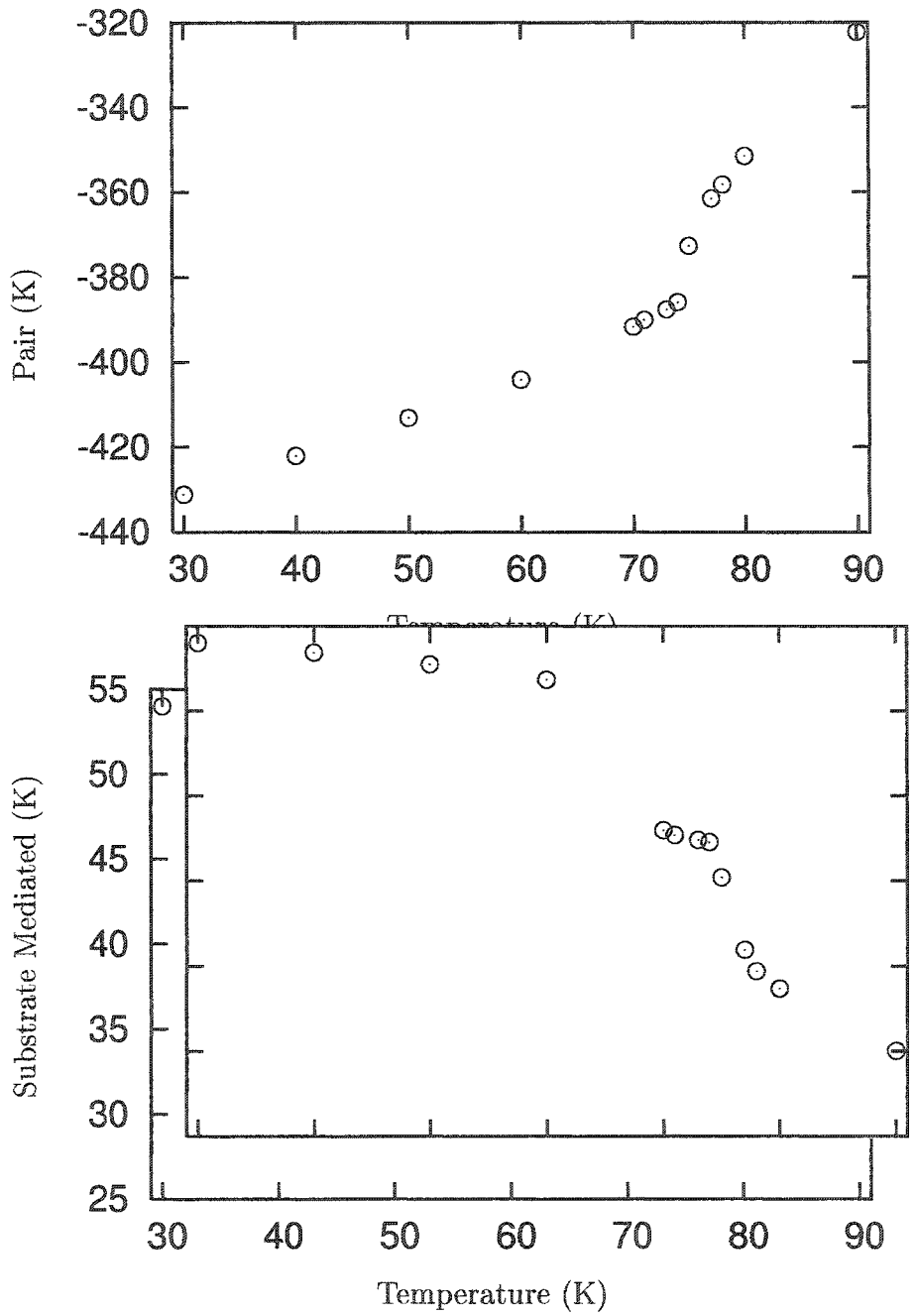

Figure 4.74: The average argon-argon energy (top) and the average substrate mediated energy (bottom) for $\rho = 1.31$.

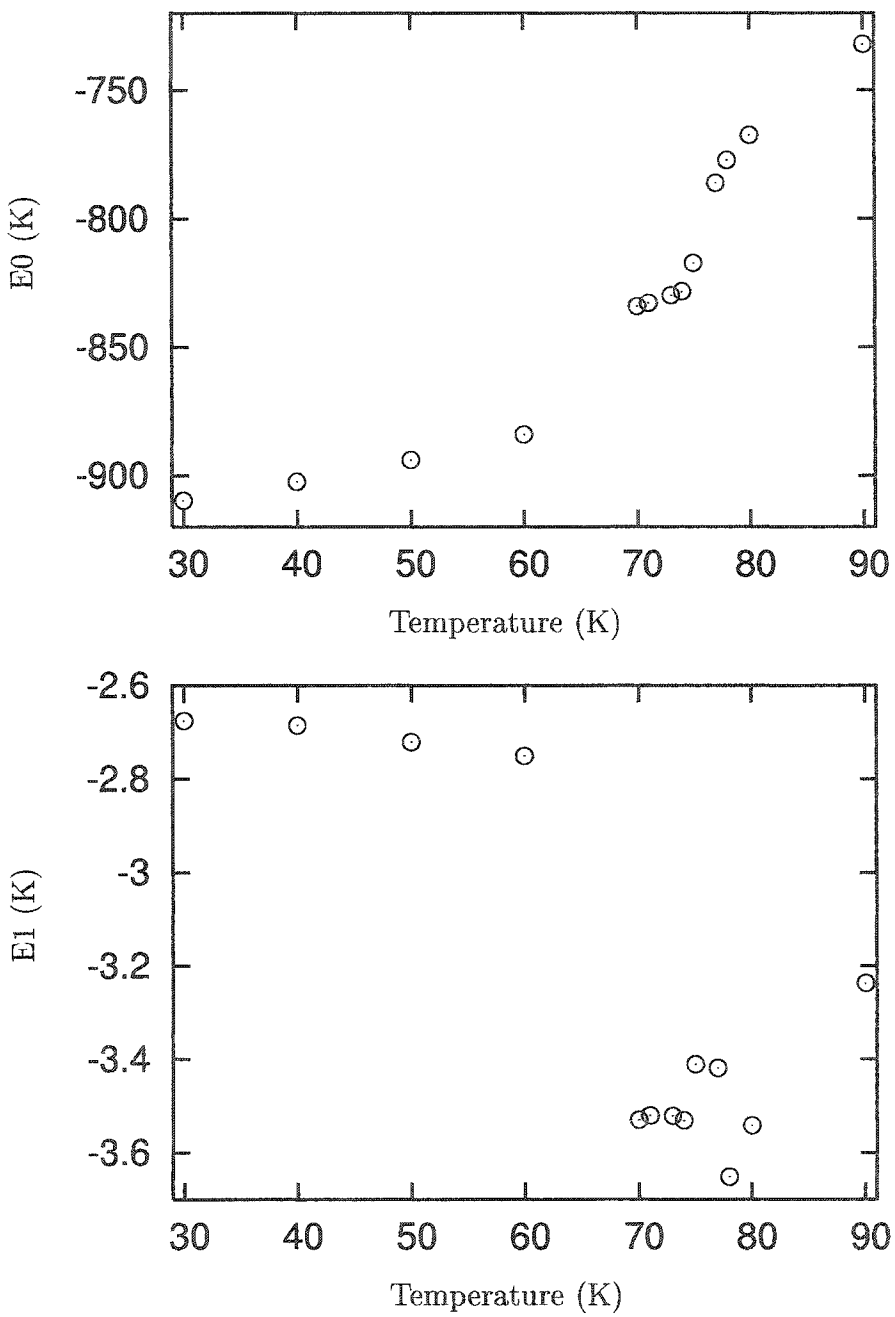

Figure 4.75: The average E0 energy (top) and the average E1 energy (bottom) for $\rho = 1.31$.

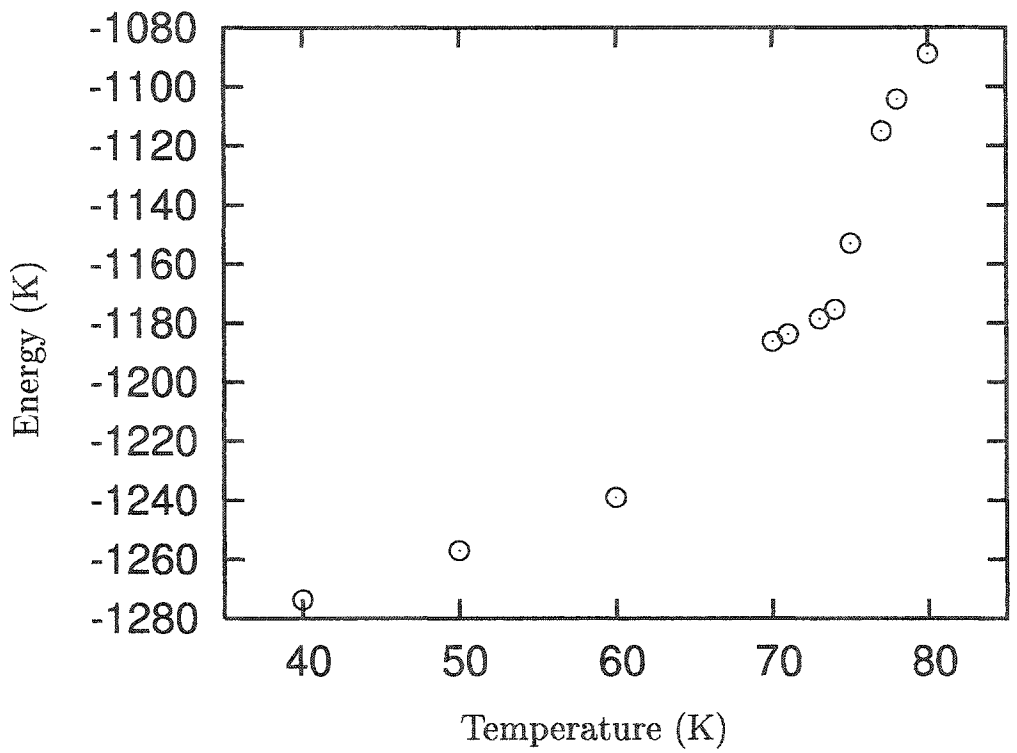

Figure 4.76: Sum of all the energy terms for $\rho = 1.31$.

Chapter 5

Discussion

These simulations have been able to accurately reproduce the experimental phase diagram for submonolayer and monolayer argon physisorbed on graphite. For $\rho \leq 1.00$ and below 47K, the argon atoms form a two dimensional solid which is rotated with respect to a $(\sqrt{3} \times \sqrt{3})$R30° symmetry direction. At $T = 47.4 \pm 0.2$K, for densities less than 1.07, the argon atoms undergo a phase transition in which the solid aligns with a symmetry direction of the graphite substrate. At the rotational transition there is also an increase in the rate of thermal expansion of the argon solid.

The rotation angle and the rotational transition is due to the competition between the pair interaction and the argon-substrate interaction. The argon atoms are displaced from the equilibrium positions they would have if there were no lateral variation of the substrate potential. The displacement results in the argon atoms being

more likely to be found in the center of the carbon hexagons, and could be due to the formation of mass density waves.

A calculation by Shiba[45] predicts that the rotation angle decreases as the lattice constant of the argon solid approaches the $\sqrt{3} \times \sqrt{3}$ value of 4.26Å. According to Shiba's theory, the argon solid aligns with a symmetry direction of the substrate when the lattice constant is 4.064Å due to the formation of hexagonal domains. Shiba's calculation utilizes continuum elasticity theory and is a zero temperature calculation, thus it does not include the effects of entropy. The rotational transition in this work occurs when the lattice constant has reached a value between 3.95Å and 3.99Å and appears to be more dependent on temperature than the lattice constant. Simulations with larger systems would have to be done to determine if the formation of hexagonal domains played a role in the rotational transition. It is interesting to note that xenon aligns with the substrate well before melting at submonolayer densities, even though thermal expansion causes the misfit to increase with increasing temperature. Knowledge of why xenon aligns with the substrate would shed light onto why argon undergoes a rotational transition.

X-ray results at $\rho = 0.7$ suggest that the submonolayer solid argon does not undergo a rotational transition before melting. Rather the rotation angle and the lattice constant evolves continuously through the melting transition[14], figure 5.1. This is in contrast to what is observed in this work, figure 5.2, where the rotation angle suddenly goes to zero below melting and at the sharp specific heat peak, and the lattice

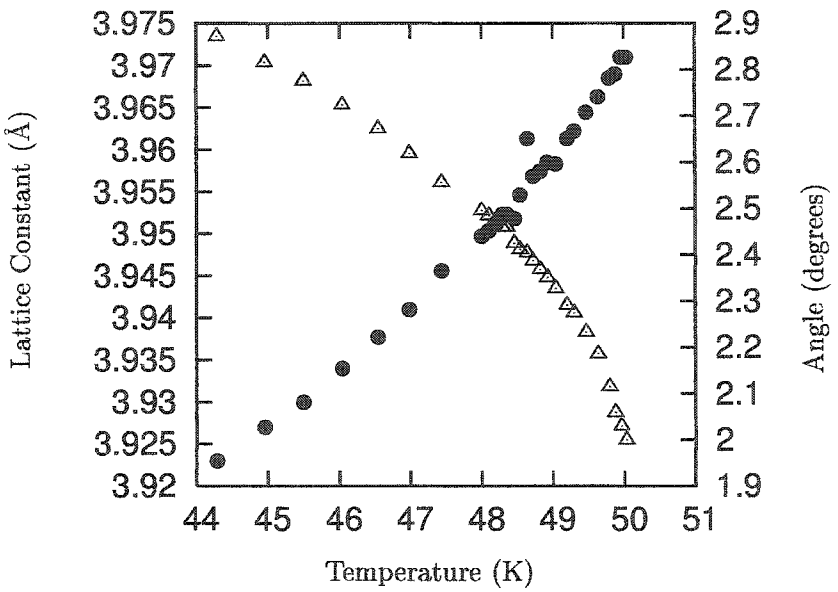

Figure 5.1: The rotation angle (△) and the lattice constant (•) obtained from the x-ray scattering experiment from a single crystal by D'Amico[14] for a density of 0.7.

constant appears to evolve continuously, although there is a sudden increase in the rate of thermal expansion at the sharp specific heat peak. In previous calculations, in which the substrate mediated potential and the argon-graphite potential was 15% stronger than in these calculations, there was a small jump in the lattice constant at the rotational transition. Also, the rotational transition was at 43.7K, 3.6K lower temperature than in these simulations. It is not known why the scattering experiments differ from these results. One possible explanation may be due to impurities in the absorbed argon. In 1998 Ma[9] measured the specific heat of argon-xenon and argon-methane mixtures, and found that the sharp specific heat peak disappeared for a xenon molar concentration of 0.015 and a methane molar concentration of 0.07.

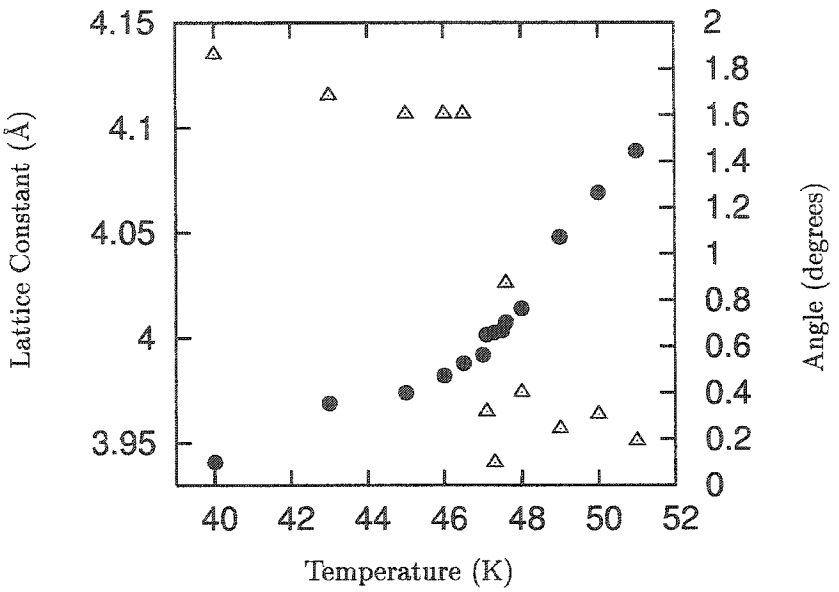

Figure 5.2: The rotation angle (△) and the lattice constant (•) for $\rho = 0.71$ from these calculations.

Thus the cause of the narrow specific heat peak is affected by impurities in the argon gas, and the impurities inhibit the rotational transition.

For densities less than and equal to 1.00, there is a change in the thermal expansion at the sharp specific heat peak. Above $\rho = 1.14$, the melting temperature depends on density and is between 70K and 80K. For a density between 1.07 and 1.14, the thermal expansion of the lattice causes the atoms to cover the whole substrate before melting. For densities greater than and equal to 1.14, the argon solid covers the whole surface at all temperatures in which the solid is present. Once the atoms cover the graphite surface, the expansion of the argon solid is restricted. The atoms tend to move perpendicular to the graphite substrate to allow the solid to expand, but motion perpendicular to the substrate costs more energy than motion parallel to the substrate. This may effect the rotational transition. At the rotational transition,

there is an increase in the rate of thermal expansion of the argon solid. For submonolayers, the increase in the rate of thermal expansion results in an increase in the pair energy, but this is partially offset by a decrease in the substrate energy. For complete monolayers, second layer promotion occurs before melting, and the solid first layer expands when second layer promotion occurs. Thus, if the rate of thermal expansion were to increase, the number of atoms promoted to the second layer would also increase. Because of the relatively large energy cost of second layer promotion, this could inhibit any phase in which there is an increase in the rate of thermal expansion.

For densities equal to and above 1.14, some atoms are promoted to a second layer before melting. The effect on the first layer of promoting the atoms into the second layer is that the lattice constant of the first layer increases, i.e. the two-dimensional solid is allowed to expand. At monolayer completion, the argon solid cannot expand unless atoms are promoted to a second layer, but there needs to be enough thermal energy for second layer promotion to occur. At some temperature between 60K and 70K, there is enough thermal energy, and the atoms start to populate a second layer. This allows the first layer to expand and increases the space available for self diffusion of the argon atoms. The importance of second layer promotion was demonstrated by conducting simulations in which the atoms were not allowed to fluctuate perpendicular to the substrate. The melting temperature increased if the atoms were not allowed to move perpendicular to the substrate, and the increase was very dramatic for the higher densities.

Migone and Chan[6] argued that the melting of argon absorbed on graphite is first order, because they identified the narrow specific heat peak with melting. In this work, it was shown that the broad specific heat peak is associated with the melting transition, and the narrow specific heat peak is not associated with melting, but rather a rotational transition. If the narrow specific heat peak is not attributed to the melting transition, all the other experimental evidence suggests a continuous melting transition. The structure factor peak evolves continuously through the melting transition[11, 14], and the peak in the compressibility at the melting transition is twenty times smaller than the methane on graphite[8], a known first order transition.

While it is impossible to prove the order of the melting transition in these simulations, some evidence of the order of the transition can be obtained from these simulations. The order parameter Ψ_6 evolves continuously through the melting transition in a temperature interval of 10K around the melting transition. In comparison, in simulations of 256 N_2 molecules absorbed on graphite[46], Ψ_6 evolved from the high temperature value to the low temperature value in a range of 2K. Thus for simular system sizes, the evolution of the order parameter for a known first order transition occurs overs a much smaller temperature interval. Also, examination of the pair distribution function, and examination of the particle configurations all suggest a continuous melting transition of argon absorbed on graphite.

The theory of Kosterlitz, Thouless, Halperin, Nelson, and Young (KTHNY) provides a description of continuous melting transition which requires two second-order

transitions. The theory is difficult to test in computer simulations, and requires simulations of large systems so that the long range decay of correlation functions can be measured accurately. The KTHNY theory predicts an unobservable essential singularity in the specific heat at the critical point, and a broad specific heat peak associated with the gradual unbinding of disclinations. The specific heat measured in these simulations is similar to what would be expected if argon on graphite underwent dislocation mediated melting according to the KTHNY theory.

These simulations have been able to answer a long standing question about the interpretation of Migone's specific heat results. Since all the other rare gas atoms on graphite exhibit first order melting, the narrow specific heat peak was originally associated with the melting transition. We know that the broad peak must be melting, and the narrow peak is associated with a change in the rotation angle and a change in the rate of thermal expansion in these simulations. For densities between 0.39 and 1.00, the argon solid undergoes a rotational transition at 47.3K to a two-dimensional solid phase which is aligned with a symmetry direction of the graphite substrate. We have also been able to show the importance of the motion of the absorbed atoms in the direction perpendicular to the substrate on the melting of complete monolayers since the atoms in the first layer have more room to self diffuse.

Chapter 6

Summary

This work was conducted to provide a better understanding of the behavior of submonolayer and monolayer argon absorbed on graphite. A Monte Carlo simulation utilizing accurate potentials was conducted to allow for a quantitative comparison with experiment. The simulations reproduced many aspects of the system very accurately. The calculated specific heat and lattice constant, corrected for size effects, were within the experimental values for the densities in which experimental information was available. The calculated specific heat also agreed very well with the specific heat experiment of Migone[6, 44]. For submonolayers, we calculated the narrow, 0.3K full width at half maximum (FWHM), specific heat peak at around 47.3K and the broad, 10K FWHM, specific heat peak at around 50K which was measured by Migone. It was found that the narrow specific heat peak was due to a rotational transition, where the argon solid rotates from an angle of between 1.6° and 2.5°, depending on density,

with respect to a symmetry direction of the substrate to aligned with a symmetry direction of the substrate. At the narrow specific heat peak, there was also a small, but abrupt, change in the rate of thermal expansion of the argon solid. Melting, which is identified with the loss of six-fold bond orientational order, occurred at the same temperature as the broad specific heat peak, and occurred around 50K.

For densities greater than one monolayer, the melting temperature was higher for the higher densities. It was found that the promotion of atoms into a second layer played an important role in melting for densities greater than a monolayer. At a temperature between 60K and 70K, the atoms started to populate a second layer, and the first layer argon solid expanded when the second layer promotion occurred. For simulations in which the atoms were not allowed to fluctuate in the direction perpendicular to the substrate, the melting temperature increased for densities in which second layer promotion was observed, but the melting temperature did not change for the densities in which second layer promotion did not occur. Thus second layer promotion is important in the melting of complete monolayers.

Bibliography

[1] J. M. Kosterlitz and D. J. Thouless. *J. Phys. C*, **6**:1181, 1973.

[2] D. R. Nelson and B. I. Halperin. *Phys. Rev. B*, **19**:2457, 1979.

[3] A. P. Young. *ibid*, **19**:1855, 1979.

[4] P. A. Heiney, R. J. Birgeneau, G. S. Brown, P. M. Horn, D. E. Moncton, and P. W. Stephens. *Phys. Rev. Lett.*, **48**:104, 1982.

[5] J. A. Litzinger and G. A. Stewart. *Ordering in Two Dimensions.* North-Holland, 1980.

[6] Z. R. Li A. D. Migone and M. H. W. Chan. *Phys. Rev. Lett.*, **53**:810, 1984.

[7] M. Nielsen, J. Als-Nielsen, J. Bohr, J. P. McTague, D. E. Moncton, P. W. Stephens. *Phys. Rev. B*, **35**:1419, 1987.

[8] Q. M. Zhange and J. Z. Larese. *Phys. Rev. B*, **43**:938, 1991.

[9] E. D. Carter J. Ma and H. B. Kleinberg. *Phys. Rev. B*, **57**:9270, 1998.

[10] T. T. Chung. *Surf. Sci.*, **87**:348, 1979.

[11] J. Bohr J. P. McTague, J. Als-Nielsen and M. Nielsen. *Phys. Rev. B*, **25**:7765, 1982.

[12] S. C. Fain C. G. Shaw and M. D. Chinn. *Phys. Rev. Lett.*, **41**:955, 1978.

[13] J. P. McTague and A. D. Novaco. *Phys. Rev. B*, **19**:5299, 1979.

[14] K. L. D'Amico, D. E. Moncton J. Bohr, and D. Gibbs. *Phys. Rev. B*, **41**:4368, 1990.

[15] D. Frenkel and J. P. McTague. *Phys. Rev. Lett.*, **42**:1632, 1979.

[16] S. Toxvaerd. *Phys. Rev. Lett.*, **44**:1002, 1980.

[17] D. Henerson J. A. Barker and F. F. Abraham. *Physica A*, **106**:226, 1981.

[18] L. W. Bruch J. M. Phillips and R. D. Murphy. *J. Chem. Phys.*, **75**:5097, 1981.

[19] G. H. Gilmer J. Q. Broughton and J. D. Weeks. *Phys. Rev. B*, **25**:4651, 1982.

[20] C. Udink and J. van der Elsken. *Phys. Rev. B*, **35**:279, 1987.

[21] C. Bruin A. F. Bakker and H. J. Hilhorst. *Phys. Rev. Lett.*, **52**:449, 1984.

[22] J. A. Zollweg K. J. Strandburg and G. V. Chester. *Phys. Rev. B*, **30**:2755, 1984.

[23] P. D. Frenkel M. P. Allen and W. Gignac. *J. Chem. Phys.*, **78**:4206, 1983.

[24] A. D. Novaco and P. A. Shea. *Phys. Rev. B*, **26**:284, 1982.

[25] F. F. Abraham. *Phys. Rev. B*, **29**:2606, 1984.

[26] M. W. Roth and M. Salazar. *Surf. Sci.*, **441**:270, 1999.

[27] J. K. Kjems H. Taub, K. Carneiro and L. Passel. *Phys. Rev. B*, **16**:4551, 1977.

[28] N. D. Merimin and H. Wagner. *Phys. Rev. Lett.*, **17**:1133, 1966.

[29] Y. Imry and L. Gunther. *Phys. Rev. B*, **3**:3939, 1971.

[30] B. Jancovici. *Phys. Rev. Lett.*, **19**:20, 1967.

[31] N. D. Mermin. *Phys. Rev.*, **176**:250, 1968.

[32] R. A. Aziz and H. H. Chen. *J. Chem. Phys.*, **67**:5719, 1977.

[33] R. A. Aziz and M. J. Slamen. *J. Chem. Phys.*, **92**:1030, 1990.

[34] W. E. Carlos and M. W. Cole. *Surf. Sci.*, **91**:339, 1980.

[35] W. A. Steele. *Surf. Sci.*, **36**:317, 1973.

[36] Private Communications.

[37] G. Vidali and M. W. Cole. *Phys. Rev. B*, **29**:6736, 1984.

[38] E. Flenner and R. D. Etters. *Phys. Rev. Lett.*, **88**:106101, 2002.

[39] L. Bruch. *Surf. Sci.*, **125**:194, 1983.

[40] K. Binder and D. W. Heermann. *Monte Carlo Simulation in Statistical Physics.* Springer, 1997.

[41] K. Binder. *Phys. Rev. Lett.*, **47**:693, 1981.

[42] K. Binder and D. P. Landau. *Phys. Rev. B*, **30**:1477, 1984.

[43] D. P. Landau M. S. S. Challa and K. Binder. *Phys. Rev. B*, **34**:1841, 1986.

[44] A. D. Migone. *Heat Capacity Study of Nitrogen and Argon Adsorbed on Graphite.* PhD thesis, Pennsylvania State University, 1984.

[45] H. Shiba. *J. Phys. Soc. J.*, **48**:211, 1980.

[46] M. Roth and R. D. Etters. *Phys. Rev. B*, **44**:6581, 1991.